

# **Polymer, Metal, and Ceramic Microtubes by Strain-driven Self-rolling**

DISSERTATION

zur Erlangung des akademischen Grades

Doktor rerum naturalium

(Dr. rer. nat.)

vorgelegt

am Fachbereich Chemie

der Fakultät Mathematik und Naturwissenschaften

der Technischen Universität Dresden

von

**Kamlesh Kumar**

**geboren am 19 Juli 1980 in Jaipur, Indien**

Gutachter: Prof. Dr. M. Stamm

Prof. Dr. H.-J. P. Adler

Eingereicht am:

Tag der Verteidigung:

**Dedicated  
To  
My Family**

## Acknowledgement

The completion of this thesis would not have been possible without the support, hard work and endless efforts of a large number of people. I wonder if I can convey my heartfelt appreciation and gratitude in any way possible to all people who are connected direct or indirect to this thesis.

I am deeply indebted to Prof. Dr. Manfred Stamm for providing me an opportunity to carry out this work in IPF, and whose guidance, advice, constant motivation and encouragement, helped me in all the time of research and writing of this thesis. The efforts and help he extended made me to feel at home.

I thank my advisor Dr. Valeriy Luchnikov for his valuable guidance and help during this thesis work. His wide knowledge and constant encouragement provided a good basis for my dissertation. I am also grateful to Dr. Bhanu Nandan for the help and support which I received from him during my stay in Dresden. The way both helped me to complete my thesis is wonderful and it is not easy to express in words.

I gratefully acknowledge Dr. Frank Simon and Dr. Petr Formanek, respectively for their help in XPS, SEM measurement; Dr. Martin Müller and Gudrun Adam for FTIR measurements. I thank Mrs. P. Scheppan and Dr. U. Burkhardt from Max Planck Institute for Chemical Physics of Solid, Dresden for their help in EDX analysis. I also thank Dr. Jens Ingolf Mönch from Leibniz Institute for Solid State and Materials Research Dresden (IFW) for deposition of gold patterns.

I would like to specially thank Prof. I. K. Varma for her tacit knowledge and moral support in very difficult times. Furthermore I would like to express my gratitude to Dr. V.

Senkovskyy for the synthesis of poly(4-bromostyrene) and Dr. A. Kiriya and Dr. E. Bhoje Gowd for their nice suggestions during my work. I also thank to my colleagues Mukesh Kumar Vyas, Prashant Sinha, Fabio Crobu, Smrati Gupta, Eva Herold, Marko Kuntzsch, Konstantin Demidenok, Vera Bocharova, Martha Horchea and Sina Burket for their cooperation and support in my work.

I would also like to thank my friends Bitu, Stefan, Prashant Menezes, Sameer, Pradyumn, Dipti, Alok, Vishal, Vikram, Manoj, Saurabh, Satpal, Biplap, Sunil and Deepa. Without their help would have been difficult to live so far away from family and to complete thesis.

To my family, I thank them for always being there for me and for giving me unconditional support and love. Words are inadequate to thank my parents, brother, and sisters, whose inspiration, understanding, patience and support have always been a source of encouragement in carrying out the work. I would like to specially thank Satish, Mahesh, Mukesh, Shimbu, Neelu, Reenu, and Meenu for accommodating my work and encouraging me to strive for more at each step.

This research work was made possible by the financial support from IPF Dresden.

## Abstract

A thin polymer bilayer film was transformed into micro- and nano-tubes using strain driven self-rolling phenomena of polystyrene (PS)/poly (4-vinyl pyridine) (P4VP) film. Polymer bilayer was produced by consecutive deposition of PS and P4VP, from toluene and chloroform solutions, respectively, by dip-coating technique. The object formation proceeds from a opening in the film made by photolithography or by mechanical scratching followed by immersion of patterned sample in dodecylbenzene sulfonic acid (DBSA) solution. DBSA forms supramolecular complexes with pyridine rings of P4VP and increases the specific volume of the polymer. Since the solution is neutral to PS layer, bilayer film develops strain due to unequal swelling of polymers in solution of DBSA and hence the film bends and scrolls in order to minimize its free energy and form tubes. The length of the tubes and the direction of rolling are determined by mechanical patterning of the film. UV-photolithography is used to fabricate patterns of polymer bilayer in order to create tube in a precise manner. The kinetics of the tube formation was studied with respect to acidity of the solution and UV dose. Rate of rolling increased with the acidity of the solution. Tube diameter and rate of rolling decreased with the increase of the UV exposure time. Films with 2-dimensional gradients of layer thicknesses were prepared to study a broad range of parameters in a single experiment.

Furthermore, polymer micro-toroids and triangles were also fabricated using self-rolling approach of PS/P4VP layer. Moreover, the kinetics of toroid formation is also studied in the present work. The equilibrium dimensions of toroid are determined by the balance of the bending and the stretching energies of the film. The width of the rolled-up bilayer is larger for the films with higher values of the bending modulus and smaller values of the effective stretching modulus.

Moreover, self-rolling phenomena of polymer layer was also explored as a template to fabricate metal, ceramic and metal/ceramic hybrid tube. In order to fabricate metallic and

bimetallic tube, the cross-linked polymer film is capped by metallic layer. After rolling, polymer template is removed by pyrolysis resulting in pure metal microtubes. The fabrication of silica and silica/gold hybrid tubes of high aspect ratio is also demonstrated. Polydimethylsiloxane (PDMS) is used as a precursor of the silica and it is converted into silica by pyrolysis at high temperature. Entire polymer moiety is also removed at this temperature. In order to fabricate hybrid tube of silica with gold, a thin gold layer is deposited on the polymer layer by physical vapour deposition.

Self-rolling of polymer bilayers is a very convenient approach for interfacing the interior of microtubes with external electrical circuits and it can be used in particular for creating devices as micro-bubble generators exploiting electrolytic decomposition of fluids. A demonstration of microbubble generation inside the polymer tube is shown in this work.

Possibility to functionalize the hidden walls of the tubes is one of the major advantages of the self-rolling approach. One can modify the surface of the film prior to rolling by magnetron sputtering of metal and upon rolling, tube and toroids with metallized inner surface could be obtained. The tube and toroids with metallic inner surface are promising for the future research as IR-frequency range resonators. Polymer and metallic microtubes fabricated by self-rolling approach may find applications in such fields as IR-waveguiding, microfluidics, enzyme bi-reaction, chemical and biochemical sensing. The silica and silica/gold hybrid tubes have potential use in optoelectronic devices and in catalytic applications.

# TABLE OF CONTENTS

## Chapter 1: Introduction

1.1 Preface and Motivation	1
1.2 Goal	4
1.3 Outline	5

## Chapter 2: Mechanism of strain-driven self rolling in thin multi-layer films

2.1 Theoretical background	8
2.2 Self-rolling of semiconductor thin films	12
2.3 Swelling behaviour of polymers, networks and super absorbers	14
2.4 Self-rolling of polymer bilayer films	17

## Chapter 3: Experimental

3.1 Materials	21
3.2 Characterization techniques	
3.2.1 Null ellipsometry	22
3.2.2 Optical microscopy	24
3.2.3 Fluorescence microscopy	25
3.2.4 Scanning electron microscopy	27
3.2.5 Atomic force microscopy	29
3.2.6 Infrared spectroscopy	30
3.2.7 X-ray photoelectron spectroscopy	33
3.2.8 Energy dispersive X-ray Analysis	35

## Chapter 4: Formation of Self-rolled Polymer Microtubes Studied by Combinatorial

### Approach

4.1 Introduction	39
4.2 Fabrication of tube	41
4.3 Results and discussion	42
4.3.1 Parameters affecting the diameter of tube	45
a) Effect of the thickness of the polymer layer on the tube's dimensions	46
b) Effect of UV exposure dose on tube diameter	49

c) Rate of rolling	50
(i) The effect of UV irradiation doses on the rate of tube rolling	51
(ii) The effect of concentration of the acidic solution on the rolling rate	51
d) Effect of acid concentration on tube diameter	52
4.3.2 Fluid transport in rolled-up polymer tube	53
4.4 Discussion	57
4.5 Conclusions	59

## **Chapter 5: Fabrication of polymer microtoroids**

5.1 Introduction	61
5.2 Experimental	62
5.3 Results and discussions	64
5.4 Kinetics of micro-toroids formation	66
5.5 Model for the micro-toroids formation	67
5.6 Discussion	70
5.7 Conclusions	71

## **Chapter 6: Formation of metallic/bimetallic microtubes**

6.1 Introduction	74
6.2 Experimental	75
6.3 Results and Discussions	75
6.4 Kinetics of tube formation	85
6.5 Conclusions	91

## **Chapter 7: Fabrication of silica and metal/silica hybrid tubes**

7.1 Introduction	93
7.2 Experimental	94
7.3 Results and discussion	95
7.4 Discussion	104
7.5 Conclusions	105



<b>Chapter 8: Bubble generation inside the tube</b>	
8.1 Introduction	108
8.2 Fabrication of bubble generation device	110
8.3 Results and discussions	112
8.4 Discussion	120
8.5 Conclusions	121
<b>Chapter 9: Summary and outlook</b>	123
<b>References</b>	130
<b>Appendixes</b>	146

# *Chapter 1*

# 1. Introduction

## 1.1 Preface and Motivation

The formation of tubular structures of micron and sub-micron dimensions is an emerging area because of potential applications of these objects in various fields such as micro and nanofluidic systems [Thu06, Teg04], wave-guide [Kip06], electronics [Tak08] and nanojet printing [Voi01]. Mesoscopic dimensions of the tubular-based devices allow for precise control over the tiny amounts of gas, chemicals and solvents, and permit to manipulate with the thermodynamical parameters of the system (temperature, pressure) with high rate and precision [Squ05, Ho98, Lei04, Het05, Mal99]. Moreover, the behaviour of fluids geometrically constrained to small, micron and sub-micron natural or artificial compartments is known to differ considerably from the bulk characteristics [Guo06]. Miniaturisation and reduction of the energy requirements of these systems are additional advantages of these systems.

There exist numerous approaches to the production of micro- and nanoscale tubular structures. The template based [Mar94] and template free [Hop04] methods are widely used to fabricate tubes of polymers, semiconductors, metals and other materials on a micro and nanoscopic scale. Typically, a membrane which contains nanopores of uniform diameter is used in a template method. With the help of porous membrane monodisperse nanocylinders of the desired material, whose dimensions can be carefully controlled, are obtained. Polymer, metal and hybrid nano- and mesotubes can also be synthesized by coating on degradable polymer template fibers [Bog00]. Extremely thin degradable polymer fiber templates are first coated with the desired wall materials and later subjected to selective removal of the core material forms the tubes.

Although the template methods of the mesotube's fabrication are simple, cheap and permit high output, however, they allow only reduced control over the functionalization of the

inner walls of the tubes and lower aspect ratio object formation. The physiochemical properties of the tube's inner surface are of primary importance for the proper functioning of the device. For instance, the balance of hydrophobicity and hydrophilicity is important for the transport of water solutions through the tubes. Selective response of the tube's orifice (chemical gating) is explored in smart filtration devices [Ion06]. Unfortunately the possibility to engineer the interior of the tubes produced by traditional methods is very limited or impossible for many modern surface functionalization methods such as micro-contact printing [Mar98, Xia98], plasma oxidation [Kac02, Nar95], photolithography [Fuj06, Pru98] and metal sputtering [Fuj98, Kel00].

The problem of the restricted access to the tube's interior and lower aspect ratio tube formation can be resolved with a relatively new approach of micro- and nanotube formation via strain-driven self-rolling of thin bilayer or multi-layer planar films [Pri00, Pri01, Sch01a, Sch01b, Vor02, Gol01]. Before rolling one can modify the top layer by the above-mentioned surface treatment methods. After rolling, the functionalized layer forms the inner wall of the tube. In this way, arbitrary complex functionalization, including complex geometrical patterning of the inner walls can be designed.

Bending moment in thin multi-layer films arises due to unbalanced in-plane forces in the top and bottom layers of the film, which can have different physical origin, such as misfit of crystal lattice of the top and bottom film, different thermal expansion of the layers etc. Initially self-rolling method was developed for epitaxially grown semiconductor multi-layers [Sch01c, Sch02a, Sch02b, Den02, Pri02, Pri03a, Pri03b, Gol04, Zha04, Pri04a, Pri04b, Nas05, Gol05], in which the bending and rolling was initiated and driven by the crystal lattice misfit between the consecutive layers. Several studies have shown the ability of semiconductor layers to form various structures like, tubes, rings, and helices of micro- and nanometric dimensions. The

tubes prepared by this method are promising for many advanced applications including nano-syringes for intra-cellular surgery and nano-jet printing [Pri03c], X-ray and visible light waveguides [Den06a].

Recently, the self-rolling mechanism was generalized to the production of polymer micro-tubes from bilayer polymer films [Luc05, Luc06, Luc07, Luc08]. The self-rolling in the polymer bilayer structures is generated by different swelling of the top and bottom layers in selective solvents. Polymer films are easy in processing, enable the control of physiochemical characteristic in broad limits and have multiple application fields. Another advantage of polymers is their good biocompatibility and, in some cases, biodegradability.

In this thesis, we systematically study the self-rolling process in the polymer films, and explore the fabrication of a few simple tube-based devices from these rolled-up polymer tubes. We investigated the kinetics of the tube formation with respect to acidity of the solution and UV radiation dose. The influences of different thickness of the film, solvent concentration and UV radiation dose on the tube diameter were studied. Moreover, the rate of rolling as a function of the UV exposure dose and solvent selectivity are examined. Furthermore, we explored the self-rolling approach of polymer layers for the fabrication of new architectures such as micro-toroids.

The combination of metals and polymers in hybrid materials is a growing research area since they combine the best properties of both components and have more potential applications compare to only polymer and metal objects. We have explored the application of self-rolling phenomenon of polymer layers for the formation of hybrid polymer-metal objects. It was observed that thin metal film stripe like gold could be enrolled by rolling of a polymer

bilayer film. These partially rolled gold stripes could be used as an electrode and electrolysis reaction is shown inside the polymer tube.

Furthermore, the polymer tubes could also be used as templates to create new 3-D metallic objects as micro- and nanotube, solenoid and nano-springs. In the present thesis we have demonstrated a novel two step very simple and inexpensive approach for fabricating single and bimetallic (Gold, Titanium) (Au, Ti, Au/Ti) microtubes with very high aspect ratio from self-rolled polymer templates. The metal layer was enrolled in the polymer tube in the first step and polymer was removed by pyrolysis in the second step. Moreover, ceramic and ceramic/metal hybrid tubes were also fabricated from self-rolled polystyrene/poly(4-vinylpyridine) (PS/P4VP) templates. Poly(dimethylsiloxane) (PDMS) was used as a precursor of the silica and PDMS was thermally converted in silica.

## **1.2 Goals**

The main aim of this work is the systematic study of fabrication of free standing polymer micro- and nano-objects with excellent control on the structure, position and geometry and also to explore the application of self-rolling of polymers. Generalization of the self-rolling technique to polymeric materials is the main aspect of the thesis because polymers allow for the tuning of chemical, mechanical, optical and electric properties in broad limit. Moreover, polymers can be used in medical and biological applications due to biocompatible and biodegradable properties.

Therefore, the thesis is mainly divided in three parts. First part of the thesis is focused on photolithography assisted polymer microtube formation by self-rolling approach and studies of various parameters which affect the dimension of the microtubes. There were two main aims of the studies presented in the first part, (1) polymer microtubes formation in large amount of

uniform and good quality and, (2) experimental study of dependence of the tube's characteristics on the dimensions of rolling bilayer and the fabrication parameters.

The second part of the work emphasizes on the formation of tubes with novel architectures from self-rolling approach of polymer film. The formation of polymer microtoroids and kinetics of toroid formation are studied in this part. The principle features of the microtoroids formation process are captured by a simple analytical model.

The self-rolling method is applicable only for bilayer or multilayer films, hence, so far, only bimetallic or multimetallic tubes have been fabricated by this method. Moreover, since only a specific combination of different metals can be used for the rolling, multimetallic tubes with desired combination is not possible. In this third part of thesis we have explored the self-rolling approach of polymer for the synthesis of metallic or ceramic tubes. For this, self-rolled polymer bilayers used as the template whose inner wall is metallized with pre-desired materials and then the polymer template is removed by pyrolysis to obtain pure metallic/ceramic tube. Ceramic/metal hybrid tubes were also synthesized from the self-rolling of polymer template. The method described in the thesis is versatile because of the fact that any pure metallic or combination of multimetallic tubes can be fabricated using the present approach.

The last part of the thesis focusses on the application of the polymer tube based device. The electrolytic decomposition of fluids via microbubble generation in the polymer tube was shown here which could have potential application in nano-jet printing.

### **1.3 Outline**

The thesis is divided in 9 chapters and 2 appendixes. A general introduction about micro- and nanotubes or channels and their synthesis by strain driven rolling method have been

reported in Chapter 1. The motivation and goal of the work are also included in Chapter 1. This strain driven self-rolling effect was explored for the formation of semiconductor nanotubes as well as polymer and hybrid polymer/metal microtubes and a detailed description of the strain driven rolling mechanism of bilayer films is presented in Chapter 2. Experimental techniques which include characterization techniques and materials are reviewed in Chapter 3.

Chapter 4 is dedicated to the study of photolithography assisted polymer microtube formation and the experimental parameters which affect the dimensions of the microtubes and rate of rolling. The application of self-rolled polymer tube as a transport of fluid on the substrate surface is also demonstrated in Chapter 4. Experimental and theoretical study of microtoroidal cavities by the self-rolling approach is presented in Chapter 5. The applications of the self-rolling method and fabricated microtubes in different fields are shown in Chapters 6, 7 and 8. The fabrication of single and multimetallic tube with the help of polymer self-rolling approach is reported in Chapter 6. The synthesis of gold, titanium, and Au/Ti microtubes are defined in this chapter. The kinetics of polymer/metal hybrid tube formation is also studied in Chapter 6.

In the next chapter (Chapter 7), the synthesis of silica tube using self-rolled polymer template is considered. The thermal transformation of PDMS/PS/P4VP tubes into silica tube was observed and discussed in detail in this chapter. Chapter 8 is devoted to the design of the bubble generation device based on the polymer microtube with incorporated metal electrodes. Chapter 9 discusses the summary of this work and outlook of the research work. References are given at the end of the thesis.



## *Chapter 2*

## **2. Mechanism of Strain-driven Self Rolling in Thin Multi-layer Films**

### **2.1 Theoretical Background (Description of self-rolling mechanism in frames of the elasticity theory)**

Thin film deposition of metal, polymer, insulating, conductive, and dielectric materials on a thicker substrate of another material plays an important role in a large number of manufacturing, production and research applications. The detachment of the film from the substrate and rearrangement into various micro- and nano-objects is used in thin membrane transfer techniques [Rob06], stretchable electronics [Sun06, Kha06a] and rolled-up technology [Pri00, Sch01a, Cho06]. Elastic deformation of thin films plays a major role in the detachment of the film from the substrate and synthesis of various architectures. The tremendous internal elastic energy of strain thin film was used to form micro- and nanotubes [Sch01a, Pri00].

In a general view there are mainly two methods to make micro- and nanotubes which are based on the selective removal of the thin films from the substrate. In one method, the film of arbitrary composition is etched from the substrate and folded back onto its own surface. The other method is based on inherently built-in strain within the film. The films on the substrate are usually in a stressed state because adhesion of two materials of different properties may give rise to internal stresses and magnitude of the mismatch strain is often inferred from a measurement of the curvature it induces in the substrate [Fre00]. The strain in the film can arise by different thermal expansion of layers [Tim25], epitaxial mismatch with lattice parameters [Pri00, Sch01a, Sch01b], chemical reaction with volume and/or phase change [Luc05, Luc07]. The stresses can be either compressive stress or tensile stress [Jou91, Jan07, Win92]. The films try to shrink in tensile stress or try to expand in compressive stress and the film can be deformed in case of large stress. A significant change in geometry may occur in case of higher strain.

The deformation can be converted into the film stress by appropriate mechanics using known material properties and geometrical dimensions of the film and the corresponding substrate. The Stoney equation is usually used as the tool for this purpose [Sto09]. According to Stoney a thin film curls up into close rolls to minimize its potential energy, especially when it doesn't adhere very strongly to the substrate. A steel stripe was used by him to study the tension of metallic film deposition by electrolysis. The basic form of classical Stoney formula gives a relation between the curvature of the film and stress. This can be written as follows:

$$K_{st} = 6 \sigma_f h_f / h_s^2 E_s \quad (2.1)$$

$K_{st}$  = Curvature of the substrate,  $\sigma_f$  = stress in the film,  $h_f$  = thickness of the film,  $h_s$  = thickness of the substrate,  $E_s$  = biaxial elastic modulus of the substrate

Timoshenko investigated a general theory of bending of a bimetal strip submitted to uniform heating [Tim25]. The stripes uniformly heated from  $t_0$  °C to  $t$  °C and if the coefficient of linear expansion of both metals be different, the heating will produce bending of the strip. The following general equation for the curvature of a narrow bi-metal strip was obtained.

$$\frac{1}{\rho} = \frac{6 (\alpha_2 - \alpha_1) (t - t_0) (1+m)^2}{d[3(1+m)^2 + (1+mn)(m^2+1/mn)]} \quad (2.2)$$

$\alpha_1$  and  $\alpha_2$  = coefficient of expansion of the metals (1) and (2).  $d$  = the thickness of the strip ( $d_1 + d_2$ ),  $m$  = ratio of the thickness of metal 1 and 2 ( $d_1/d_2$ ),  $t_0$  = initial temperature,  $t$  = heating at a particular temperature,  $\rho$  =curvature of a bi-metal strip,  $n$  = Young's moduli of the layers ( $Y_1/Y_2$ )

Stoney's formula has been modified many times for the purpose of evaluating bilayer and multilayer structures with arbitrary layer thickness ratios [Kim99, Din98, Bro07]. The

curvature of the bilayer film or diameter of the tube depends on the strain and thickness of the film and it can be represented as:

$$D = \frac{d [3(1+m)^2 + (1+mn) \{m^2 + (mn)^{-1}\}]}{3\epsilon (1+m)^2} \quad (2.3)$$

$D$  =Diameter of tube,  $\epsilon$  = strain in the film,  $d$  = thickness of the bilayer ( $d_1 + d_2$ ),  $n$  = ratio of Young's moduli of the layers ( $Y_1/Y_2$ ),  $m$ = ratio of thickness of layer ( $d_1/d_2$ )

The strain ( $\epsilon$ ) is introduced due to lattice mismatch between two layers. Assuming  $Y_1 = Y_2$ , then the resulting tube diameter can be presented by a continuum mechanical model as the following equation [Sch01b, Tsu97]:

$$D = \frac{1}{3\epsilon} \frac{(d_1 + d_2)^3}{d_1 d_2} \quad (2.4)$$

The multilayer-modified Stoney's formula which predicts the stress contribution of each individual layer is proposed and verified through experiments and numerical analysis [Kim99]. Closed-form estimate of curvature for self-positioning multilayer hinged structures and tubes has been also derived [Nik03]. According to this the curvature radius for hinge of different width ( $R$ ) is calculated as

$$R = [(x - x_0)^2 + (y - y_0)^2] / [2 (y - y_0)] \quad (2.5)$$

where  $x$  and  $y$  are horizontal and vertical coordinates of some point selected for the radius determination;  $x_0$  and  $y_0$  are coordinates of the hinge detachment from the substrate.

The internal strain distribution offers the opportunity to extend the above fundamental investigations to a new diversity of material systems and geometries. Hence, a new technique based on the use of internal elastic stresses in thin film is developed and known as self-rolling

technique. According to self-rolling method, tube, toroids and other complicated structures of prescribed size and shape are formed with the use of elastic energy of initial strained films of nanometer thickness by highly selective and directed detachment of the film from the silicon substrate. A thin film minimizes its potential energy by bending and scrolling when film is allowed to relax and it tends to acquire a new equilibrium shape for which their elastic energy is minimal.

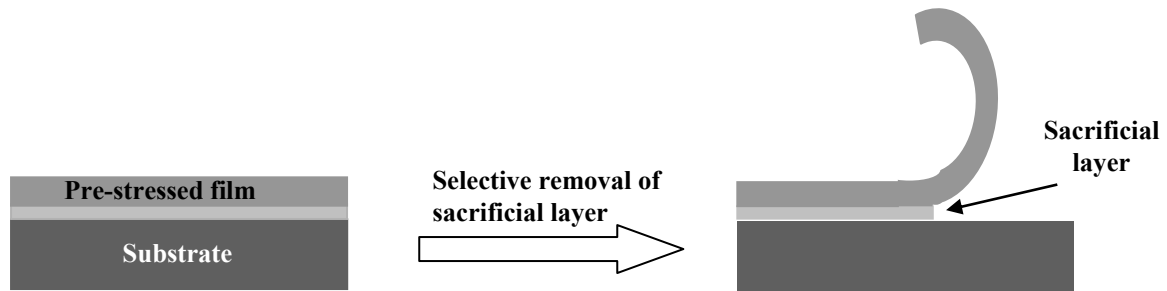


**Figure 2.1:** A schematic view of self-rolling of pre-stressed film via selective removal of sacrificial layer

In order to make various kinds of structures from the self-rolling approach, a nanometer thin film is deposited on the silicon wafer. The strain in the film is generated either during the deposition or after deposition. The deposited layers were in-depth microstructured (windows or scratches) so that the etch solution reaches up-to silicon-oxide depth. The formation of microstructured windows is the essential step in design of self-rolled device. The position and orientation of rolling objects are determined through these windows. Photolithography [Hua05], electron beam lithography [Hua05, Pri01], direct mechanical patterning with a sharp razor blade [Men04, Luc05] and focus ion beam [Luc06] were used for the structuring of the bilayer to access the substrate by etch solution. The microstructured samples were immersed in the etch solution to remove the sacrificial layer. The strained layer is released from the substrate by removing the sacrificial layer through the lithography windows and spontaneously rolled and formed micro- and nanotubes. The principle of self-rolling of stressed film is schematically depicted in Figure 2.1.

## 2.2 Self-rolling of semiconductor thin films

The strain driven rolling was started for semiconductor films and fabrication of semiconductor nanostructures followed with a precise control in structure, geometry and position. A wide variety of different objects in the nanometer to micrometer range have been synthesized using strain driven self-rolling [Pri00, Sch01a].

The strain in semiconductor films is generated from mismatch of lattice constants. Epitaxial mismatch of the crystal lattice is the driving force for the self-rolling of semiconductor thin films. In a compressed state the lattice constant of the grown film is greater than the substrate. For example, a thin film of InAs grown on a GaAs substrate show 7.2% compression strain [Mön01]. A schematic view of strain-induced self-rolling of semiconductor layers (GeSi/Si) followed by formation of tube is shown in Figure 2.2.

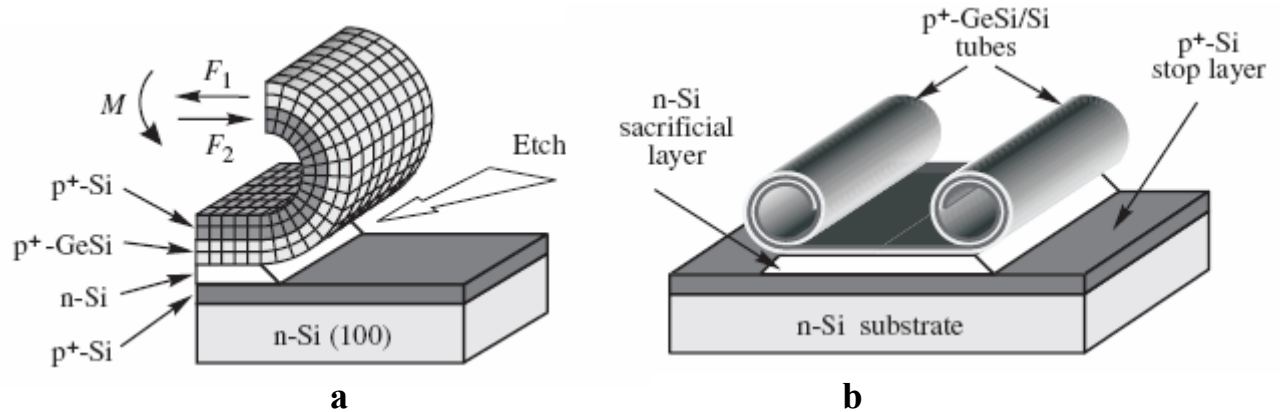


**Figure 2.2:** Schematic presentation of strain induced rolling of semiconductor layers (a) Scrolling of the GeSi/Si bilayer after its partial detachment from the substrate during selective etching of the underlying n-Si sacrificial layer. (b) Self-rolling of P<sup>+</sup>-Si/GeSi bifilms during etching of the sacrificial layer. [Figures adopted from (Gol01)]

According to this method, an elastically strained GeSi/Si film is grown on the silicon substrate using molecular-beam epitaxy (MBE). The GeSi film is in a compressed state due to lattice parameter mismatch and the upper Si film remains in an unstrained state. The micropatterns are

formed on the strained films by lithography and this 2-D patterned strained film is transformed into 3-D objects by selective etching of the sacrificial layer. Etching solvent breaks the adhesion of the substrate and film followed by bending of the film. Two elastic forces,  $F_1$  and  $F_2$ , exist when sacrificial layer is selectively removed. These are elastic forces which are oppositely directed, and they give rise to a non-zero moment of forces  $M$ , which tends to bend the bifilm and form tubular shape.

The structure and size of these objects can be varied over a wide range from nanometer to micrometers. Dimension of these objects could be precisely controlled by film thickness and by the strain incorporated within the two-dimensional layers by lattice mismatch. There is a critical value of thickness of strained layer to start the plastic deformation. In order to start the deformation the thickness of the strained layer should not exceed than this critical value. The number of roll in the fabricated tube is defined by the distance from the edge of the lithographic scratch at which the film starts to roll. The relaxation and redistribution of internal elastic stresses between layers occur during the scrolling of layers and the value of strain in each layer become lower than the value in the initial flat layer with the maximum stress [Pri06].

Semiconductors like InGaAs/GaAs [Pri00, Sch01c, Ste08], SiGe/Si [Sch01a, Sch01c, Sch01b, Gol01, Zha04], SiGe [Sch02b, Cav07] and InGaP [Sch02d] micro- and nanotubes, spiral, and rings have been fabricated onto silicon substrate by strain driven rolling approach using lithography. This method transforms precisely defined two-dimensional structures (epitaxial layers) into free-standing three dimensional objects [Pri00, Sch01c, Sch02a, Men04, Den04a, Den06b]. In fabrication of semiconductor tubes not only molecular beam epitaxy (MBE) grown strained films were used [Pri01, Gol04] but also ultra-high vacuum chemical vapour deposition (UHV-CVD) method was used [Zha04].

The anisotropy of elastic and chemical properties of the semiconductor films allow to fabricate many complicated three dimensional structures such as helical coil, toroids, rectangular, triangular, squared, circular etc. [Pri01, Gol01, Sch02c, Sch02b, Pri06]. Moreover, complex objects with laterally modulated properties have also been obtained using self-rolling method. It is also possible to make ohmic contacts to rolled-up tube. There are two way to obtain near-ohmic contacts to the tubes, first conductive strips are prepared on the film surface and later rolled the film, second method is overgrowing the tubes by a heavily doped wide band-gap material followed by local selective etching and opening some fraction of the buried-in tubes [Pri00]. These external contacts are compatible with the mature integrated-circuit technology which allows us to anticipate its wide practical applications, hence this method automatically resolves the problem of creating ohmic contacts to tubes.

Furthermore, the strain-rolling approach is practically applied not only for semiconductor heterostructures but also for the multi-layered hybrid structures such as metal, dielectric, magnetic layers and epitaxial hybrid structures. Different semiconductor/metal, bimetallic and multi-metallic films, for example, In/Al/GaAs/InAs, SiGe/Si/Cr, Ti/Au, Ti/Au/Ag, Pt/ (Co<sub>0.3nm</sub> / Pt<sub>0.8nm</sub>)<sub>x8</sub>, Si<sub>3</sub>N<sub>4</sub>, Al<sub>2</sub>O<sub>3</sub> and Si<sub>3</sub>N<sub>4</sub>/Ag, Pd/Fe/Pd, SiGe/Si/Si<sub>x</sub>N<sub>y</sub>/Cr were used for fabrication of micro- and nanotubes by stress driven rolling of layers. This would substantially broaden the possible applications of such objects in micro- and nano-electronics, mechanics and fluidics. The free standing magnetic objects such as Cr, Co, Ni, Mn, or Fe could be used in magnetic memory chips, quantum magnetic rings, and hard disk [Wol01].

### **2.3 Swelling behaviour of polymers, networks and super absorbers**

Strain in the polymer film can arise by different behaviour of polymers with respect to the sorption of solvents and gases. Depending on the chemical nature of the polymers this sorption leads to polymer swelling. Hydrogels is a class of polymer materials which has the ability of



swelling in water and retaining a significant fraction ( $> 20\%$ ) of water without dissolving in water [Bra90, And76, Kul89, Po94, Omi08]. Hydrogels absorb aqueous solutions through hydrogen bonding with the water molecule and increase the volume. Hydrogels become very flexible due to their large water content and they can be used in tissue engineering (as a scaffolds), environmental sensing (pH, Temperature etc.), drug delivery, disposal diapers and contact lenses.

A special class of hydrogels is called as superabsorbent polymers (SAP) (also called slush powder) widely used in disposal diapers and in granules for holding soil moisture in arid areas. SAP are hydrophilic polymers that can absorb and retain huge amounts of water or aqueous solutions relative to its own mass [Ich96, Day99, Zoh08]. They can uptake water as high as 100,000%. According to original sources SAPs are divided into two main classes (a) synthetic (petrochemical-based) (b) natural (e.g., polysaccharide- and polypeptide-based). Cross-linked polyacrylates and polyacrylamides, hydrolyzed cellulose-polyacrylonitrile (PAN) or starch-PAN graft copolymers and cross-linked copolymers of maleic anhydride are mainly used SAP.

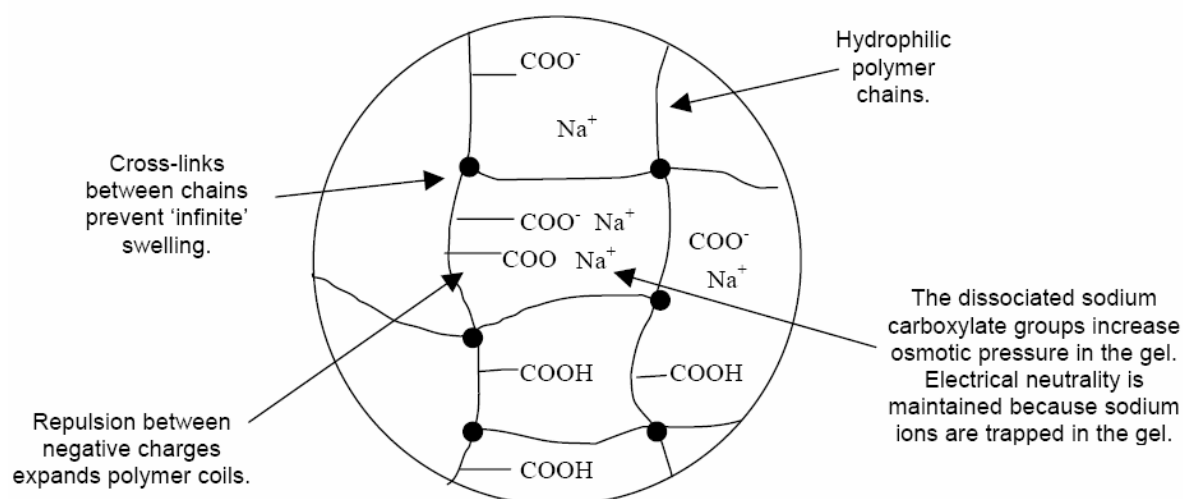


**Figure 2.3:** Schematic view of SAP network. The polymer backbone contain  $-\text{COOH}$  group which form hydrogen bond with water and facilitates hydration.

In case of cross-linked polymers, the interaction between solvent and polymer plays very important role. A cross-linked polymer can be viewed as a network consisting of flexible chains connected to multifunctional nodes (cross-linking sites). When a cross-linked polymer is put in a liquid, it swells up to a point. The swelling of the cross-linked network vary in different solvents. It depends on the thermodynamic interaction between polymer and liquid and it can be swelled to a large extent from its original size. In good solvent, network swell more due to favourable thermodynamic interaction between polymer and liquid. The total absorbency and swelling are also controlled by the type and degree of cross-linking of the polymer. A low density cross-linked polymer generally has a higher absorbent capacity and swells to a larger extent. These types of polymers also have a softer and more cohesive gel formation. Highly cross-linked polymers exhibit lower absorbent capacity and swell to a smaller extent. The gel strength is firmer and can maintain particle shape even under modest pressure.

Cross-links between the polymer chain form a three dimensional network and prevent the infinite swelling of network by the elastic retraction forces of the network chains [Figure 2.3]. These chains tend to maintain a random coil distribution for the distance between chain ends (between crosslinks). It is accompanied by a decrease in the entropy of the chains, as they become stiffer from their originally coiled state. In case of high crosslinking, the network swells less because the chains between crosslinks are shorter. Hence, the maximum swelling is determined by the equilibrium between these two forces, the polymer–liquid mixing tendency, and the elastic response of the network chains. The variable parameters which can affect the swelling are temperature, pressure, pH, electric field, ionic concentration, composition of the solvent. The Van der Waals forces, hydrogen bonding, hydrophilic-hydrophobic interaction and ionic interaction between solvent and polymer also determine the extent of swelling.

The mechanism of swelling of ionized, crosslinked polymer networks is based upon the concept of osmotic pressure. In ionic SAP the overall neutrality is maintained by the balance of negative and positive ions. According to Flory [Flo53], the polymer acts as a semi-permeable membrane which does not allow charge substituents to exit the polymer into the surrounding solution. This is because the ionized monomeric units contain fixed charges which attract and fix ions from the outer solution. Therefore, a charge gradient is set up, in which the concentration of free ions is greater outside of the polymer. Therefore, the osmotic pressure exerted by the gradient causes the polymer chain to swell as further ions diffuse in.

The thermodynamic state of the system, where the interaction between the polymer and another component(s) or solvent play a significant role, is characterized by Flory–Huggins interaction parameter ( $\chi$ ). The conformations of polymers change when they interact with solution and it is accompanied by additional entropy and energy changes. According to Flory-Huggins equation the free energy of mixing ( $\Delta G_m$ ) is presented as below:

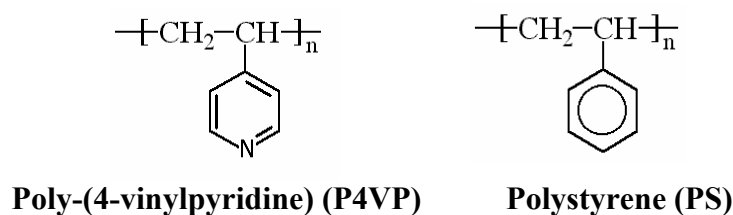
$$\Delta G_m = RT [n_1 \ln \phi_1 + n_2 \ln \phi_2 + n_1 \phi_2 \chi_{12}] \quad (2.6)$$

here  $n_1$  is the number of moles and  $\phi_1$  volume fraction of solvent (component1). The number of moles and volume fraction of polymer (component 2) are denoted by  $n_2$  and  $\phi_2$ , respectively.  $\chi$  is the Flory–Huggins interaction parameter which take account of the energy of interdispersing polymer and solvent molecules. R is the gas constant and T is the absolute temperature.

#### **2.4 Self-rolled polymer bilayer films**

Recently, strain driven rolling of polymer layer [Luc05, Luc06, Luc07, Luc08] has been developed and it attracts more attention due to easy processing and broad possibilities for tailoring physical and chemical properties. Polymers are generally biocompatible and biodegradable and therefore the polymer-based tubes can be more advantageous for the

medical, biotechnology and biological applications. Different swelling properties of chemically unlike polymer films in selective solvent are an important aspect in case of stress driven self-rolling phenomena of polymers. In self-rolling method, the lateral forces, which generate the bending moment, arise due to an unequal change in the specific volume of the components of the film. The polystyrene/poly (4-vinylpyridine) bilayer constitutes a good choice for the self-rolling of polymer layer.



These polymers show opposing effect in the aqueous solution of acid. P4VP has weak basic behaviour due to presence of nitrogen atom in the pyridine ring and it forms acid-base complex in presence of acid whereas the PS layer remains unchanged in presence of acid. So after immersion of sample in the acidic solution, the P4VP layer swells due to acid-base complex formation whereas upper PS layer remains stiff. Consequently strain arises in the film due to unequal swelling of polymers in selective solvents. The acidic water causes protonation and swelling of the P4VP layer simultaneously. The PS layer plays double role in the self-rolling approach, first it opposes the swelling of the P4VP layer, and thus induces the bending moment. Secondly, it also protects the P4VP layer from direct contact with acidic water at the interface between this and the rolling front. The schematic presentation of self-rolling mechanism of PS/P4VP bilayer is shown in Figure 2.4. Combinations of other polymers and solvents could be used if they produce similar mechanical effect. In addition, hybrid objects could be synthesized by combining polymer with other materials such as metal. UV-photolithography is an effective way to produce uniform and large number of good quality microtubes in case of polymer [Luc07].

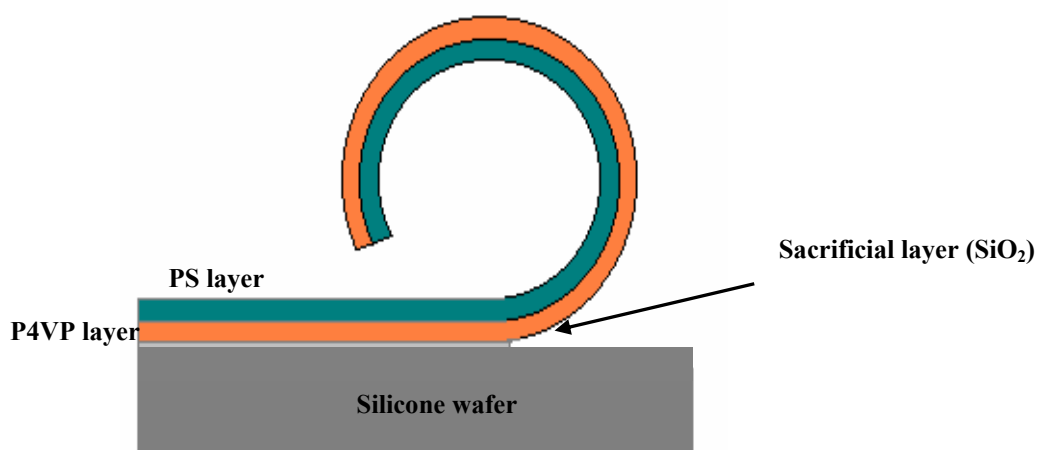


**Figure 2.4:** Schematic presentation of self rolling of P4VP/PS bilayers. Rolling occurs due to etching of  $\text{SiO}_2$  layer by the acidic solution which releases the polymer film from the substrate.

According to the elasticity theory, in case of semiconductor films, the curvature of the bending layers is defined by the mechanical strain, stiffness of the materials and thickness of the layers but in terms of polymer materials, theoretical analysis of tube's dimension is more complicated. In case of polymers, these parameters also depend on the degree of crosslinking, swelling in selective solvent and plastic deformation of the polymers (described in detail in Chapter 4).

## *Chapter 3*

## 3. Experimental

### 3.1 Materials

#### 3.1.1 Substrate

Silicon wafers were used as the substrate throughout all the experiments. These wafers were purchased from the Silchem Handelsgesellschaft GmbH (Freiberg, Germany) or Wacker-Chemicronics GmbH (Burghausen, Germany). Silicon wafers were cut into appropriate sizes using diamond cutter before start of the cleaning process of the wafers. Silicon wafers were cleaned by sonication in dichloromethane for 15 min followed by heating in H<sub>2</sub>O<sub>2</sub>, NH<sub>4</sub>OH and Millipore water solution (1:1:2) for 1 h at 65 °C [Ker70]. Subsequently the silicon wafers were rinsed 3-4 times with millipore water and dried under nitrogen stream.

#### 3.1.2 Solvents

Millipore water was used to make the acidic solution. Chloroform, Toluene, THF, diethyl ether, and hexane were purchased from Sigma-Aldrich. Toluene, chloroform and dichloromethane were purchased from Acros Organic and used as received.

#### 3.1.3 Polymers and other chemicals

Poly(4-vinylpyridine) (P4VP) {M<sub>n</sub> = 45900, M<sub>w</sub> = 82500} and Polystyrene-block-Poly(4-vinylpyridine) (PS-b-P4VP) {M<sub>n</sub> = 35000 - 2700} were obtained from Polymer Source Inc and used as received. Poly(4-bromostyrene) (PS) was synthesized from 4-bromostyrene by nitroxide mediated radical polymerization. 10 g of freshly distilled 4-bromostyrene (0.055mol) and 0.032g of 2,2,5-Trimethyl-3-(1-phenylethoxy)-4-phenyl-3-azahexane, alkoxyamine [Ben99] (0.1mmol) were placed in a round bottom flask equipped with magnetic stirring bar and sealed with a rubber septum. Argon was bubbled through the mixture using stainless steel needle for 30 minute. After that the mixture was heated at 123°C for 2 hours.

The viscous polymer solution so obtained was diluted with tetrahydrofuran (THF) and poured into hexane. The solid was filtered, redissolved in dichloromethane and precipitated into tenfold excess of diethyl ether and dried in vacuum at 50°C. Yield – 8g (80%). GPC:  $M_n = 25000$ ,  $M_w = 46000$ ,  $PDI = 1.77$ . 4-bromostyrene was purchased from Sigma-Aldrich and distilled under reduced pressure before use. Poly(dimethylsiloxane) (PDMS, Sylgard 184) and Dodecylbenzene sulfonic acid were obtained from Dow Corning and Acros Organic, respectively.

### 3.2 Characterization Techniques

#### 3.2.1 Null ellipsometry

The thickness of polymer layers was measured by null ellipsometry. Ellipsometry is sensitive to several material characteristics, such as layer thickness, optical constants (refractive index and extinction coefficient), surface roughness, composition, and optical anisotropy. Therefore, ellipsometry is a simple, versatile, and powerful characterization technique to measure the dielectric properties of thin film. Ellipsometry analyses a change in polarization of light upon reflection or transmission from a sample. The nature of polarisation depends on the thickness and refractive index of the sample. The detail description of the ellipsometry can be found in literature [Tom05, Azz87, Ohl00]. A simple principle of the ellipsometry is shown in Figure 3.2.1 a.

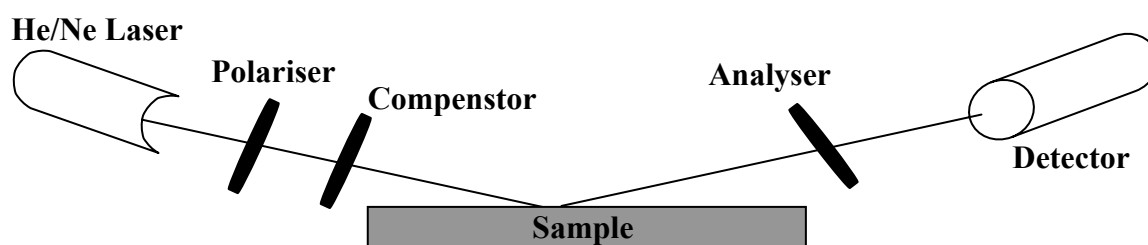


*Figure 3.2.1 a: Principle of ellipsometry*



An ellipsometer can measure thicknesses less than a nanometer to several micrometers. Monochromatic light is emitted by a light source and is elliptically polarized by a polarizer. The coordinate system used to describe the ellipse of polarization is the p-s coordinate system (Figure 3.2.1 b). The p-direction is defined by the intersection of the surface and the plane of incidence (corresponding to x), and the s-direction perpendicular is to the p-direction in the plane of surface (corresponding to y), whereas the z-axis is directed inward into the sample, perpendicular to its surface.

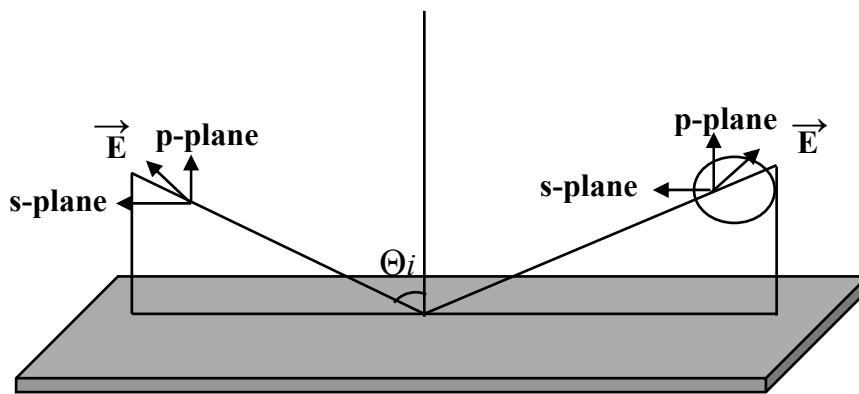


**Figure 3.2.1 b:** Schematic view of the geometry of an ellipsometry measurement

After polarization the laser passes through a compensator and it falls on the sample. The sample reflects the radiation and the change of phase between s and p components of light depends on the sample thickness and refractive index. After reflection radiations pass through an analyser and are detected by a detector. Therefore the position of the analyser and polarizer are measured at the maximal and minimal intensities. The basic principle of ellipsometry is presented in Figure 3.2.1b.

Ellipsometry does not measure thickness directly, it measures the change in polarization state of light reflected from the surface of a sample and gives the value of  $\Psi$  (amplitude parameter) and  $\Delta$  (phase parameter). The ellipsometry measurement is generally expressed by the following equation [Azz87]:

$$\tan(\Psi) \cdot \exp(i\Delta) = r_p/r_s \quad (3.1)$$

Here  $r_p$  is the complex Fresnel reflection coefficient of the sample in the plane of incidence (p) while  $r_s$  is the coefficient perpendicular (s) to the plane of incidence. The ratio of Fresnel coefficient contains phase information in  $\Delta$ , which makes the measurement very sensitive. The fit of the determined value of  $\tan(\Psi)$  and  $\Delta$  parameter of an optical model provides layer thickness and optical constants of layered substrates. For proper working of ellipsometry the sample must be composed of a small number of discrete, well-defined layers that are optically homogeneous and isotropic. Violation of these assumptions will invalidate the standard ellipsometric modeling procedure, and more advanced variants of the technique must be applied.

In the present work, the SENTECH SE-402 microfocus null-ellipsometer was used to measure the thickness of polymer layer. It consists a light source (He/Ne laser) to emit monochromatic light. The thickness of polymer layers were measured at  $\lambda = 632.8$  nm and  $70^\circ$  angle of incidence. The refractive indices 3.858- i0-018 for silicon substrate and 1.4598 for native silicon dioxide were used for the calculations. Polymer layer thickness were obtained by using  $n = 1.59$  for PS [Iye03] and  $n = 1.58$  for P4VP [Bie00]

### **3.2.2 Optical microscopy**

The microtubes, toroids and rolling of layers were observed by optical microscopy, in the present work. Optical microscopes are the simplest and most widely used instruments for viewing or magnifying the objects that are hardly visible to the naked eye. An optical microscope consists of a light source, a condenser, an objective lens, and an ocular or eyepiece, which can be replaced by a recording device. The eyepiece and objective lens magnify the image of the specimen and project it onto the viewer's retina or onto the film plane in a camera. The condenser lens focuses a cone of incident light onto the specimen. Visible wavelengths of

light are used in optical microscope. Optical or light microscope involves passing visible light transmitted through or reflected from the sample through single or multiple lenses to allow a magnified view of the sample. The resulting image can be detected directly by the eye and captured digitally. There is a movable stage which holds the specimen in the optical path and allows the specimen to be moved in and out of the focal plane and even left, right and rotated about the optical axis. The detail description of optical microscopy can be found in microscopy books [Deg80, Mur00].

The optical microscope which we used for characterization, contains four Zeiss Achromplan lenses {a scanning lens (4X), low power lens (10X), medium power lens (32X) and high power lens (50X) that produce an enlarged image of an object placed in the focal plane of the lenses. The objective lens has few mm focal lengths and it creates an intermediate image. This intermediate image is further magnified by ocular or eye-piece.

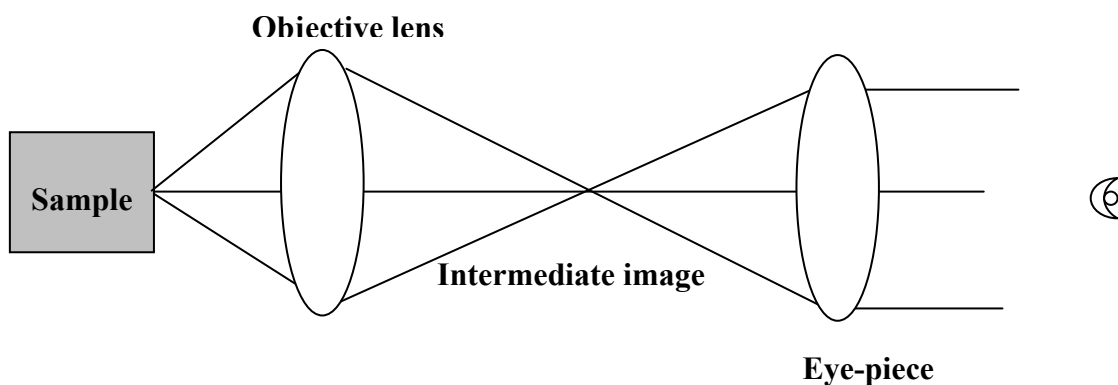


*Figure 3.2.2: Principle of optical microscopy*

### **3.2.3 Fluorescence Microscopy:**

The fluorescence microscope is a high power compound light microscope fitted with a mercury or xenon lamp, a dichroic fluorescence filter cube, and fluorescent objectives [Lic05]. The most significant difference between fluorescent microscopy and normal bright field microscopy system is that the light shown on the specimen is not the same light as viewed

through the eyepieces, in fluorescent microscopy. The light incident is used as an excitation light and the image viewed is the light that has fluoresced from the specimen. The fluorescence microscope is used to study physiological and biochemical properties of organic or inorganic substances using the phenomena of fluorescence and phosphorescence instead of absorption and reflection [Bar96, Ros91, Ros95].

The fluorescence microscope is based on the phenomenon that certain material emits energy detectable as visible light when irradiated with the light of a specific wavelength [Lak99]. The sample can either be fluorescing in its natural form like chlorophyll and some minerals, or treated with fluorescing dyes. In present study, polystyrenesulfonic acid (PSA) molecules in polymer tube were detected by fluorescence microscopy. PSA molecules were labelled by Rhodamine 6G dye and Carl Zeiss Axio Imager fluorescence microscope used to detect PSA molecule inside the tube.

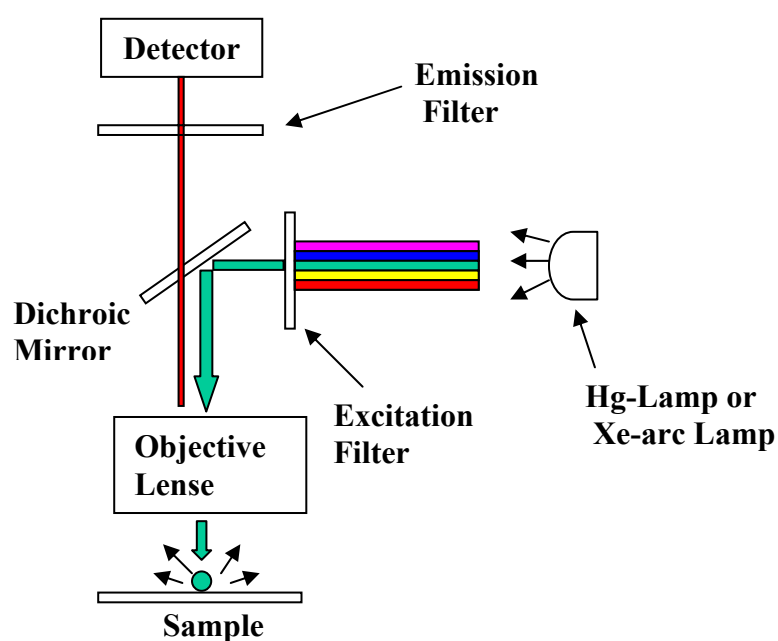


*Figure 3.2.3: Schematic view of a fluorescence microscope*

Fluorescence microscope contains a mercury or xenon lamp to emit ultraviolet light. A dichroic mirror is used in the fluorescent microscope to reflect one range of wavelengths and to allow another range to pass through. The dichroic mirror reflects the ultraviolet light up to the specimen. The ultraviolet light excites fluorescence within molecules in the specimen. The objective lens collects the produced fluorescent-wavelength light and this fluorescent light passes through the dichroic mirror and emission filter. The emission filter eliminates wavelengths other than fluorescent. The allowed fluorescent light is detected by detector [Figure 3.2.3]. Here, the fact that the emitted light is of lower energy and has a longer wavelength than the light that is used for illumination. The fluorescing areas can be observed in the microscope and shine out against a dark background with high contrast.

#### **3.2.4 Scanning Electron Microscopy (SEM): Ultra 55 plus (Carl Zeiss SMT)**

SEM is an electron microscope which produces the magnified images of high resolution by using electrons instead of light waves [Che90]. The images created without light waves are rendered black and white. Higher magnification, larger depth of focus, greater resolution and ease of sample observation are main specialities of SEM. In the SEM detector the signals from the interaction of the incident electron with the sample's surface are detected and a virtual image from the signals is constructed. SEM requires a vacuum atmosphere to image a sample, because a gas atmosphere rapidly spreads and attenuates electron beams.

Figure 3.2.4 represents the schematic view of SEM with basic components. SEM requires vacuum atmosphere to analyse the sample. A beam of high energy electrons (range from 100 eV to 100 keV) is emitted by electron gun, located at the top of the column. This electron gun is made by tungsten or lanthanum hexaboride ( $\text{LaB}_6$ ) cathode. The electron beam passes through a series of condenser lenses. These lenses focus the electrons to a very fine spot (0.4 nm to 5 nm). A pair of scanning coils deflects the focused beam back and forth across the

specimen in a controlled manner. When the electron beam hits the sample and the electrons lose energy by repeated random scattering and absorption within a interaction volume. The energy exchange between the electron beam and the sample results in the emission of secondary electrons from the surface. Back scattered electrons and characteristic X-rays are also emitted with secondary electrons. Secondary electrons are collected by a detector which sends the signals to an amplifier. The final image is built up from the number of electrons emitted from each spot on the sample that corresponds to the topography of the sample [Rus85].

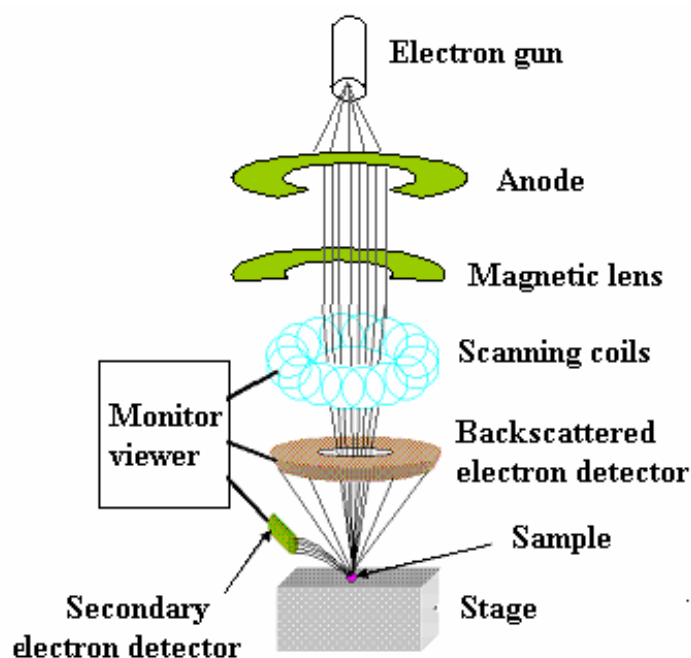


*Figure 3.2.4: Schematic view of Scanning electron microscope*

The LEO DSM 982 GEMINI microscope was used for the morphological studies of tubes and toroids. The acceleration range of this SEM is from 0.2 kV to 30 kV. It gives typical resolutions of 1nm at 30kV and 4nm at 1kV. A thin layer of gold was covered by sputtering to introduce electrical conductivity in the samples which increase the emission of secondary electrons thereby inducing contrast and enhancing the quality of images.

### 3.2.5 Atomic force microscopy (AFM)

In AFM a sharp probe is scanned across a surface and interaction between probe and sample is monitored. When the tip is brought into proximity of the sample surface, some kinds of forces are generated between tip and sample, and cantilever gets deflected in response to these forces [Figure 3.2.5a]. Depending on the force between the tip and the sample, forces are measured in AFM such as mechanical contact force, Van der Waals forces, capillary forces, chemical bonding, electrostatic forces, magnetic forces, Casimir forces, solvation forces etc [Hin06, Gie03, Zho93]. The force in AFM is not measured directly, but calculated by measuring the deflection of the lever, and knowing the stiffness of the cantilever. Therefore, the generated forces in AFM follow Hooke's law. According to Hook's law

$$F = -kz \quad (3.2)$$

F= Force, k= spring constant, z= cantilever deflection.

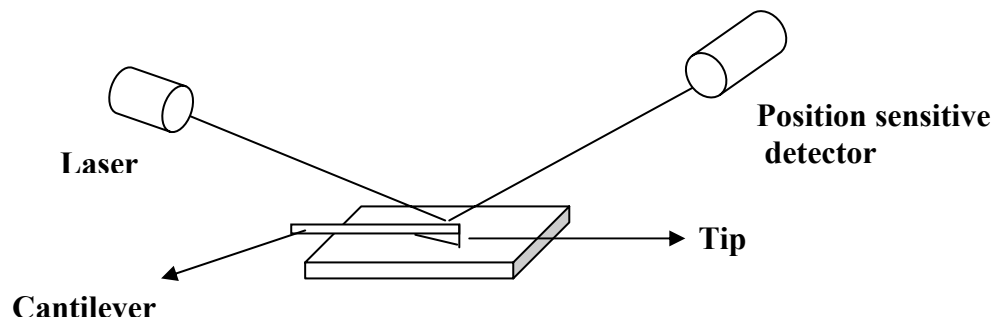


*Figure 3.2.5a: Principle of AFM*

The cantilever is typically made from silicon or silicon nitride and contains a tip with radius of curvature in the order of nanometers. The displacement of the cantilever is detected by the reflection of a laser beam focused on the top surface of the cantilever. Typically, in AFM a deflection of a reflected laser is measured by a split photodiode detector. The AFM is used to image almost any type of surface, including polymers, glass, ceramics, and composites at nanoscale with high resolution. AFM images the surface in atomic resolution and also measures the force at nano-newton scale. AFM was applied to studies of adhesion, friction, corrosion, abrasion, etching and polishing of surfaces.

Vertical movement of the scanner is monitored by the detector and is stored in form of topographic image. There are mainly three modes of AFM: (a) contact mode AFM (b) Tapping mode AFM (c) Non contact mode AFM. In contact mode, tip scans the sample in close contact with the surface and a feedback loop maintains a constant deflection between the cantilever and the sample by vertically moving the scanner. The force between the cantilever and the sample remains constant due to constant cantilever deflection. In tapping mode AFM, cantilever is oscillated at or near its resonance frequency with amplitude ranging from 20 nm to 100 nm. The tip taps on the sample surface during the scanning procedure. In non-contact mode the cantilever is oscillated slightly above the cantilever resonance frequency with amplitude less than 10nm. The corresponding force vs probe-sample distance curve is shown in Figure 3.2.5 b

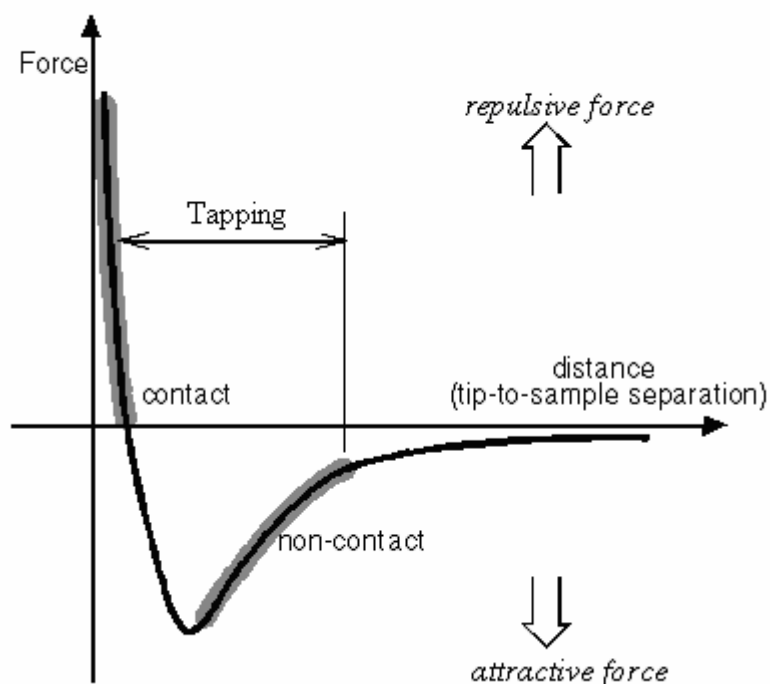


**Figure 3.2.5b:** Curve between force vs probe distance from the sample

### 3.2.6 Infrared Spectroscopy (IR)

IR spectroscopy is a powerful technique to determine the functional group in a sample or molecular structure of materials, whether organic or inorganic. Infrared radiations contain wave



lengths between the visible and microwave regions. Photon energies associated with the infrared radiation (from 1 to 15 kcal/mole) are not much sufficient to excite electrons, but may induce vibrational excitation of covalently bonded atoms and groups. The covalent bonds in molecules are not rigid sticks or rods, they behave like stiff springs that can be stretched or bent. Infrared radiation is absorbed by organic molecules and converted into energy of molecular vibration, either stretching or bending. For the vibration to be infrared active there should be a change in the dipole moment during the vibration. Detailed description of the IR can be found in the literature [Gri86, Sil88, Smi79].

The infrared region is divided in near, mid and far infrared regions and the wave lengths of these regions are  $14000\text{-}4000\text{ cm}^{-1}$ ,  $4000\text{-}400\text{ cm}^{-1}$  and  $400\text{-}10\text{ cm}^{-1}$  respectively. The  $4000\text{-}400\text{ cm}^{-1}$  frequency region is predominantly used for chemical analysis in IR spectroscopy which corresponds to change in vibrational energies within the molecule. All the atoms in the molecule vibrate with respect to each other at above absolute zero temperature and when the vibration frequency is equal to the frequency of the IR radiation directed on the molecule, it absorbs the radiations. A particular functional group absorbs at a characteristic frequency and IR measures these absorption frequencies of infrared region. An IR spectrum shows the curve between wavenumber (X-axis) and percent transmittance (Y-axis) or absorbance. An IR spectrum of a particular compound is unique and therefore it can serve as a fingerprint for this compound [Cro93, Sil81, Bli94].

Older dispersive infrared techniques experience difficulties due to the 'one wavenumber at a time' nature of data acquisition and it leads to either a poor signal to noise ratio in a spectrum or a very long time needed to obtain a high quality spectrum. Poor signal to noise gives inherent large errors and long time prohibits in-situ work. These problems can be resolved using Fourier transform infrared spectroscopy (FTIR). The data is collected and

converted from an interference pattern to a spectrum in FTIR. Therefore FTIR instruments are faster and more sensitive than the older dispersive instruments.

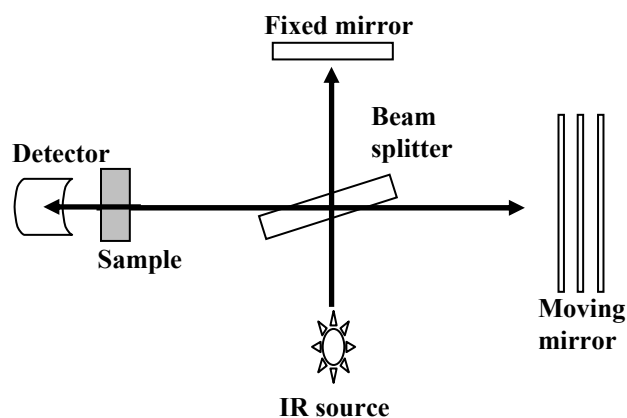


**Figure 3.2.6 a:** A schematic view of FTIR spectrometer typical

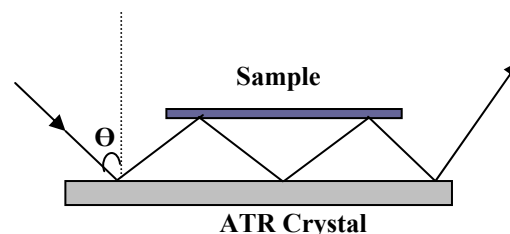


**Figure 3.2.6 b:** Attenuated total reflection ATR plate showing path of light.

Michelson interferometer is a widely used interferometer. It contains two perpendicular mirrors (fixed mirror and moving mirror) and a beam splitter [Figure 3.2.6 a]. The IR radiations are emitted from IR source and splitted by a beam splitter on fixed mirror and movable mirror. The beam splitter is made from an infrared transparent material, such as KBr. The fixed mirror reflects the light back to the beam splitter. The moving mirror moves at a known velocity, back and forth along the direction of light. This mirror also reflects the radiation back to the splitter and some of the light combines with the light reflected from the fixed mirror. Therefore relative position of the moving mirror to the fixed mirror is changed and consequently an interference pattern is generated [Figure 3.2.6 b]. The resulting beam then passes through the sample and is focused on the detector. The detectors are sufficiently fast to cope with time domain signal changes from the modulation in the interferometer. FTIR spectrometer IFS 66v/s [Bruker, Germany] was used in the present work. The spectra were recorded in the transmission mode for the sample on silicon wafer. The FTIR spectrum of the sample was obtained after subtraction of the neat silicon wafer spectra.

### 3.2.7 X-ray Photoelectron Spectroscopy (XPS)

A sample is irradiated with a beam of monochromatic x-rays and the energies of the resulting photoelectrons are measured in XPS [Figure 3.2.7]. A detail description of XPS can be found on the literature [Cha95, Ade91, Mou95]. The XPS is a surface analytical technique which is used to study the composition and electronic state of the sample surface. Non-conducting materials can be analyzed with the help of low energy charge compensation in XPS. XPS is based on photo-ionization and energy dispersive analysis of the photoelectrons. The surface is irradiated by X-ray photons of 200 - 2000 eV in the XPS measurement. The irradiated photons are absorbed by the core electron of the atom and if the photon energy is higher than binding energy of the core electron, the electron emits from the surface.

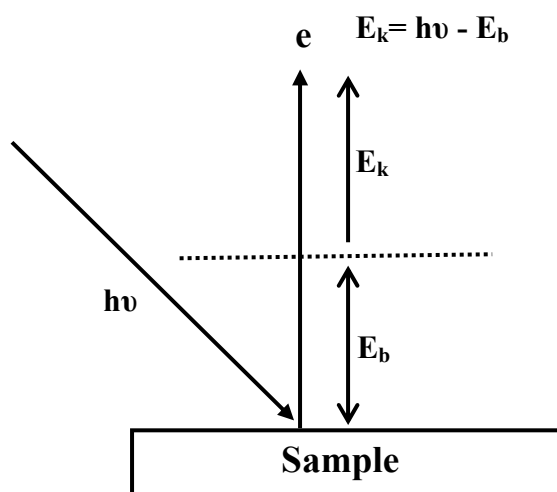


*Figure 3.2.7: Schematic view of principle of XPS*

The kinetic energy can be represented by the following formula:

$$E_k = h\nu - E_b \quad (3.3)$$

where  $E_b$  is the energy of the electron emitted from one electron configuration within the atom.  $h\nu$  is the energy of the X-ray photons being used, where  $h$  is Planck's constant,  $\nu$  is the frequency of light.  $E_k$  is the kinetic energy of the emitted electron as measured by the instrument. The kinetic energy of emitted electron depends on the photon energy and binding

energy of the electron to the surface. The core electron of an element has a unique binding energy and by measuring the binding energy of an electron the elements can be identified. The binding energy of an electron also depends on the chemical environment of the element. This variation of the binding energy assists to study the chemical status of the element in the surface. Therefore, it is also known as electron spectroscopy for chemical analysis (ESCA).

The binding energy of the electrons reflect the oxidation state of the specific surface elements and the number of electrons reflect the proportion of the specific elements on the surface. Measurement of the binding energy and the number of emitted electrons from the surface of the material gives the XPS spectra. The number of detected electrons is plotted against binding energy in XPS spectrum. Each element shows characteristic XPS peaks of particular binding energy that indicate the presence of the particular element in the surface being analyzed. XPS can be used to not only identify the elements but also quantify the chemical composition because the number of photoelectrons of an element is dependent upon the atomic concentration of that element in the sample. After the value of peak intensity (the peak area after background removal) is obtained, the atomic concentration of an element,  $C_i$ , can be expressed as [Oco92]:

$$C_i = \frac{I_i / S_i}{\sum_1 I_i / S_i} \quad (3.4)$$

where  $I_i$  is the peak intensity for element  $i$ , and  $S_i$  is the sensitivity factor for the peak  $i$ .

In the present study, XPS spectra were recorded by an AXIS ULTRA photoelectron spectrometer (Kratos Analytical, Manchester, England). The spectrometer was equipped with a monochromatic Al  $K\alpha$  ( $h\nu = 1486.6$  eV) X-ray source of 300 W at 15 kV. The kinetic energy of the photoelectrons was determined with a hemispherical analyzer set to pass energy of 160 eV for wide-scan spectra and 20 eV for high-resolution spectra. During all measurements,

electrostatic charging of the sample was compensated using a low-energy electron source working in combination with a magnetic immersion lens. Later, all recorded peaks were shifted by the same amount, which was necessary to set the C 1s peak to 285.00 eV for saturated hydrocarbons [Bri98]. The take off angle  $\Theta$  is kept  $0^\circ$  for the measurement. The take off angle  $\Theta$  is the angle between the surface and electron optical axis of the spectrometer. Quantitative elemental compositions were determined from peak areas, using experimentally determined sensitivity factors and the spectrometer transmission function. Background spectrum was subtracted according to Shirley [Shi72]. The high-resolution spectra were deconvoluted using a computer routine. The free parameters of component peaks were their binding energy (BE), height, full width at half maximum, and the Gaussian-Lorentzian ratio.

### **3.2.8 Energy Dispersive X-ray Analysis (EDX)**

EDX is an analytical technique used for the elemental analysis or chemical characterization of samples [Ade90, Gol81, Ros03]. This technique is performed in conjunction with SEM and is based on the interactions between electromagnetic radiation and matter. EDX works by analyzing x-rays emitted by the matter in response to being hit with charged particles. This technique is non-destructive and has a sensitivity of  $>0.1\%$  for elements heavier than C. EDX detectors cannot detect the presence of atomic number less than 5 elements because intensity of x-ray is very weak in light elements. The fundamental principle of EDX is based on the fact that atoms of different chemical elements emit X-rays of different characteristic energy. These energies are characteristic of an element's atomic structure which can be identified uniquely from each other [Gol03]. The evaluation of the energy spectrum collected by an energy dispersive Si(Li) or SDD X-ray detector allows the determination of the qualitative and quantitative chemical composition of the sample at the current beam position.

In this technique an electron beam of 10- 20 keV strike the surface of a sample. The electron beam can be precisely controlled and according to electron beam the EDX spectra can be obtained either from a specific point/particle on the sample, giving an analysis of a few cubic microns of material or alternatively the beam can sweep over a selected area of the sample to identify the elements in that region. The bombarded electrons strike the specimen atom's electron resulting in some electrons being ejected and creation of a hole. This hole is eventually occupied by a higher energy electron from an outer shell and the excess energy of those electrons is released in the form of X-ray photons [Figure 3.2.8a].

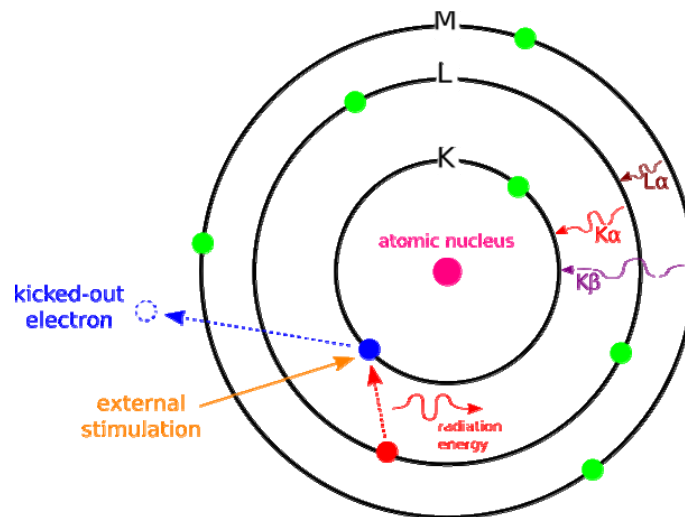


**Figure 3.2.8 a:** Principle of EDX (Figure adopted from <http://en.wikipedia.org/wiki/File:EDX-scheme.svg>)

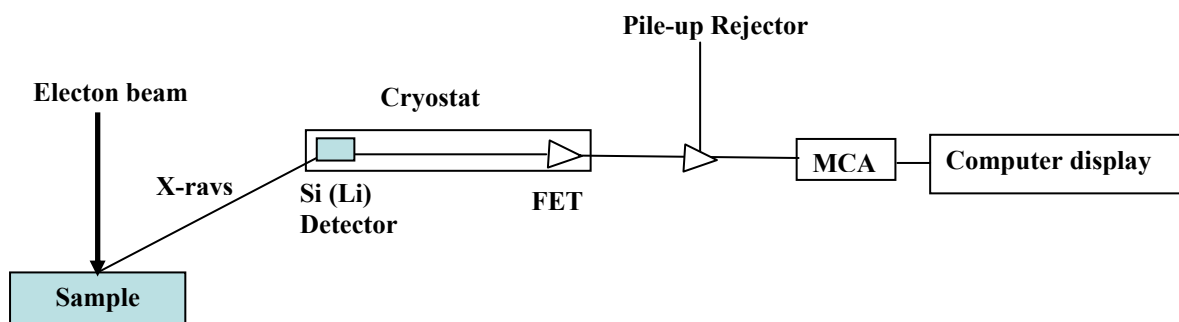


**Figure 3.2.8b:** Schematic presentation of EDX

EDX detector counts the ejected x-ray photon with respect to their energy. In the MCA (multi-channel analyser) the pulses are digitized and stored as pulse height spectrum [Figure

3.2.8b]. A spectrum of the kinetic energy versus relative counts of the detected x-rays is obtained in energy dispersive spectrometer. This spectrum is used to determine the qualitative and quantitative values of the elements present in the sampled volume [Rus96]. EDX is not a surface science technique because in this X-rays penetrate the surface about 2  $\mu\text{m}$ . In the present study, EDX of the samples was carried out in a Philips XL30 scanning electron microscope.

## *Chapter 4*



## **4. Formation of Self-rolled Polymer Microtubes Studied by Combinatorial Approach**

### **4.1 Introduction:**

Polymer micro- and nanotubes have been demonstrated to possess remarkable applications in various fields such as microfluidic devices [Sha06], chromatography [Eba06], biotechnology [Mar03], medicine [Mca03], and chemical sensors [Bra03]. Specific functions performed by microtubes may include encapsulation, liquid and catalyst carriers, flow control, heat exchange, reinforcement, detection, filtration, sensing, optical waveguiding, etc. A decade ago a simple and versatile approach was introduced for production of micro- and nanotubes via strain-driven self-rolling of multi-layer thin films released in controlled manner from the substrate [Pri00, Pri04a, Pri01, Pri02, Vor02, Sel03, Sch01c, Den02, Sch02c, Son06a, Nas05, Men04]. This micro-mechanical effect was explored for the formation of semiconductor nanotubes [Pri00, Pri04a, Pri01, Pri02, Vor02, Sel03, Sch01c, Den02, Sch02c, Son06a, Nas05, Men04, Hua05] as well as metal tubes. The bending moment in the films can be caused by such different factors as misfit of crystal lattices of the top and the bottom layers [Pri00, Pri04a, Pri01, Pri02, Vor02, Sel03, Sch01c, Den02, Sch02c, Son06a, Nas05, Men04, Hua05] or different coefficients of thermal expansion [Tim25].

Recently the self-rolling approach has been generalized to polymer and composite polymer/metal films [Luc05, Luc06]. Polymers allow for tuning the mechanical, optical, electrical and chemical properties of the tube in broad limits. Polymers can be easily combined with other materials such as metals and form the hybrid objects. Strain in the case of a polymer bilayer film can be developed due to unequal swelling of chemically distinct polymers which constitute the top and the bottom layers in a selective solvent. The film minimizes its potential energy by bending and scrolling when it is allowed to relax. The rolled up layers stick together

thus forming a perfectly bonded tube wall. The main advantage of self rolling technique is the possibility of complex engineering of future inner walls of the tubes [Luc07, Hua05]. The small dimensions and the remarkable physiochemical properties of their inner walls are important for the micro and nanofluidic systems because ion and chemical transport can be regulated by molecular-recognition sites on the channel wall [Hub03] [Detail is given in Chapter 2].

The position and orientation of the tube were precisely determined by mechanical structuring of the polymer films by a razor blade [Luc05] or focussed ion beam (FIB) [Luc06]. Recently photolithography has been used to define critical feature size in the fabrication of the larger number of microtubes [Luc07]. Short wave UV-radiations were used for the curing of bilayer and TEM grid used as a photo-mask. The use of photolithography creates symmetric patterns which results mainly in twin tubes instead of single tubes.

Although there exist quantitative description of bending metallic bilayers via the famous Timoshenko formula [Tim25], it is hardly applicable to the case of bending polymer bilayers because of the cooperative action of many factors involved in the tube formation process, such as strong adhesion of the polymers to the substrate, plasticity of polymers, swelling in solvents and yielding of polymers upon strong elongation. By this reason, an experimental study is indispensable for understanding the tendencies of the polymer tube formation.

In this chapter we describe a modified photolithography process which avoids the formation of twin tubes and permits parallel production of large amount of uniform, high quality tubes. A detail experimental systematic study of the polymer microtube formation in various fabrication conditions is performed. The collected information can be used as a reference for the future fabrication of the tubes of desired dimensions. We explore the dependence of the tube's diameters on the thickness of each of the polymer layers in the

double-layer structure. Then, the dependence of the tube's diameters on the degree of short-wavelength UV cross-linking is investigated. Finally, the rate of rolling as a function of the UV exposure dose and solvent selectivity are obtained.

#### **4.2 Fabrication of Tube**

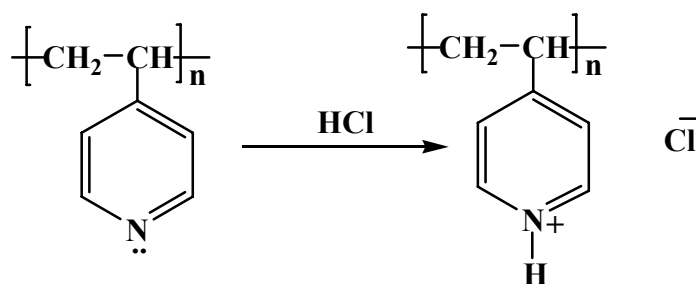
A polymer bilayer was created by consecutive deposition of P4VP and PS, from chloroform and toluene solutions, respectively, by dip-coating technique. A 4 – 5 nm thin layer of PS-b-P4VP block copolymer was deposited on the P4VP layer before deposition of PS, in order to provide a better adhesion between the PS and P4VP layers. Polymer bilayer was crosslinked by UV-radiation. Crosslinking of polymer bifilm provides finite elasticity to the polymer. Without crosslinking, the mechanical strain in the P4VP layer can be relaxed by expansion in the normal direction. UV lamp (G8T5, TecWest Inc., USA) having a 2.5W output at 254 nm was used to irradiate the P4VP/PS bilayer. The estimated exposure dose was 4.11 J/cm<sup>2</sup>. Irradiation with < 280 nm UV light is known to lead to generation of free radicals, chain scission and crosslinking of PS [Ran75] and P4VP [Har05]. TEM copper grids (400 lines per inch) were used as a photo mask. Irradiation with short-wave UV ( $\lambda = 254\text{nm}$ ) causes photo-crosslinking of PS and P4VP in irradiated regions. The pattern was developed by washing the uncured polymer (both PS and P4VP) using a non-selective solvent (chloroform). The microstructured polymer bilayer was dipped in aqueous solution of hydrochloric acid (HCl). The released polymer film is detached from the substrate and forms the microtubes via rolling. The tubes were characterized by the SEM and optical microscopy.

PS and P4VP provide a good combination of different swelling behaviour in selective solvents. Samples with deposited polymer layers were exposed to UV-light through the TEM grids to create the photopatterns. The regions of the polymer film exposed to UV-light show good stability in organic solvents (chloroform, dichloromethane) while the unexposed regions

are easily washed away by these solvents. Hence, the UV-radiations solve two tasks a) introducing finite elasticity in the bilayer, and b) structuring of polymer bilayer using TEM grids. The microtubes were produced by immersion of the micro structured samples in aqueous solutions of HCl.

#### 4.3 Results and Discussion:

The lone pair electron of nitrogen of P4VP form a bond with proton ( $H^+$ ) of HCl (Scheme 4.1). Protonation of nitrogen atom in the pyridine ring results in coulombic repulsion of the 4VP units and selective swelling of the P4VP layer. The swelling of P4VP layer, opposed by the stiff PS layer, gives rise to the bending moment in the film, that leads to the film detachment from the substrate and curling. Since the PS layer acts as the protective layer for the P4VP one, the rolling starts and proceeds from the opening in the film, produced by photopatterning. A detail description of the self-rolling phenomena in P4VP/PS layers with the schematic presentation is given in section 2.4.



*Reaction scheme 4.1: Protonation of 4VP unit by acidic unit*

Self-rolling from uniform openings in the bilayer, produced either by photolithography or any other approach (e.g. mechanical scratching) results usually in twin tubes [Luc05, Sch02d]. We fabricate asymmetric polymer stripe to introduce directional rolling in order to avoid the formation of twin tubes. A schematic view for the process of asymmetric pattern fabrication is given in Figure 4.1.

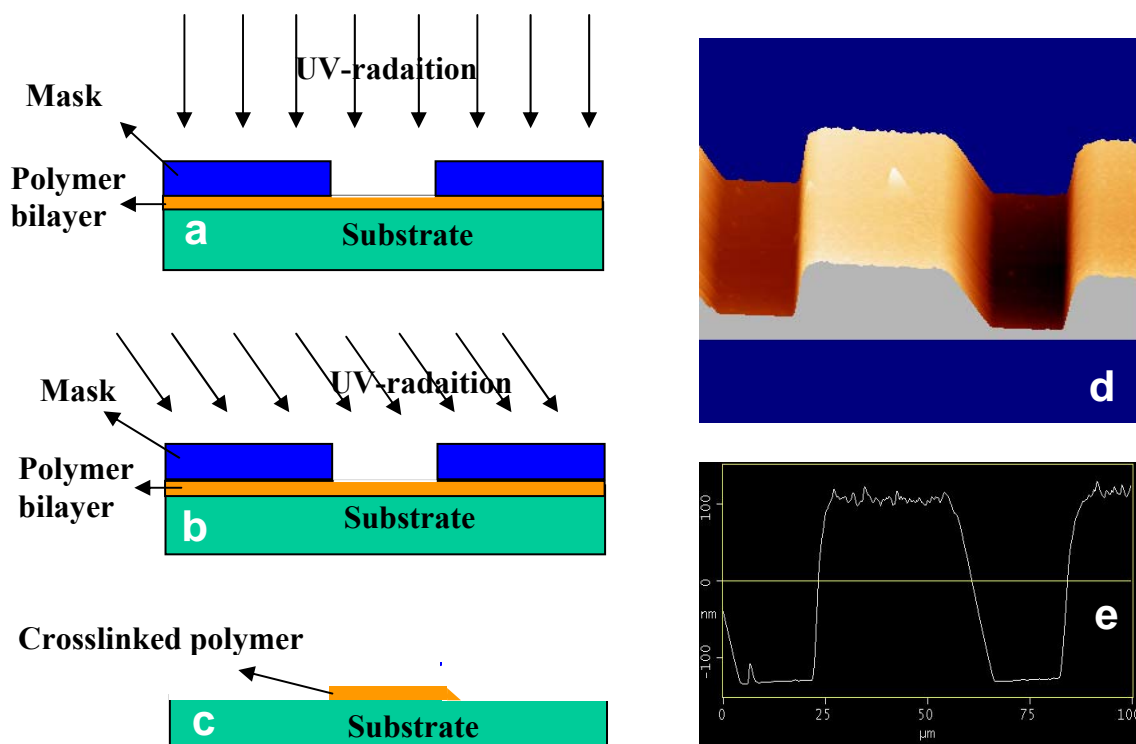


**Figure 4.1:** The photolithography process and schematic way of formation of asymmetric pattern (a-c). (a) Sample exposed to UV-light at normal incident angle, (b) sample exposed to UV-light at sharp incident angle, and (c) development of pattern after washing away uncrosslinked polymer. (d) Three dimensional AFM image of an asymmetric polymer stripes, and (e) section profile of AFM image.

In order to create asymmetric polymeric stripes, polymer bilayer is exposed twice to the UV light, once at the normal incident angle [Figure 4.1 a], and then at a certain inclination [Figure 4.1 b]. After the development of the pattern in chloroform, the asymmetric ratchet-like profile of the bilayer is obtained [Figure 4.1 c]. A three dimensional AFM image of an asymmetric polymer stripes is given in Figure 4.1 d, followed by section profile of this AFM image [Figure 4.1 e].

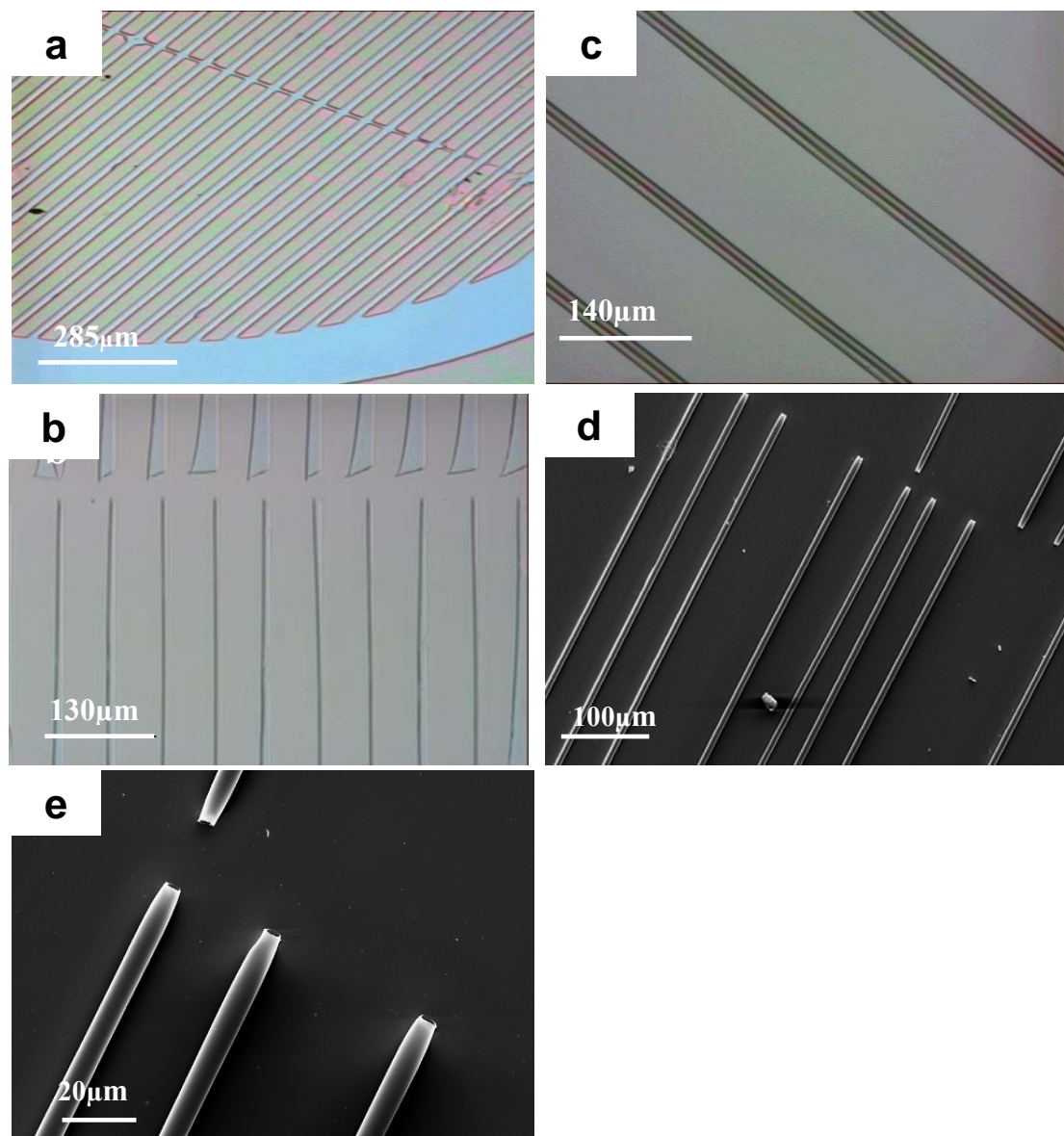


**Figure 4.2:** Tube formation by self rolling of photo-structured bilayer film (a) Pattern developed by washing away uncrosslinked polymer with chloroform. (b) Unidirectional rolling of asymmetric polymer stripe in 0.1wt% aqueous solution of HCl. (c) Formation of twin tube from the symmetric polymer stripes. (d) and (e) SEM micrographs of tube arrays.

In case of asymmetric patterns the formation of polymer tubes starts by rolling from the steeper edges of the polymer stripe. This is so because the adhesion energy does not depend on the thickness of the film, although the bending energy does. At the thin side of the profile, the gain of energy via rolling is insufficient to prevail the adhesion to the substrate, whereas at the

steep side the bending moment is strong enough to detach the film from the surface. Optical micrograph of polymer bilayers with typical developed patterns is shown in Figure 4.2 a, where the polymer bilayer and the regions of silicon wafer are identified by the brown and blue colors, respectively. The asymmetry of the polymer layers strips is clear from the difference in the intensity of the brown color on the edges. Dark brown line indicates the thicker edge whereas thinner edge is indicated by light brown line. The unidirectional rolling of the asymmetric stripes in the acidic solution can be seen by the presence of short bow-like structure which are present only at one side of pattern, immediately after immersion of the sample in acidic solution. An optical micrograph showing unidirectional rolling which starts from the thicker edge is shown in Figure 4.2 b. Unlike of unidirectional rolling from asymmetric pattern, bidirectional rolling from the control symmetric pattern resulted in formation of twin tubes (Figure 4.2 c). SEM micrographs of a polymer tubes is shown in Figures 4.2 d and e which were fabricated from the unidirectional rolling.

#### ***4.3.1 Parameters affecting the diameter of tube***

The diameter of the tubes depends on a number of factors, the most important being the thickness of each of the components of the bilayer, the stiffness of the polymer networks in the collapsed and the swollen states, the degree of swelling, and the strength of adhesion to the substrate. In the present study, we do not attempt to make a more detailed comparison of the experimental data with a theoretical model. This comparison is not possible at the present state of our knowledge about the system for several reasons. First, such parameters entering in the model as Young moduli of the polymers in the glassy and swollen states are not known and their measurement in the bilayer film needs the development of special techniques. Second, the Timoshenko formula, derived for the limiting case of linear elasticity theory of the materials, may not be adequate for the description of the polymer bilayer films. Such effects like yielding of the glassy polymer layers upon elongation, and non-linear stress-strain relation of the

polymer networks upon strong elongation should be taken into account. For this reason, we constrain the goal of the present study to tracing the main tendencies of the tube's formation process, with the purpose to elaborate the practical recommendation for the microtube fabrication procedures, and with the aim to provide the material for future theoretical analysis.

***a) Effect of the thickness of the polymer layer on the tube's dimensions***

Thickness of the PS and the P4VP layers are the characteristics of the bilayer that can be most easily controlled during the fabrication process. Dip-coating technique permits to control the thickness of the polymer layer simply by varying the rate at which the sample is withdrawn from the solution. According to the model of Landau and Levich, the effect of the solution viscosity on the film thickness ( $h$ ) is as significant as the effect of the withdrawal speed ( $u_0$ ), which can be described by  $h \propto (u_0)^{0.67}$  [The99]. Remarkably, the dip-coating technique also allows easy creation of samples with a gradient of the film thickness along the sample length, via accelerating (or decelerating) the rate of the sample withdrawal from the solution. This enables to explore the tube's formation for a continuum of the layer thickness values in a single experiment. This so-called combinatorial approach is nowadays broadly used in chemistry and material science [Ita06].

In order to simplify the study of the bilayer films, we create samples with 2D-film thickness gradients. First, the P4VP layer is deposited so that its thickness increases from top to bottom along the conventional X direction. The thickness of the layer is measured at several points along the X direction and linearly interpolated that gives the thickness of the layer as the function  $g(X)$ . Then, the sample is rotated by  $90^\circ$  and the PS layer is deposited with the thickness gradient along the conventional Y axis. The thickness of the bilayer is again measured by ellipsometry, this time along the Y direction, and the thickness of the PS layer is



interpolated by the function  $f(Y)$  (the thickness of the P4VP layer is deduced). Then, the thickness of the bilayer film at any point of the sample can be calculated as  $h(X,Y)=g(X)+f(Y)$ .

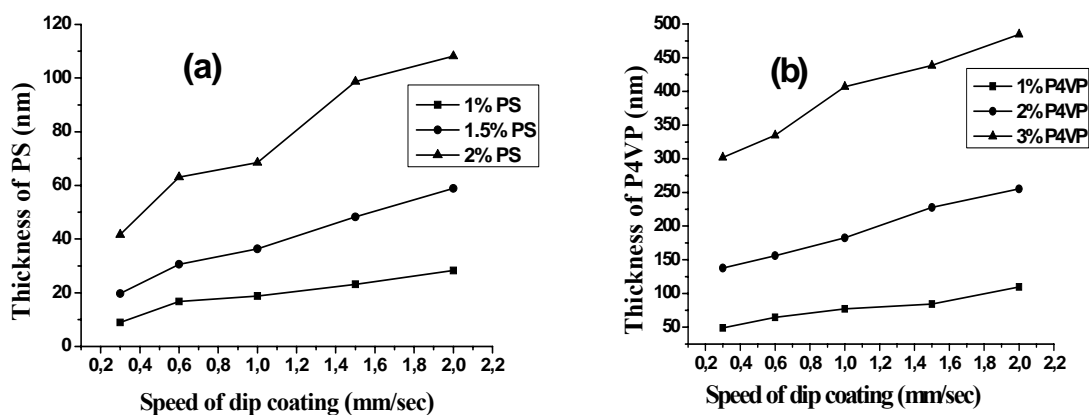


**Figure 4.3:** The dependence of film thickness on P4VP and PS solution concentration and speed of dip coating. (a) Thickness of PS vs speed of dip coating from toluene. (b) Thickness of P4VP vs Speed of dip coating from solution in chloroform.

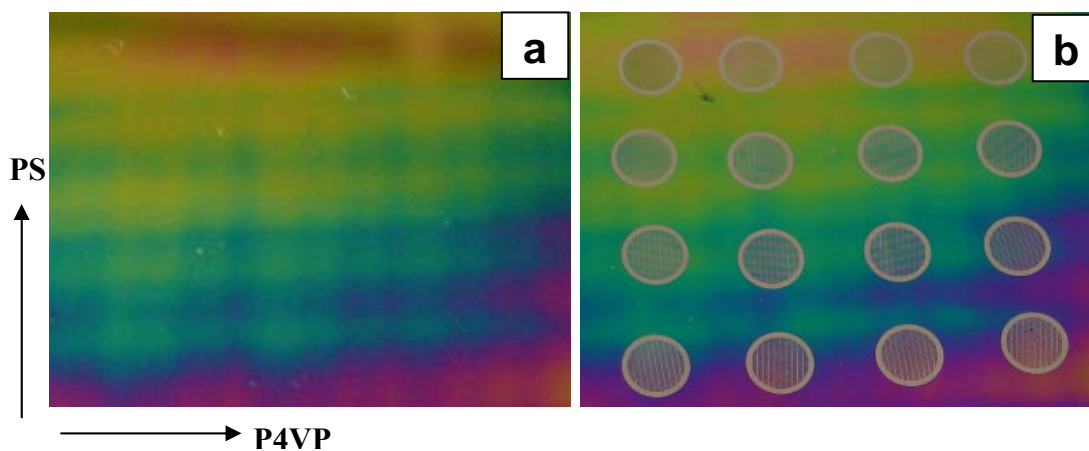


**Figure 4.4:** (a) The PS/P4VP film with gradient thickness. (b) Patterning of the sample a. TEM grids were used as a mask to create pattern. On the image, the thickness of PS and P4VP increases along the vertical and horizontal directions, respectively. The arrows show the direction of increasing thickness of PS and P4VP.

In Figure 4.3 the dependence of the PS and P4VP film thickness on the rate of dip-coating is presented, for different solution concentrations. The PS/P4VP film with 2D-gradient of the bilayer thickness and photo patterning of the sample is shown in Figure 4.4.

The tubes were formed by immersion of the patterned bilayer in the 0.1 w.t.% aqueous HCl solution. In the present work, we omit the study of the dependence of the tubes's diameters on the solvent quality. The HCl concentration chosen by us is optimal in the sense that it is not only sufficiently high for the initiation and proceeding of the rolling, but it is also sufficiently low to avoid very rapid scrolling, that usually leads to defects and irregularities in the tube shapes. With the dip-coating technique, we were able to generate gradient films with the thickness increasing approximately by 100% along the sample, both for PS and P4VP layers. There exists a minimal thickness of the P4VP layer (approximately 35 nm) that is required to provide the bilayer films sufficient bending moment, necessary to overcome the adhesion to the substrate.

Figure 4.5 shows the dependence of the tube's diameters on the thickness of the PS layer (before swelling) for several thicknesses of the P4VP layer. In this experiment, samples were irradiated with 8.22 J/cm<sup>2</sup> UV dose. In our experimental conditions the diameter of the tube grows with the thickness increase of either of the layers. It is clear however from general considerations that the radius of the curled film should have a minimal value for a certain optimal ratio of the layer thicknesses, for any fixed total thickness of the bilayer. If, for example, the bottom layer is very thin in comparison to the top layer, its expansion will not be able to generate a strong bending moment, and hence the curvature radius will aspire to infinity. If, in contrary, the bottom layer is very thick, its expansion cannot be effectively constrained by the counter-force arising in the top layer, that also results in a big radius of the curl.

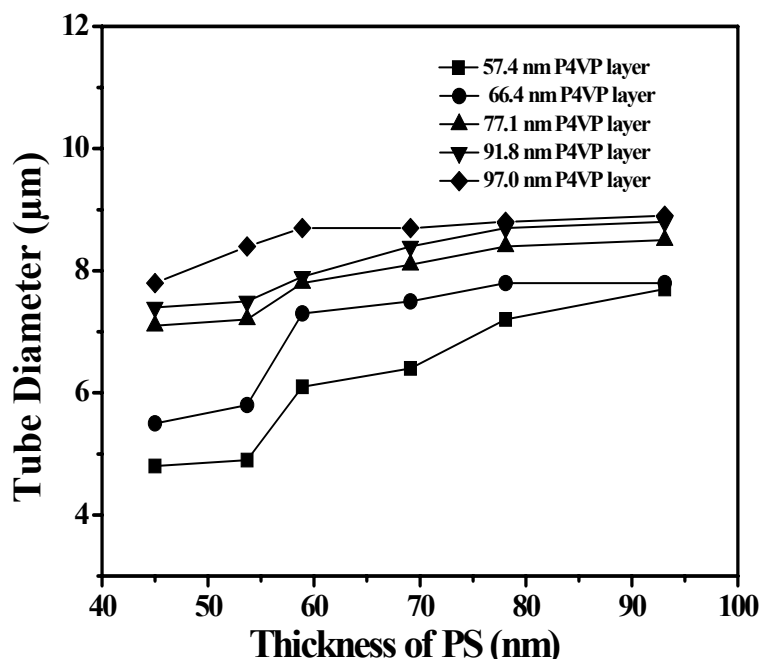


*Figure 4.5: Dependence of the diameter of tubes at different thickness of P4VP and PS*

#### *b) Effect of UV exposure dose on tube diameter*

Bilayer film with PS and P4VP of thickness 50 and 90 nm respectively were used to study the effect of UV exposure dose and concentration of acidic solution on tube diameter and rate of rolling. Samples were exposed to UV-radiation for different time to study the effect of UV exposure dose. Patterned samples were put in 0.1 wt% aqueous solution of HCl for rolling. The dependence of the tube diameters on the UV exposure dose is shown in Figure 4.6.

The following qualitative explanation of the behaviour seems to be reasonable. At very low exposure doses, the degree of crosslinking of the P4VP layer is below the percolation threshold, so that the layer has zero static elasticity modulus, and the strain due to swelling of the polymer is completely relaxed via expansion of the polymer in the direction normal to the PS layer. Thus, at the low UV doses tubes were not formed. We suppose that even after reaching the critical dose corresponding to the percolation threshold of the P4VP layer, the P4VP layer remains too soft and easily deforms in the normal direction upon swelling, without generating sufficiently strong bending moment required to overcome the adhesion force

between substrate and the bilayer. We observed that only the films exposed to the minimum irradiation dose  $0.96 \text{ J/cm}^2$  are able to roll in the acidic solution.

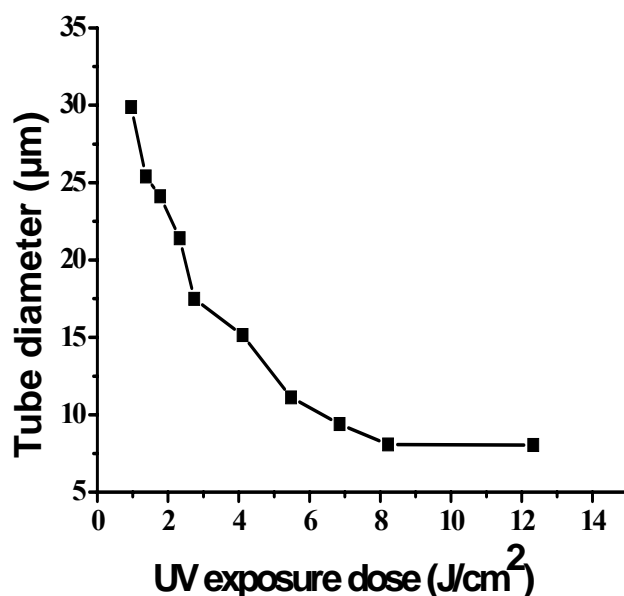


*Figure 4.6: Dependence of tube diameter on dose of UV exposure.*

The experiment shows that tube diameter continuously decreases with increasing the exposure time, until the radius of the tubes reaches some saturation value, after which no further change was observed. This means that the increase in the cross-link density of the P4VP makes the layer more and more stiff, and it generates more and more intense bending moment upon the swelling. However, the crosslink density has, supposedly, some limiting degree, determined by the micro-structure of the polymer. This density puts correspondingly the lower limit to the diameter of the tubes, for the given composition of the bilayer.

***c) Rate of rolling***

It is observed that diameter of the tube can be changed either by changing the thickness of the polymer film, changing the dose of UV-radiation or changing the concentration of acidic solution or by stopping the rolling process at some desired stage just by taking the sample out from acidic solution. One of the interesting aspects in the self-rolling process is the rate of

rolling, it is obvious that rate of rolling will be changed with UV-dose and concentration of acidic solution. Hence, it was crucial to make a systematic study of rate of rolling in different conditions. In the following study we made a detailed study on rate of rolling as dose of UV-radiation and concentration of acidic solution were varied.

**(i) The effect of UV irradiation doses on the rate of tube rolling**

UV irradiation affects not only the geometrical dimensions of the tubes, but also the rate of the tube's formation, as shown by the Figure 4.7. The rolling process of polymer bilayer were video-recorded and the rate of their formation was determined as the distance passed by a tube's axis in the time unit.

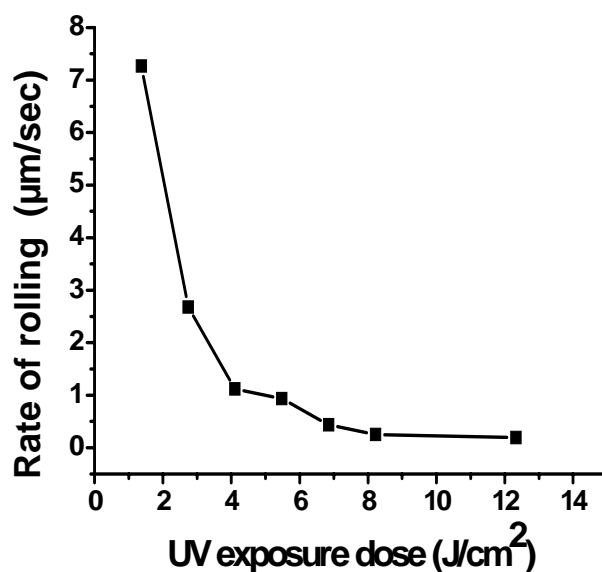


**Figure 4.7:** Rate of rolling in 0.1 wt% HCl: rate of rolling vs UV exposure dose

It is clear from Figure 4.7 that rate of rolling decrease with increase of UV-radiation. There can be two reasons for the deceleration of the tube's formation with the increasing UV dose. Higher crosslinking degree may slow down the mobility of polymer chains and the rate of swelling of the P4VP network in the solvent. It is also known that UV irradiation may cause

covalent binding of polymers to SiO<sub>2</sub> substrates [Yan03]. Then, the rolling at higher irradiation doses may be decelerated by more dense chemical links between the layer and the substrate.

***(ii) The effect of concentration of the acidic solution on the rolling rate***

The rate of rolling of the tubes can be controlled in broad limits by the concentration of acid in the aqueous solution. According to Figure 4.8 which shows the dependence of the rate of rolling on acid concentration, a minimal concentration exists, below which the tube's rolling was not observed. Apparently, the rate and the degree of P4VP layer protonation depend strongly on the pH of the solution. The rate of protonation of P4VP is higher in case of high acid concentration (low pH) and results in higher rate of rolling while rolling is found slower in case of lower acid concentration.

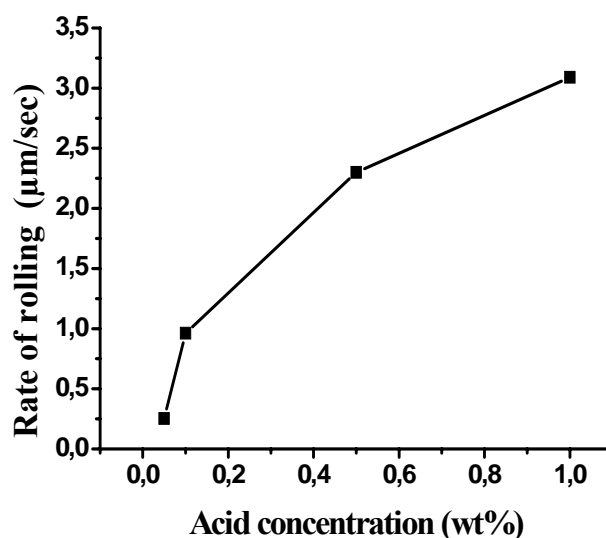


**Figure 4.8:** The rate of rolling at different acid concentration. Irradiation dose is 5.48 J/cm<sup>2</sup>.

***(d) Effect of acid concentration on tube diameter***

Patterned bilayer film was rolled in different concentrated solution of HCl to observe the effect of acid concentration on tube diameter. Irradiation dose for the samples is 5.48 J/cm<sup>2</sup>. It was observed that diameter of tubes decreased with increasing the concentration of acidic solution [Figure4.9]. It is observed that in less acidic solution the rate of rolling is slower due

to less protonation of the P4VP than in the more acidic solution. It is worth to note that lower rates of rolling result usually in more perfect tubes, because swelling of the P4VP layer proceeds more homogeneously, and defects, which have some extra free energy cost, have more time to relax.

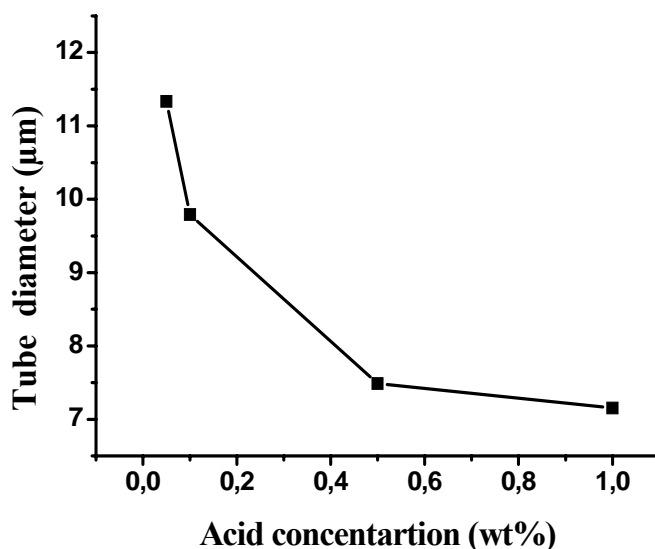


**Figure 4.9:** The dependence of the tube's diameter on the acid concentration. Irradiation dose is  $5.48 \text{ J/cm}^2$ .

#### 4.3.2 Fluid transport in rolled-up polymer tube

Rolled-up semiconductor tubes have been demonstrated as transport media for the liquid solutions [Den04b]. The self-rolled polymer tubes can also be used for the same purpose. When a drop of rhodamine 6G solution in water is placed on an open end of a tube, the liquid inside the polymer tube rises due to capillary action [Figure 4.10 a, b]. On the figures,  $h_1$  indicates the initial stage of solution meniscus, whereas  $h_2$  shows its position after a certain time.

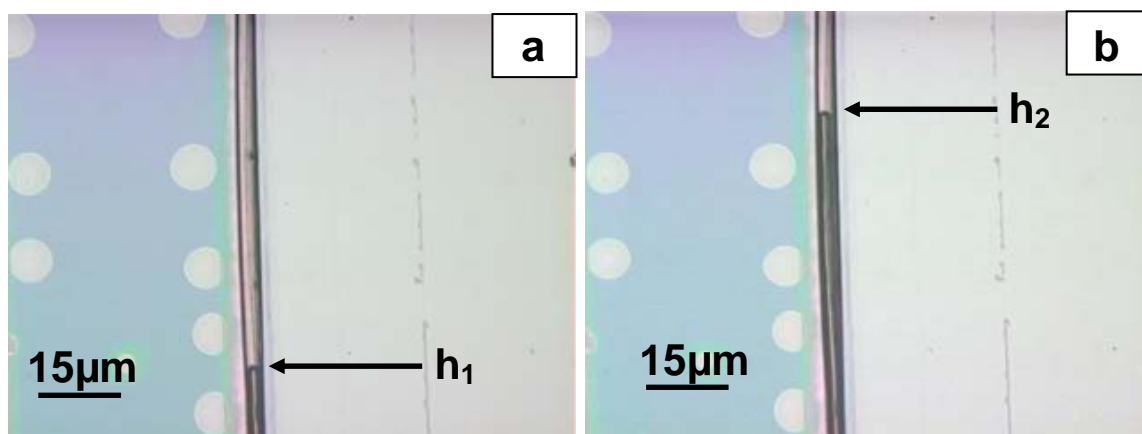


**Figure 4.10:** Optical micrograph of flow of dye solution in polymer tube (a) Initial stage of flow ( $h_1$ ) (b) flow stage after a certain time ( $h_2$ )

Furthermore, we were able to detect single polyelectrolyte molecules inside the polymer tube during the flow of polyelectrolyte solution (polystyrene sulfonic acid) by means of fluorescent microscopy [Figure 4.13]. Polyelectrolyte molecules are labeled with rhodamine 6G dye.

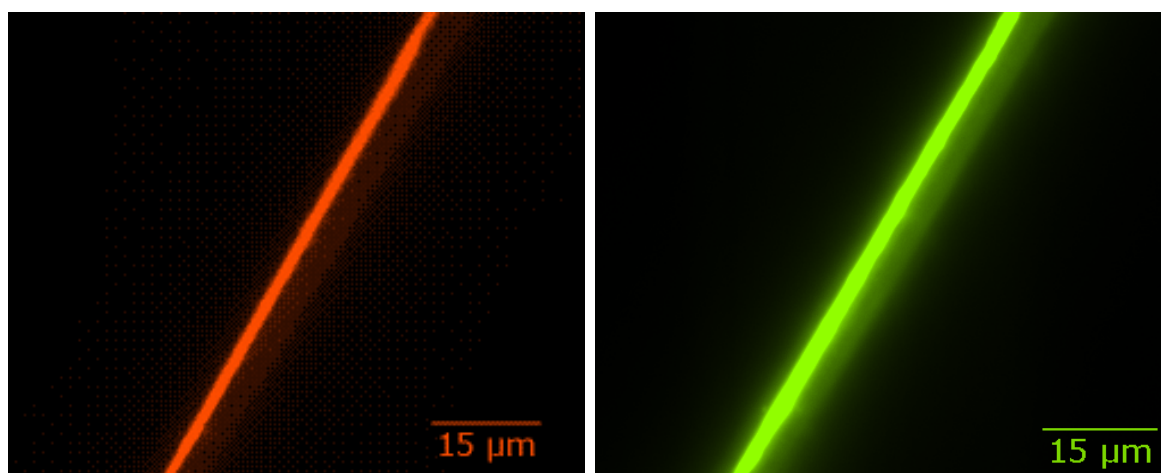


**Figure 4.11:** Fluorescence image of P4VP/PS tube by different filters

In course of these experiments it was necessary to overcome the following difficulty. It was observed that P4VP/PS tubes formed according to the scheme described above show themselves fluorescence even without insertion of any dye solution. [Figure 4.11].



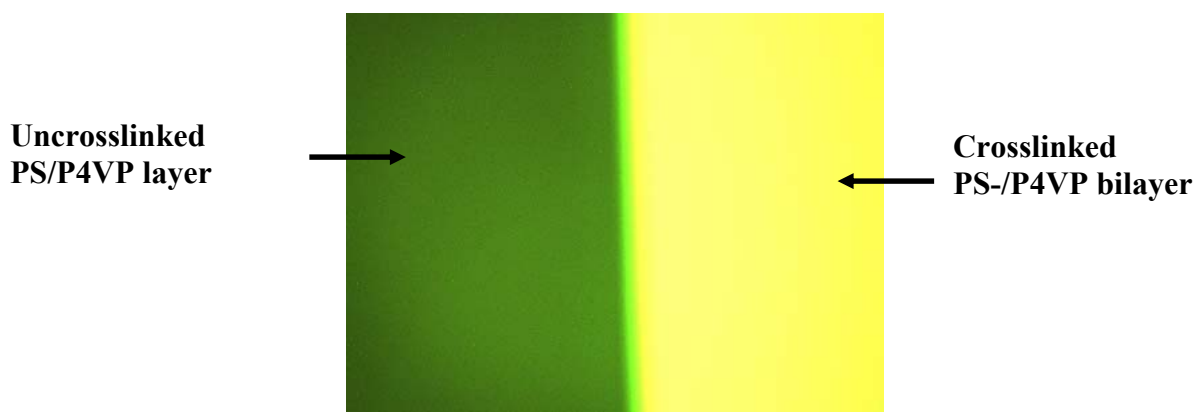


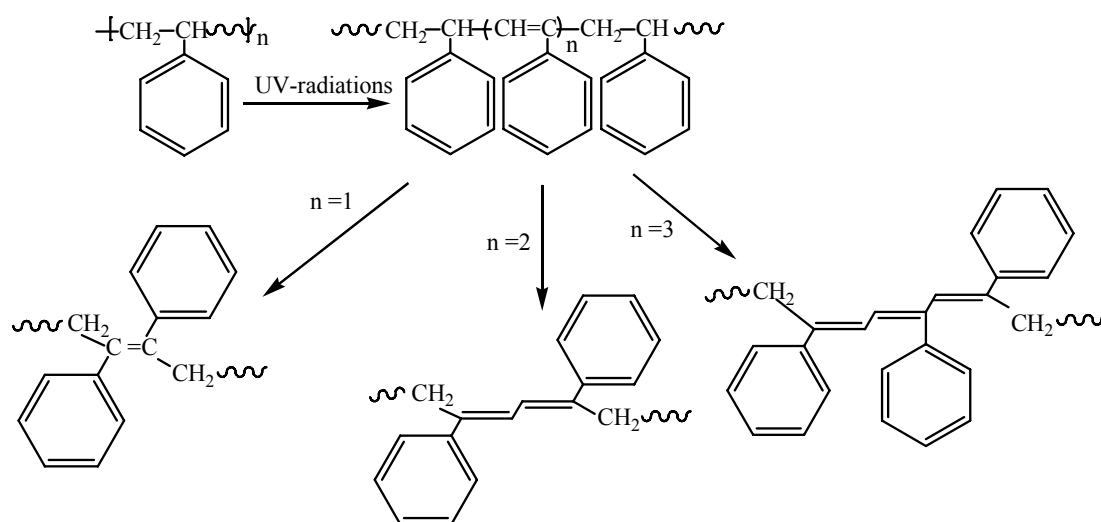
**Figure 4.12:** *PS/P4VP bilayer with crosslinked and uncrosslinked areas*

However, PS and P4VP have the absorbance and emission bands in the 240-330 nm range and should not therefore produce bright images in the visible range by the fluorescent microscopy. In order to find the reason of this fluorescence a control experiment was performed. Half of the polymer bilayer of a sample was exposed to UV-radiations and remaining part masked and remained unexposed. Examination of this sample under the fluorescence microscope revealed that UV-exposed part was fluorescent unlike the unexposed part [Figure 4.12].

Therefore, the exposure of the polymer layers to UV light causes changing in its luminescent spectral properties. It is known that UV-radiation can cause photodegradation of polymer alongside with crosslinking of bilayer [Scheme 4.2]. This photodegradation initiates formation of new fluorescence and absorption optical centres in the polymer [Nur06, Cac87] which absorb and emit light in the fluorescence range (330-520nm).

In order to avoid fluorescence of the tubes, the P4VP/PS bilayer were chemically crosslinked via 1, 4- diiodobutane. Figure 4.13 shows an optical micrograph of polymer tube fabricated from chemically crosslinked P4VP/PS bilayer. 0.01 % aqueous solution of polystyrene sulfonic acid (PSA) was inserted in the tube via capillary action. Rhodamine 6G

dye was used for the labeling of PSA molecules. After placing a drop of PSA solution inside the polymer tube by capillary action an image was recorded using fluorescent microscope. Each bright spot inside the tube corresponds to the molecule flowing through the tube. The average number of the spots corresponds to the concentration of PSA in water.



**Reaction Scheme 4.2:** Formation of new fluorescence and absorption optical centres in the polymer by UV-irradiations



**Figure 4.13:** Self-rolled P4VP/PS tube with PSA molecules labeled by Rhodamine 6G dye

Thus, we observed that self-rolled polymer tube can be used for the transport of fluids. Moreover, optical transparency of the polymer tubes enables optical detection of individual

macromolecules by means of fluorescent microscopy. These results are encouraging for future possible studies such as stretching of macromolecules inside a polymer tube via hydrodynamic flow, or investigation of single living cells in confined geometry of a polymer tube.

#### **4.4 Discussion**

The formation of micro- and nano-tube by self-rolling approach was first introduced by Prinz et al using strain induced self-rolling of  $\text{In}_x\text{Ga}_{1-x}\text{As}/\text{GaAs}$  [Pri00]. Later this concept was applied to Si-Ge, III-V, II-VI semiconductors [Son06a], metals [Nas05] and polymers [Luc05, Luc06]. The basic concept for self-rolling approach was based on different lattice constant or different thermal expansion or different swelling behaviour of the different material layers. In the case of semiconductors, when a thin layer with lattice constant higher than the substrate is selectively released from the substrate, the material deforms and results in a wide range of novel three-dimensional micro- and nano-meter sized objects [Pri00, Scho01a, Sch01c]. Such objects include folded and rolled-up nanotubes [Scho01a, Sch01c, Pri00, Sch02b, Gol01], nanorods [Sch02a], helices [Pri00, Gol01], and rings [Sch01c, Sch02a, Sch02b, Zha04]. A sacrificial layer is essential between the substrate and upper layer which then can be selectively etched off.

The basic steps in order to fabricate self-rolled object are similar in each case. In the first step a bilayer film of semiconductor or metal or polymer with the sacrificial layer underneath is deposited on the silicon substrate and in next step the sacrificial layer is removed with the etchant so that the bilayer can be released from the substrate. In order to expose the sacrificial layer to etchant the mesostructured path in the layers can be made by simply making a scratch on the film [Sch02b, Sel03, Luc05] or by selectively growing on the side wall [Pri02]. Recently, lithographic patterning was introduced as a more controlled, systematic, and easier way to make patterns on the substrate [Sch05, Pri06, Yeo06, Oca03, Chu08, Qin05].

The photolithography patterning of semiconductor film has been carried out by two different methods. The first method involved the SiO<sub>2</sub> deposition, photolithographic patterning and freon reactive ion etching (RIE) steps to transfer the pattern to the silica layer and inductive coupled plasma etching to transfer the pattern to the epitaxial structure down to the sacrificial Al<sub>x</sub>Ga<sub>1-x</sub>As/GaAs layer [Chu08]. In the second method, photolithographic patterning was done directly on the epitaxial structure and wet chemical etching was used to transfer the patterns [Li08].

In the past, the patterning in the polymer bilayer for the self-rolling was done either by a sharp razor blade [Luc05] or by focus ion beam [Luc06]. In the present study we carried out patterning of polymer bilayer by photolithography. The ability to define intricate patterns of the polymer bilayer on the surface of the silicon wafer was main advantage of photolithography. These photopatterns can be further rolled in selective solvent in order to form microtube. Therefore, polymer microtube of good quality and higher quantity were obtained using photolithography.

Furthermore, the effect of various parameters on the fabrication process of tube has been studied in the present thesis. In the past the formation process of In<sub>x</sub>Ga<sub>1-x</sub>As/GaAs tube was monitored in real time as a function of sacrificial layer etching time [Den04b, Den04c]. In this case it was observed that the roll-up process is highly nonlinear in the beginning, linear at an intermediate stage, and ceases for long etching times. The rolled-up semiconductor tube was also filled with red dye and their fluorescence signal was recorded to show that these tubes can act as nanopipelines for fluid transport over long distances or as light emission sources on a substrate surface. In this chapter, we studied in detail, various parameters which affect tube's dimensions like thickness of polymer layer, UV-radiation dose, concentration of acidic solution, and rate of rolling, which helps in controlling the dimensions of a tube. Moreover, the fluorescence properties of polymer tube are also studied in the present thesis.

## 4.5 Conclusions

Photolithography route allows the formation of polymer rolled-up tubes in good quantity and of good quality. Asymmetric photopatterning permits to program the direction of rolling of bilayer films and was found to be suitable for producing single tubes instead of twin tubes. In this chapter, we presented the first systematic experimental study of the formation of polymer tubes. Combinatorial approach (preparation of films with 2D gradient of the film thickness) was applied to study a broad range of parameters in a single experiment. The dependence of the tube's dimensions on the characteristics of the bilayer films and fabrication parameters such as effect of UV radiation exposure time and effect of acid concentration on the rate of rolling are analysed.

The main results can be summarized as follows. (a) thickness of the bilayer film was found to be the dominating factor to determine the tube's diameters, (b) diameter of the tubes decreased with increase in the UV irradiation dose applied for the crosslinking of the polymer, and (c) the rate of rolling and the diameter of the tubes can be effectively controlled both by the dose of the UV irradiation and the quality of the solvent (i.e. in the given system, the acidity of the water solution). In this study, we constrained ourselves to qualitative explanations of the observed dependencies, because many of the process parameters yet need to be experimentally determined. Furthermore, we observed the successful detection of fluorescent molecule inside the solution in the polymer microtube. Possible applications of polymer microtubes are in microfluidic device, biotechnology, sensor and chromatography field. The kinetics of tube formation reported here can be used to make tubes with tailored diameter based on the end application.

## *Chapter 5*

## 5. Fabrication of Polymer Microtoroids

### 5.1 Introduction

Engineered micro- and nanocavities attract much attention as a means to trap light and matter in mesoscale volumes for the studies of confinement effects, such as inhibition or enhancement of spontaneous radiation rate [Pur46] and depression of the melting point [Alc05, Kan06]. The cavities of toroidal shape are particularly interesting as quasi-one-dimensional compartment with periodic boundary conditions. Recently, dielectric micro-rings produced of fused silica have been explored as high-finesse optical resonators, which have broad realm of possible applications in telecommunication and bio-sensing technologies [Arm03, Yal06]. These micro-rings can store light energy at extremely high efficiency and can be integrated into microchips for a number of potential applications.

In the strain driven self-rolling of semiconductor films, bilayers are release from the substrate and formed various free-standing objects such as tubes [Scho01a, Sch01c, Pri00, Sch02b, Gol01], rings [Sch01c, Sch02a, Sch02b, Zha04], helical [Pri00, Gol01], and rods [Sch02a]. After generalization of self-rolling approach to polymer films, microtubes were fabricated using PS/P4VP bilayer (described in Chapter4). However, it is also possible to fabricate more complex geometries using strained polymer films. In this chapter we explore the self-rolling approach of polymer films to fabrication of toroidal micro-cavities. These microtoroids are perspective as optical micro-ring resonators and micro-compartments with periodic boundary conditions. These closed looped tubes can be produced by self-rolling of a bilayer from circular openings. Self-rolling of the toroidal tubes is self-constraining: it stops when the energy gain due to relaxation of the bending moment is compensated by the work on the in-plane stretching of the film caused by the increasing radius of the torus. It is contrary from the case of the straight tubes formation, which can roll until the film is available.

## 5.2. Experimental

The formation of the micro-toroids is schematically depicted on Figure 5.1.

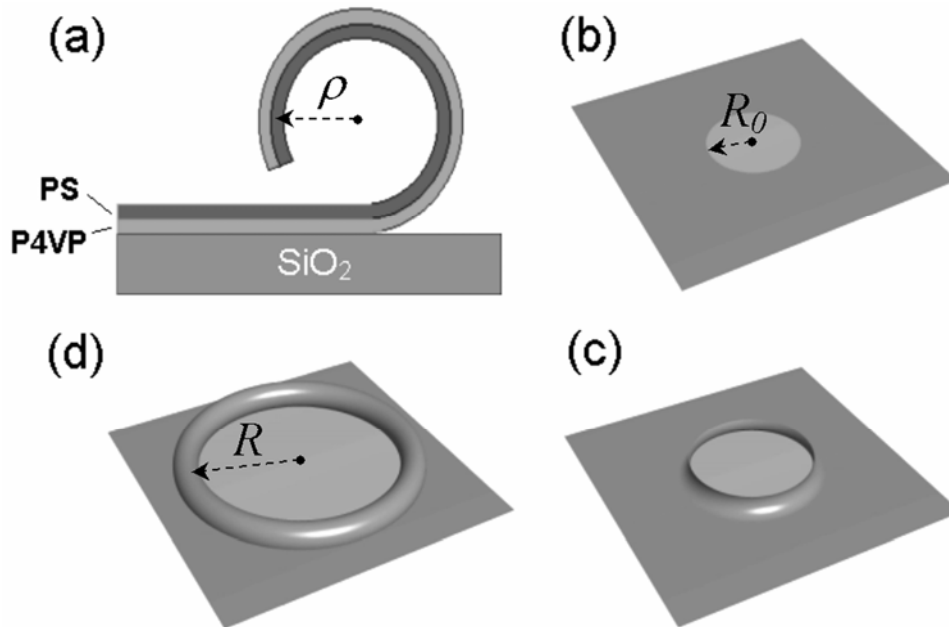


**Figure 5.1:** The schematic view of formation of the rolled up toroidal micro tubes. (a) The structure of the polymer bilayer. (b) A circular lithographic window in the film produced by photolithography approach. (c),(d) initial and the final stages of the toroid formation.

In the fabrication scheme we explore the self-rolling effect produced by unequal swelling of the top and bottom components of bilayer polymer films [Luc05] [Figure 5.1 a]. The poly(4-vinyl pyridine) (P4VP) and the polystyrene (PS) layers were deposited from solutions in chloroform and toluene, respectively, by dip coating. The thickness of the layers (measured by ellipsometry) was  $h_{p4vp} = 47$  nm and  $h_{ps} = 50$  nm. More details of the polymer bilayer film fabrication is described in Chapter 4. The rolling proceeds from an opening in the film, created by photolithography route or by mechanical scratching. The opening provides the contact of an etching agent or a selective solvent with the lower layers of the system. Following the Ref.[Pri03c], we call these openings the lithographic windows (LW). In the photolithography route, the film was patterned by irradiation of the sample through a photomask (a quartz slide



with circular metallic features) with short-wave UV ( $\lambda = 254$  nm, irradiation dose  $W = 4$  J/cm<sup>2</sup>). UV-light of the short wavelength diapason leads to photo-crosslinking of the both polymers [Ran75, Har05].

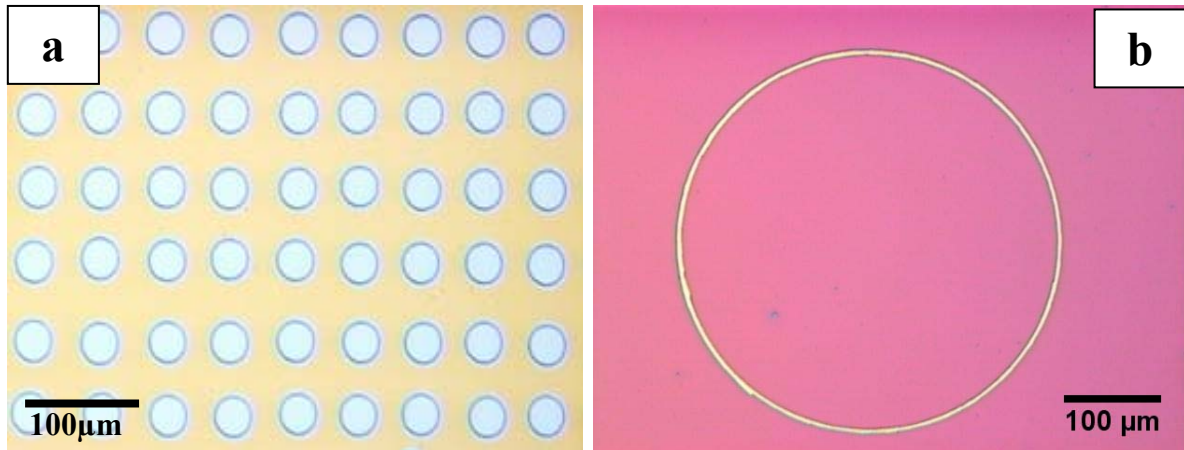
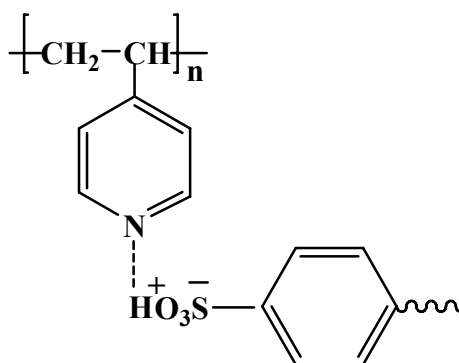


**Figure 5.2:** *Optical micrographs of circular patterns formed on the crosslinked PS/P4VP (a) patterns create using quartz slide with circular opening. (b) Circular opening made by mechanical scratching using sharp needle.*

The patterns were developed by washing non-cured polymer in dichloromethane/chloroform. In this way, the polymer films with circular openings [Figure 5.1 b, 5.2 a] were obtained. In the mechanical scratching circular LWs were produced by a sharp needle. For this purpose the sample was mounted on a rotating stage, and a sharp needle was put by a micro-positioning system into contact with the sample surface. An optical micrograph of sample with mechanical scratch is given in Figure 5.2 b. Patterned polymer bilayers were immersed in 2 wt % aqueous solution of dodecyl benzene sulfonic acid (DBSA) to start the self-rolling of layers [Figure 5.1 c]. The samples were taken out from the acidic solution after the toroids formation and dried [Figure 5.1 d]. The characterization of microtoroid was done by SEM and optical microscopy.

### 5.3 Results and discussions

The driving force for the self-rolling of bilayer is generated from the formation of supramolecular complex between the solution of DBSA and pyridine rings of P4VP [Ikk95, Ika96]. The DBSA was chosen as a acidic surfactant because it has a relatively long tail and easily form supramolecular assembly with pyridyl group. The specific volume of polymer was increased due to supramolecular complex formation (Scheme 5.1).



**Reaction scheme 5.1:** Schematic view of supramolecular complex formation of DBSA with P4VP

The stiff PS layer is neutral in the DBSA solution and it opposes the swelling of P4VP layer. Due to these two opposing actions the bending moment arises which causes curling of the film and eventual tube formation Figure 5.3 a, b are the optical micrographs of single toroid and array of polymer toroids, respectively. An optical micrograph of toroidal surface is shown in Figure 5.3 c.

SEM micrographs of micro-toroids produced by photolithography route are collected on Figure 5.4. A defect-free 128  $\mu\text{m}$ -wide toroid was formed by rolling of 3.3  $\mu\text{m}$ -wide tube from a 100  $\mu\text{m}$ -wide LW (Figure 5.4 a, b). The toroid has one completed shell, as can be deduced by comparing the width of the rolled layer (14  $\mu\text{m}$ ) and the circumference of the tube (approximately 10 $\mu\text{m}$ ). The surface of the tube is very smooth [Figure 5.4 b].

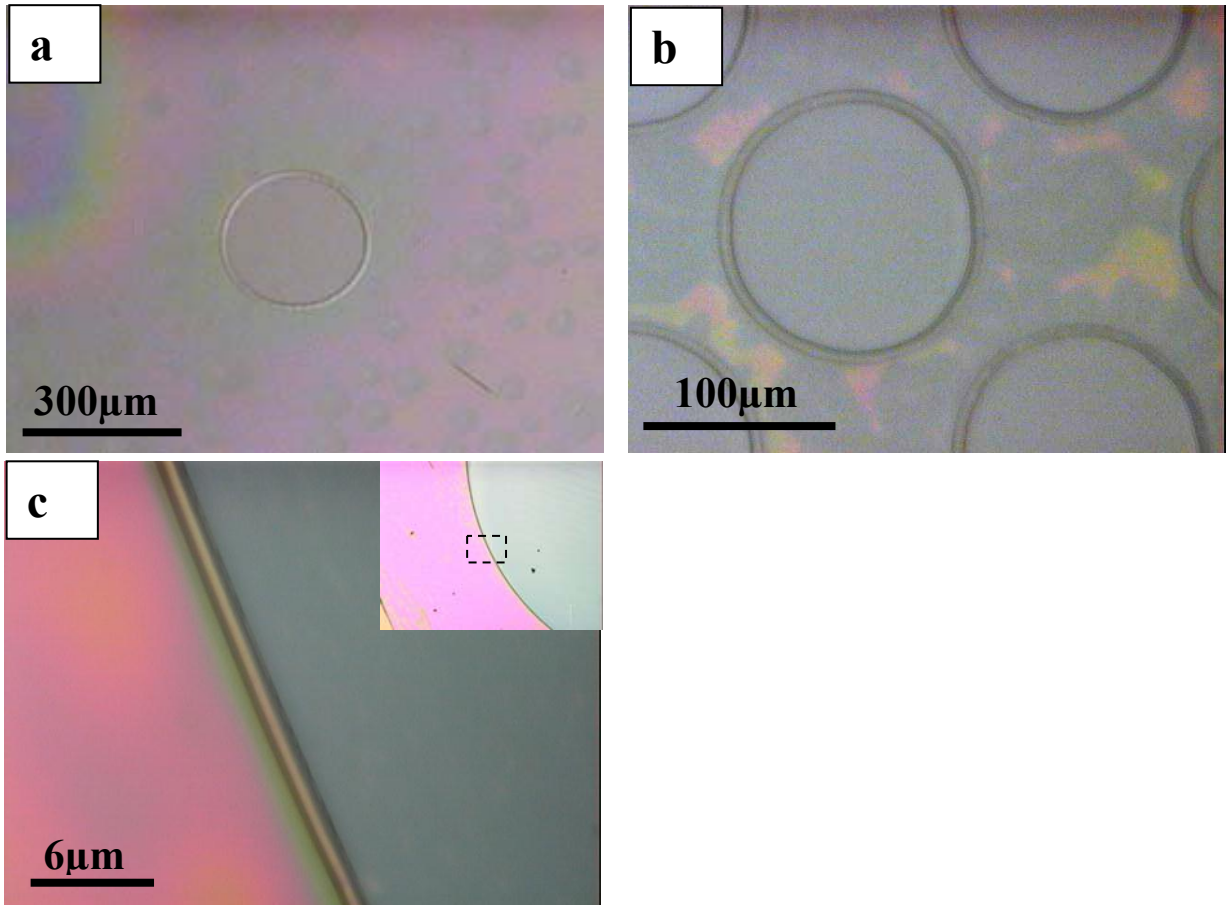


*Figure 5.3: Optical micrographs of polymer micro-toroids produced by rolling-up of the bilayers from circular openings. (a) A single microtoroid tube in dry state (b) An array of microtoroids (c) Surface of microtoroid.*

Photolithography permits to fabricate large arrays of toroids (Figure 5.3 b, 5.4 c). If the distance between the neighbouring LWs is small, the toroids can touch each other, forming characteristic twin-tube junctions [Figure 5.4 d]. In order to avoid the distortion of the toroid's shape by further rolling, the process can be stopped by removing the sample out of the solution and washing it in pure water. This operation can be done with high accuracy, because rolling proceeds sufficiently slow (typically, a few micrometers per minute).

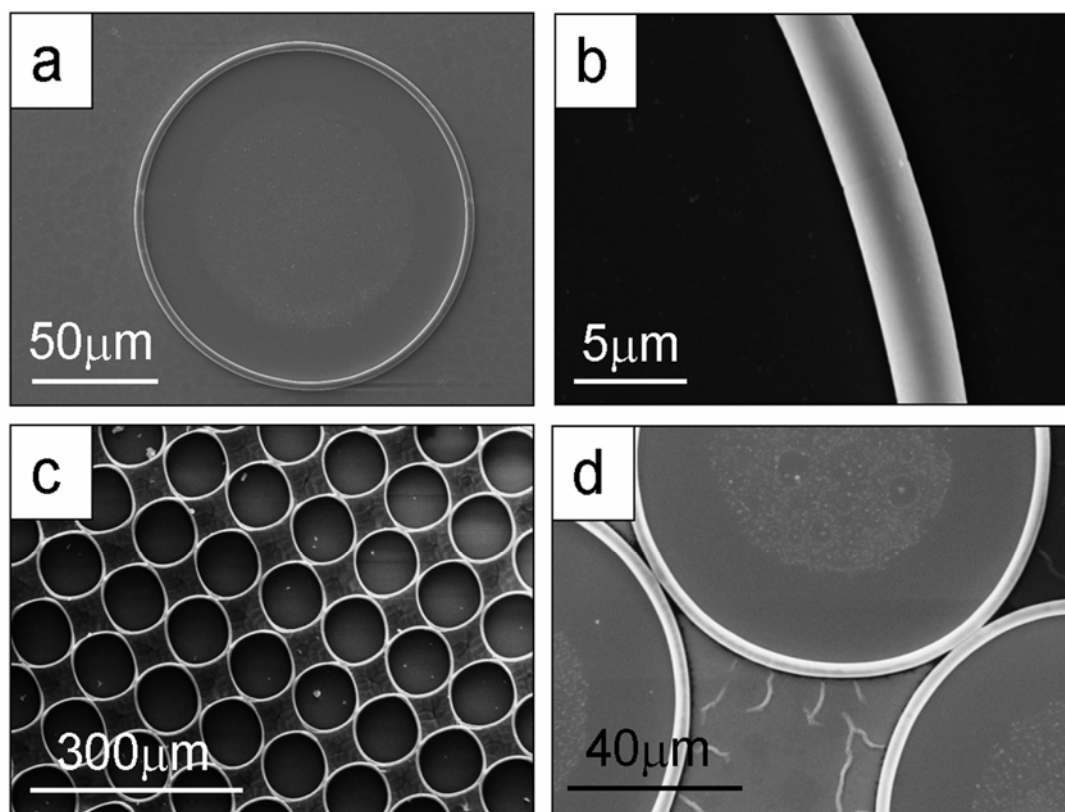


**Figure 5.4:** SEM micrographs of toroidal tubes a), a single micro-toroid. b) Magnified view of the wall of toroid. c), d) an array of micro-toroids.

#### 5.4 Kinetics of toroids formation

As pointed above, the rolling of the toroidal tubes cannot proceed unlimitedly. The increasing radius of the toroid causes lateral strain in the film, such that the strain isolines are closed concentric circles centered at the middle of the LW. To investigate the kinetics of the toroid formation, we prepared a set of concentric LWs in the bilayer film by mechanical scratching and video-recorded the film rolling.

Figure 5.5 a shows the width of the rolled-up layer  $L = R - R_0$  (notations are demonstrated in Figure 5.1) as the function of time for different LW radii. The rolling rate does not depend on the LW radius and amounts, for the given experimental conditions,  $dL/dt \approx 5.3 \mu\text{m}\cdot\text{min}^{-1}$ . Apparently, it is the rate of swelling of the P4VP film that determines the tempo

of toroid formation until the counter-forces originating in the lateral strain come into play. Rolling slows down when the width of the rolled part approaches a saturation value  $L_e$  that depends on the radius of LW (Figure 5.5 b). Larger radius of LW results in broader rolled-up stripe of the bilayer, since the effect of the curvature on the tube formation is smaller for wider LWs. This intuitive explanation of the experimental result is supported in the next section by a simple analytical model of the micro-toroid formation.

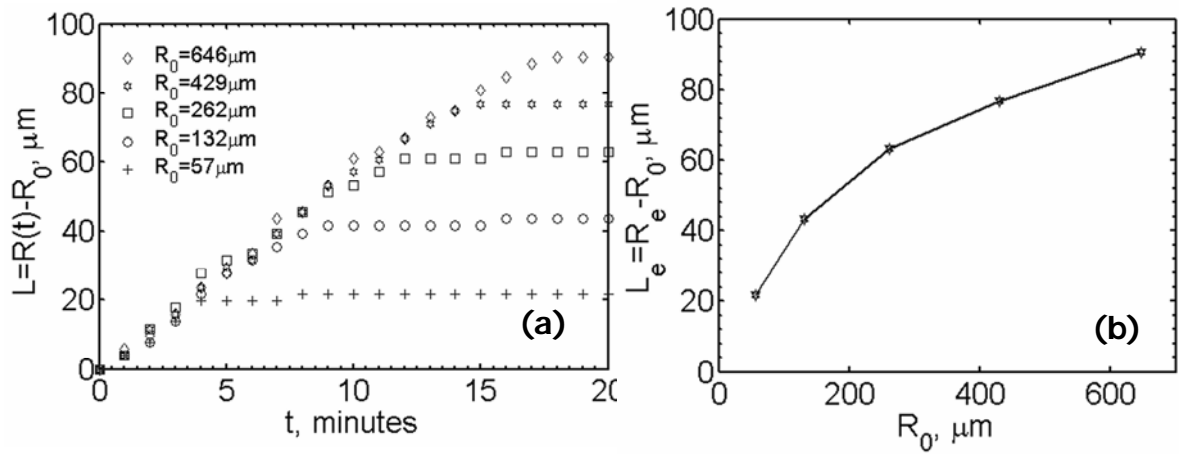


**Figure 5.5.** Characterization of the micro-toroid formation. (a) The width of the rolled-up part of the bilayer as the function of time, for different radii of the lithographic window. (b) The equilibrium width of the rolled-up part of the bilayer, as the function of the LW radius.

### 5.5 Model of the micro-toroid formation

The process of micro-toroid formation can be understood on the qualitative level by considering the following simple model. Since the thickness of the film is much smaller than its radius of curvature, one can regard the film as a 2D-surface with the spontaneous curvature radius  $\rho$ . The contribution of the elastic energy to the system's free energy can be written as [Fed06]:

$$F = \int \left[ \frac{1}{2} \kappa \left( \frac{1}{r_1} + \frac{1}{r_2} - \frac{2}{\rho} \right)^2 + \bar{\kappa} \left( \frac{1}{r_1 r_2} \right) \right] dA + \frac{1}{2} \int u_{\alpha\beta} \sigma_{\alpha\beta} dA \quad (5.1)$$

Here  $\kappa$  and  $\bar{\kappa}$  are the mean and the Gaussian curvature elastic constants, respectively,  $u_{\alpha\beta}$  and  $\sigma_{\alpha\beta}$  are the two-dimensional deformation and stress tensors, calculated in appropriate curvilinear coordinates [Hel73, Lan86]. Here we assume that bending and stretching contributions to free energy of a thin bilayer film are decoupled. The integrals are taken over the whole surface of the film. The equilibrium form and dimensions of the tube released from the substrate can be found in principle by variation of the free energy function eq. 5.1. This problem is out of scope of our present study. However, the model became easily tractable if we consider toroids originating from the LWs of large radii. In this case, it is reasonable to assume that  $\rho \ll L$ , i.e. the width of the rolled part of the film is much larger than the radius of the tube, because at the beginning of rolling the effect of the LW boundary curvature is small. Also, we suppose that the width of the rolled-up stripe of the bilayer is small compared to the radius of the LW,  $L \ll R_0$ . This condition is fulfilled if the stretching stiffness of the film is sufficiently large. Finally, for the thin looped tube one can always assume  $r_2^{-1} \ll r_1^{-1} \approx \rho^{-1}$ , i.e. the maximal curvature of any element of the tube's surface is much larger than the minimal curvature, which is approximately equal to the spontaneous curvature. Let  $Y$  be the effective Young modulus\* of the double layer film. (\*The effective Young modulus for the in-plane stretching of a bilayer film can be obtained by the rule of mixture,  $Y = (h_1 Y_1 + h_2 Y_2) / (h_1 + h_2)$ , where  $h_i$   $Y_i$  are the thickness and Young modulus of the  $i$ -th layer). Then, the difference of the free energy of the film in the rolled and the unrolled states can be easily integrated (see Appendix A1) and reads, in the dimensionless units  $\Delta\tilde{F} = \Delta F / (\pi Y R_0^2)$ ,  $x = L / R_0 \ll 1$  as:

$$\Delta\tilde{F}(x) = -A \cdot [x^2 + 2x] + (1+x)^2 \ln(1+x) - x - \frac{3}{2}x^2 \approx -A \cdot [x^2 + 2x] + \frac{x^3}{3} \quad (5.2)$$

where  $A = 3\kappa / (2\rho^2 Y)$ . The function  $\tilde{F}(x)$  has the minimum at  $x_e = A + \sqrt{A^2 + 2A}$  (Figure 5.6). Self-consistency of the condition  $x \ll 1$  requires that  $A \ll 1$ , and, up to the leading term,

the position of the minimum is  $x_e \approx \sqrt{2A}$ . Thus, the equilibrium number of shells of the toroidal tube is:

$$n_e = L_e / (2\pi\rho) = x_e R_0 / (2\pi\rho) = \frac{R_0}{2\pi\rho^2} \sqrt{\frac{3\kappa}{Y}} \quad (5.3)$$

In this study, we do not make direct comparison of our model with experiment, since the mechanical properties of the P4VP films forming supramolecular complexes with DBSA are unknown. Nevertheless, the model qualitatively explains the following facts about the toroidal tube formation: a) rolling stops after reaching a certain width of the rolled-up part of the bilayer (apparently, this equilibrium width corresponds to the minimum of the free energy), and b) the equilibrium width of the rolled-up film is larger for the circular LWs of larger radii, in accordance with the experiment [Figure 5.5 b].

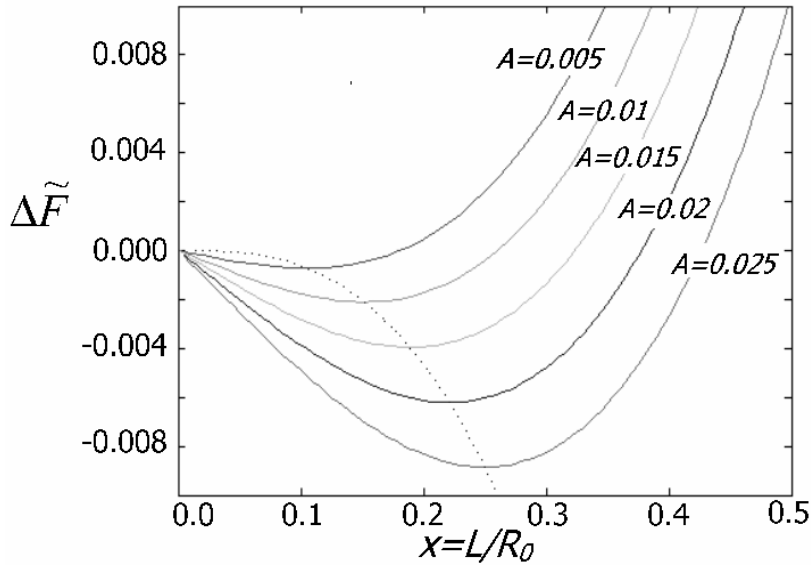


**Figure 5.6:** Free energy of the micro-toroid as the function of the width of the rolled-up layer, for different values of the parameter  $A$ . (in dimensionless units). The dotted line indicates the position of the function minimum.

However, the proportionality of  $L_e$  and  $R_0$  is not linear, as suggested by the formula (eq. 5.3). This is an indication that a more detailed theory needs to be developed. Finally, the

model supports the intuitive expectation that the number of the shells (or, equivalently, the width of the rolled-up bilayer) is larger for the films with higher values of the bending modulus (hence, providing larger energy gain via scrolling) and smaller stiffness of the in-plane stretching (that is, causing less constraint to rolling as the diameter of the toroid increases). This tendency is illustrated in Figure 5.6 by plotting several free energy graphs for increasing values of the parameter  $A$ .

## **5.6 Discussion**

The strong confinement of electromagnetic energy in microtoroids or cavities can result in functional microphotonic integrated circuits [Arm03]. Accordingly, microtoroids find applications in strong-coupling cavity quantum electrodynamics (QED), enhancement and suppression of spontaneous emission, novel sources, and dynamic filters in optical communication [Vah03]. In the past very high discrete silica microsphere resonators have been demonstrated [Wol00] with their applications in lasers and channel filters [Cai00a, Cai00b]. A combination of lithography, dry etching and a selective reflow process was used for producing silica toroid-shaped microresonators-on-a-chip [Arm03]. Recently optical microcavities were fabricated from semiconductor microtubes using a bottle-like geometry [Str08] and it has been demonstrated that the axial modes in microtubes can be controlled precisely by the preparation of specially shaped lobes in their rolling edge. These lobes turn the microtubes into bottle resonators.

Apart from semiconductor resonators, polymers are also promising materials for microresonators because of the wide range of indexes of refraction available and they can be patterned by photo processing [Rab02]. Due to the inherent mechanical flexibility of many polymers the tuning of polymer microcavities can be achieved simply by stretching the cavity [Li06]. Previously, a molding technique was used to fabricate resonators from polymers that



have either thermal or UV curing mechanisms [Arm07]. However, the main disadvantage of the fabrication process is that it requires silica toroids as a template. In the present work, we demonstrate a simple and novel method to fabricate the polymer microtoroids using a photomask. Furthermore, the microtoroids with metallized inner surface can also be fabricated using this approach and metallized toroids are known to function as IR waveguides [Har00].

## **5.7 Conclusions**

We have introduced fabrication of hollow-core toroidal micro-cavities by the self-rolling of strained polymer bilayer films. Rolling of the bilayer is due to preferential swelling of P4VP in aqueous solution of DBSA. A few micrometer wide tubes are looped in the few dozens wide toroids. The formation of the toroids is self-constrained: their equilibrium width is determined by the balance of the free energy gain due to relaxation of the bending moment and the work of the film stretching. Micro-toroid formation by the self-rolling of polymer bilayers is possible due to relatively high stretchability of polymers. The principal features of the micro-toroid formation process are captured by a simple analytical model. Our analytical model qualitatively correctly predicts the existence of the equilibrium size of the micro-toroids. However, a more detailed theory should be elaborated. In particular, coupling of bending and stretching should be taken into account while calculating the free energy of the rolling bilayer. The necessity of such a coupling in the multi-layer films is obvious from the fact that stretching the film in one direction will produce bending of the film in the orthogonal plane, as soon as the Poisson ratios of the materials of the layers differ. Also, the nonlinear stress-strain relation for the polymer film should be taken into account.

Hollow-core toroidal micro-cavities produced by self-rolling approach can be interesting for a number of advanced applications. In a few preliminary experiments, we modified the hidden walls of the tubes by magnetron sputtering of gold on the surface of the polymer film,

prior to film rolling. The circular LWs were made by mechanical scratching. Upon rolling, the micro-toroids with metallized inner surface were obtained. On the other hand, the hollow-core micro-capillaries with metallized inner surface are known to function as waveguides for IR-radiation [Har00]. Thus, the toroidal rolled-up cavities with the metallized inner walls may be interesting for the development of micro-resonators for the IR frequency diapason. Another possible field of application of the self-rolled micro-toroids is encapsulation of micro-particles of different nature (quantum dots, living cells etc). During rolling, the particles can be captured from the surrounding solution and enclosed in the toroidal geometry. This may provide new opportunities for the studies of self-assembly phenomena in confined space [Yin01].

## *Chapter 6*

## **6. Fabrication of Metallic/Bimetallic Microtubes**

### **6.1 Introduction**

Nano and microtubes have large number of potential applications in microelectronics, cell analysis, microfluidic, waveguides, chemical and biochemical sensors [Poo90, Thu06, Teg04, Tak08, Kip06, Spa07]. Metallic microtubes are promising for a number of advanced applications, for instance waveguiding of far- and mid-infrared radiation and chemical sensing [Har00], due to their electronic properties, such as high electrical and thermal conductivity, optical reflectivity, good mechanical properties, high resistance to oxidation and good magnetic properties. These advantages of metals also make them of choice in telecommunication, information technology and safety critical applications. Gold with mesoscopic channels broaden the application fields to medicinal and drug delivery because of the excellent biocompatibility, resistance to corrosion and malleability.

In this chapter we explore the application of the self-rolling approach to the formation of metallic microtubes with high aspect ratio. Here, we describe the combination of the self-rolling approach with pyrolysis of the polymer component after the tube formation. As the result, we obtain pure free-standing metallic or multi-metallic tubes. The polymer plays therefore an auxiliary role in this fabrication scheme, and is removed from the final product. The main advantage of the approach we see is the possibility of the tube formation from apparently any single metal or multi-metal films, even those that have no propensity to self-roll by themselves. Moreover, the approach enables, in principle, the fabrication of arbitrary metallic patterns on the tube's inner walls, by means of photolithography [Luc07]. This approach can be used for producing complex free-standing 3D micro-objects via release of patterns from the polymer support by pyrolysis.

## 6.2 Experimental

The bilayer of PS (50 nm) and P4VP (70 nm) was deposited on the cleaned silicon wafer from toluene and chloroform solution respectively. Dip coater was used for the deposition of bilayer. The bilayer was crosslinked by UV radiation using a UV lamp (G8T5, TecWest Inc., USA) with a 2.5W output at 254 nm. A thin film of gold or titanium was deposited on the crosslinked bilayer using direct current (DC) sputtering at pressure of  $2.6 \times 10^{-2}$  mbar and an operating voltage of -440V. The scratches were made by a sharp blade. Sample with microstructures was immersed in aqueous solution of 4 wt% DBSA. The samples were pyrolyzed at 500 °C for 3 h in oven to remove the polymers. The characterization of sample was done by optical microscopy, SEM, IR, XPS and EDX.

## 6.3 Results and Discussions

The two step method involves the use of self-rolled polymer bilayers as the template where inner walls are metallized with desired metals and then the polymer template is removed by pyrolysis. In this study we constrain ourselves to gold (Au), Titanium (Ti) and Au/Ti bimetallic tubes fabrication, although in principle any metals, sufficiently stable at ambient conditions, can be used. Figure 6.1 illustrates schematically the fabrication procedure.

A bilayer of PS and P4VP, with P4VP as the bottom layer, is deposited on the silicon wafer by dip-coating. Subsequently, a desired metal or combination of metals is deposited by physical vapour deposition on top of the bilayer. Although the fabrication of the tubes without the intermediate PS layer is also possible, we have found that inclusion of this layer in the fabrication scheme improves essentially the uniformity of the tube's shape. The obtained multilayer of polymer and metal is then micro-structured via straight scratches made by a sharp razor blade. This opens access to the dodecylbenzenesulfonic acid (DBSA) to the bottom layer of the multilayer film. Supramolecular binding of DBSA and pyridine rings [Ikk95] caused

swelling of the P4VP induces the in-layer strain in the film, is relaxed by rolling, which starts at the scratches. Note that upper layers (PS and/or metal ones) protect the P4VP layer from uncontrollable swelling apart of the front of rolling. The microtube thus formed has inner wall made of metal whereas the outer wall is that of polymer. The rate of rolling was found to be quite slow (few  $\mu\text{m}/\text{min}$ ) and can be easily controlled by acid concentration and the UV irradiation doze. Hence, it was possible to stop the rolling process when a desired number of rolls are achieved. Finally, the tube was pyrolysed at  $500\text{ }^\circ\text{C}$  for 3 h in oven in order to remove the entire polymer and thus the tube left was all made of the deposited metal.

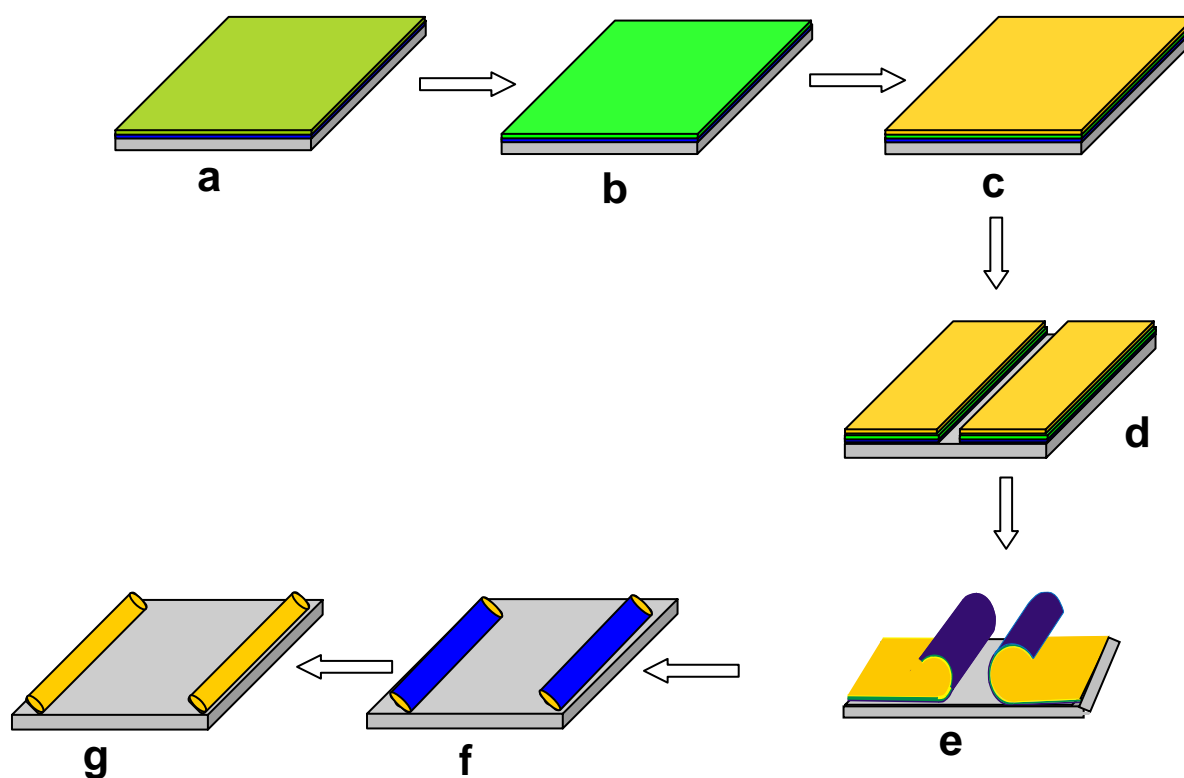


**Figure 6.1:** Schematic presentation of gold tube formation by self rolling approach, (a) deposition of P4VP/PS polymer bilayer, (b) crosslinking of bilayer by UV radiation, (c) deposition of thin layer of metal (nm) by magnetron sputtering, (d) mechanical structuring of layers by a sharp object, (e) rolling of layers in DBSA solution, (f) PS/P4VP tube with enrolled metal, (g) metal tubes after removal of polymer by pyrolysis at  $500\text{ }^\circ\text{C}$ .

We first fabricated purely polymeric self-rolled PS/P4VP microtubes having no metallic layer for the reference ones, to adjust the fabrication parameters, such as the concentration of DBSA, the UV irradiation dose, the thickness of P4VP and PS layers [Detail is given in Chapter 4]. An optical micrograph of polymer tube is shown in Figure 6.2.

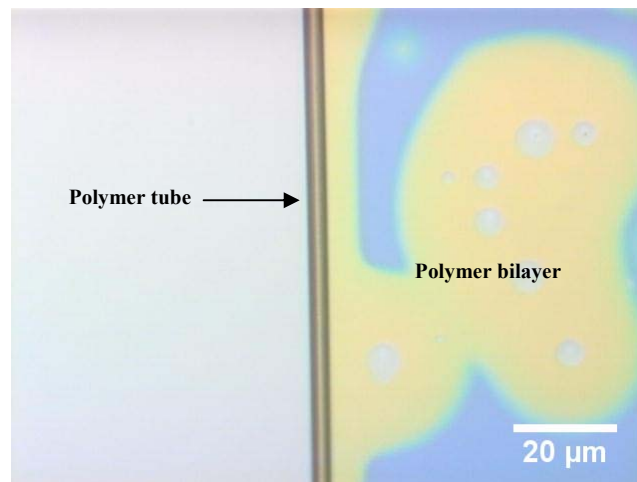


**Figure 6.2:** *Optical micrograph of PS/P4VP tube.*

The optical micrographs of the tubes before and after pyrolysis are presented in Figure 6.3 and Figure 6.4, respectively. It is observed that in most cases, we obtained tubes with perfectly cylindrical shape, although sometimes they had oval cross-section supposedly due to action of the capillary forces during the sample drying. Such shape distortions, which are due to capillary forces during sample drying, were reported also for self-rolled semiconductor tubes [Sel03, Sch02c] and represent a general problem in the field of micro and nanofabrication. Because of relatively high stiffness of the metal films compared to that of the polymer layer (the Young moduli (G) of gold, titanium and polystyrene are  $G_{Au} \sim 78$  GPa,  $G_{Ti} \sim 110$  GPa, and  $G_{PS} \sim 3$  GPa respectively), the diameter of the tubes is very sensitive to the thickness and the type of the metallic layer. Figure 6.3 a shows the P4VP/PS/Au tube, in which the Au layer is 50 nm thick, whereas in the P4VP/PS/Ti tube (Figure 6.3 b) the thickness of the Ti layer is only 10nm. However, under similar condition of rolling, the Au/polymer and Ti/polymer hybrid

tubes have comparable diameters of 12.5 and 8.8  $\mu\text{m}$ , respectively, due to higher stiffness of Ti. Figure 6.3 c shows the P4VP/PS/Ti/Au tube, in which the thickness of the Au/Ti layer is 50 nm, as for the Au in P4VP/PS/Au tube (see Figure 6.3 a). However, the polymer/bimetal tube has significantly larger diameter ( $\sim 37\mu\text{m}$ ), because the more stiff titanium constitutes 80% of the bimetal film thickness (appr. 40nm).

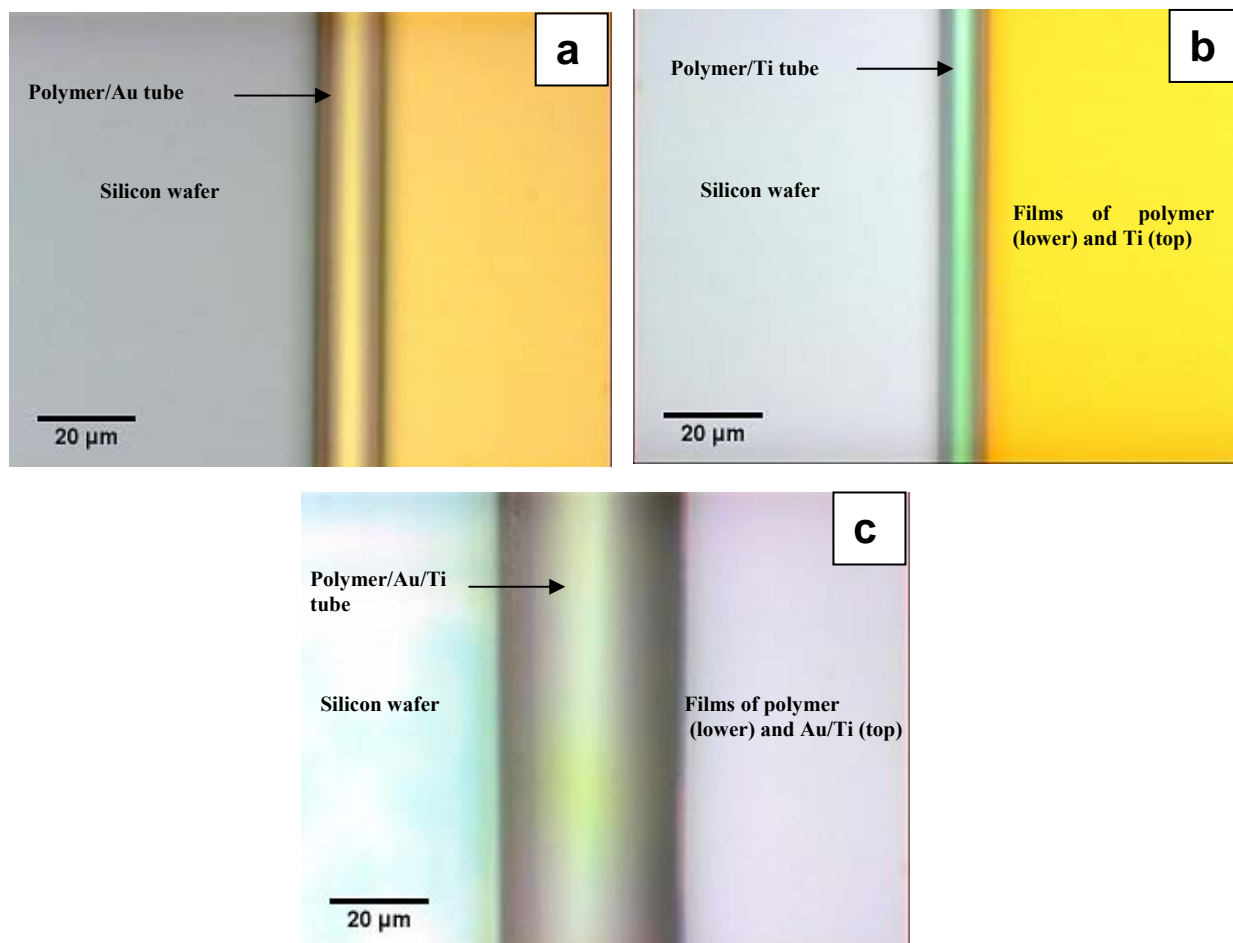


**Figure 6.3:** Optical micrographs of gold and titanium tubes before pyrolysis. (a) Au tube (thickness of film was 50nm) (b) Ti tube (thickness of film was 10nm) (c) Ti/Au tube (thickness of layer was 40/10 nm). In all the figures shown the tube rolled in the direction from left to right before the sample was removed from the DBSA solution and dried.

The metal microtubes released by pyrolysis from the hybrid tubes are shown in Figure 6.4. The cylindrical shape of the tube was found to remain intact. However, since the polymer



component was mostly removed, some shrinkage of the tube diameter was observed. Thus, the hybrid polymer/Au, polymer/Ti and polymer/Au/Ti microtubes discussed above shrink after pyrolysis to diameters 10.2, 8.1 and 28.8 $\mu\text{m}$  respectively.

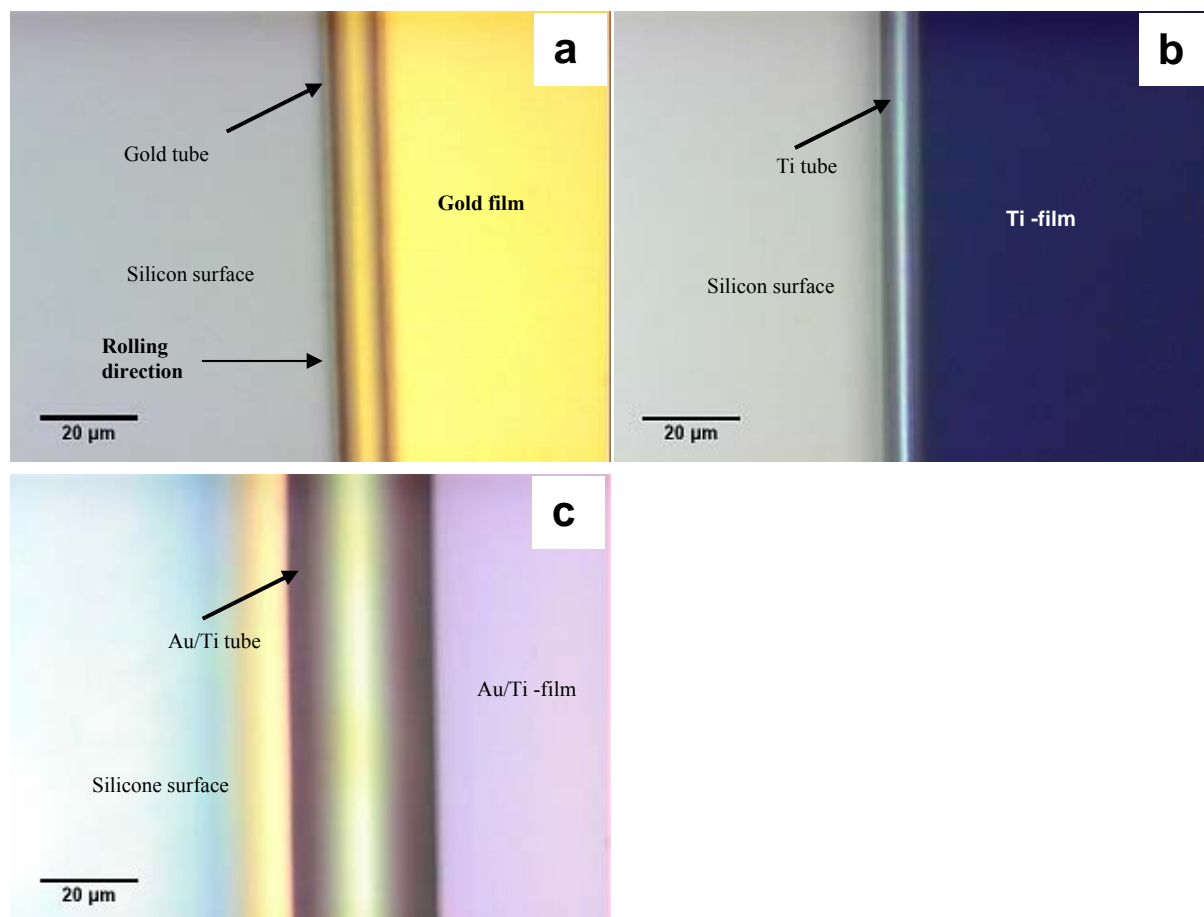
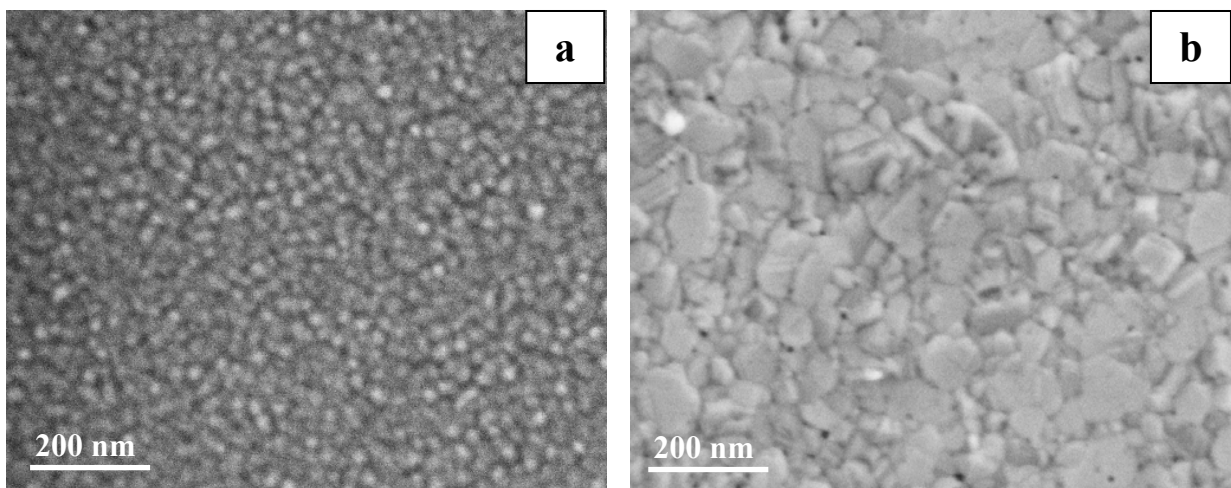


**Figure 6.4:** Optical micrographs of gold and titanium tubes after pyrolysis (a) Au tube (thickness of film was 50nm) (b) Ti tube (thickness of film was 10nm) (c) Ti/Au tube (thickness of layer was 40/10).

The shrinking of the tube diameter could be explained considering the effect of pyrolysis on gold layer structure and on the strain relaxation in the film. In the sputtering process, gold is deposited in form of nanoclusters. On the other hand, it is known that the melting point of nanoclusters is strongly depressed in comparison to the bulk material. According to the data of Buffet and Borel [Buf76] the melting point of 3 - 4 nm wide Au particles falls below 500°C.

This melting of particles, which make part of a strained gold layer, may lead to complete or partial relaxation of mechanical strain, which arises in the gold layer during rolling.

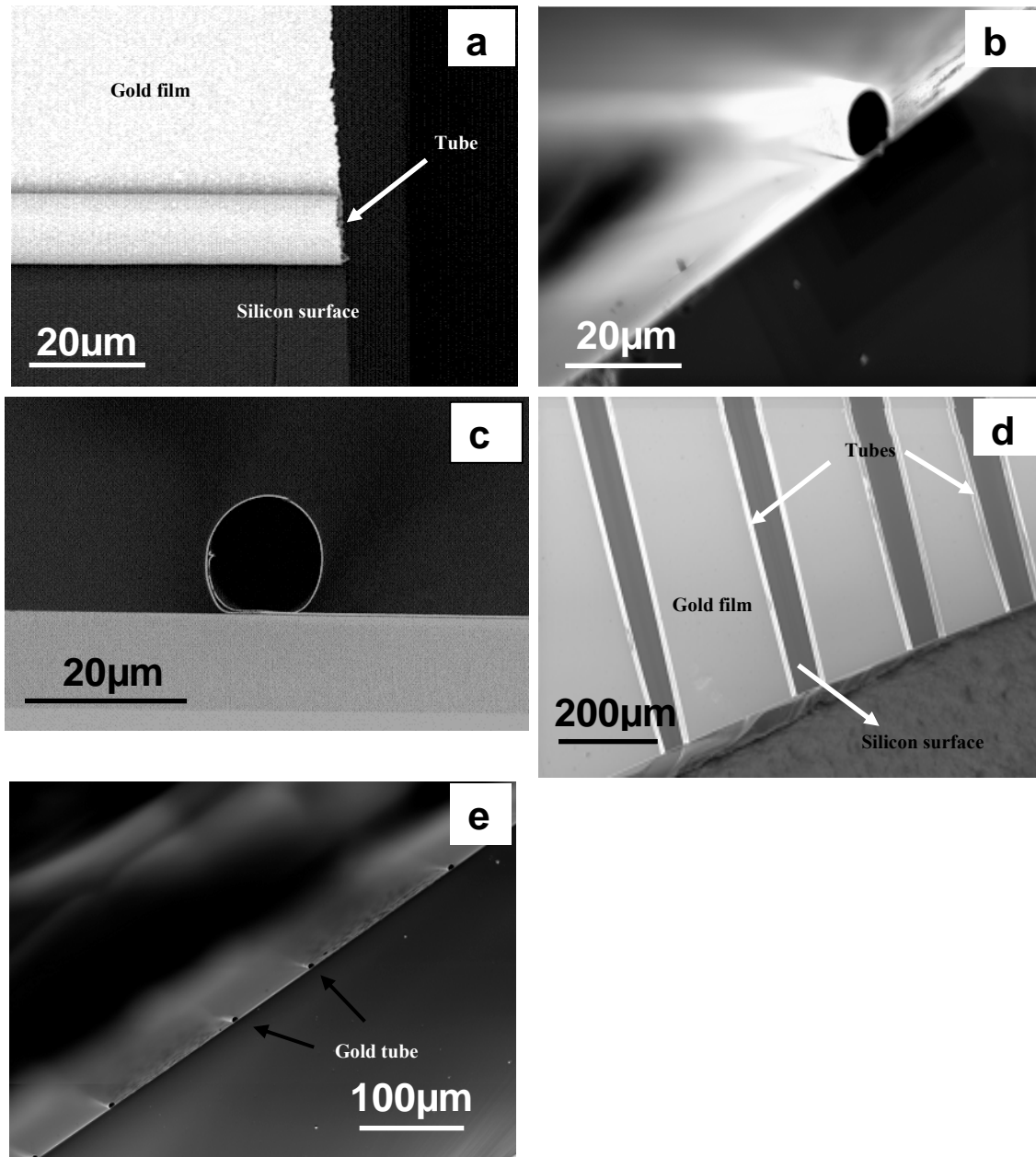
The change of the gold layer structure upon annealing is evident from the SEM micrographs, which represent the surface of the Au layer before (Figure 6.5a) and after (Figure 6.5b) heating at 500°C for 3 hours. One can say that nanocluster form of gold was transformed into polycrystalline structure. It is very likely that any macroscopic mechanical strain in the film is relaxed upon such a profound structure transformation. Shrinking of the tube's diameter upon pyrolysis may be also due to melting of gold nanoclusters and recrystallization. In this process the gaps between the clusters are filled, and the material became more dense, that might lead to diminishing of the layer dimensions. Hence, melting of gold nanoclusters and recrystallization might lead to densification of the material and it's shrinking in all directions, thus leading to decrease of the tube's diameters.



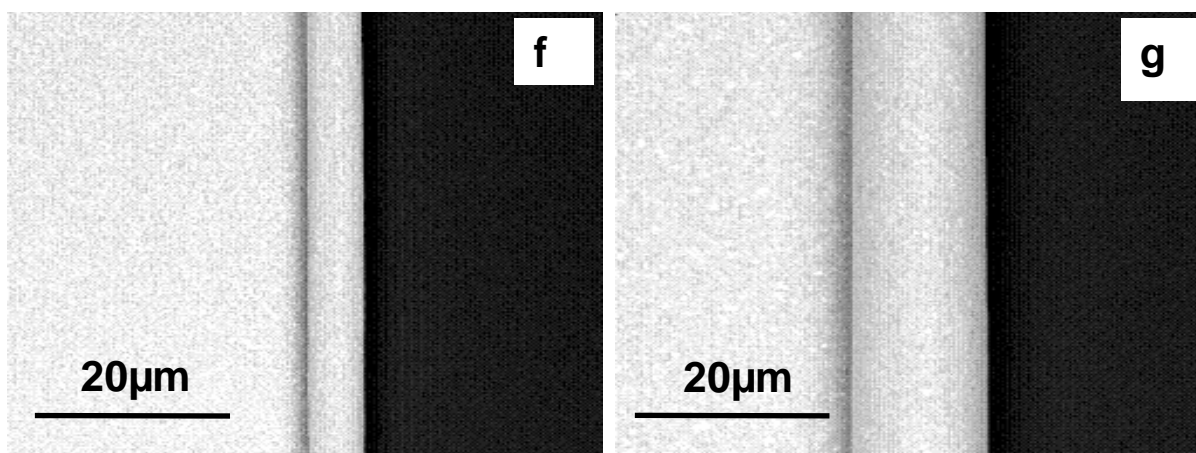
**Figure 6.5.** SEM micrograph of gold 20 nm thick layer, created by magnetron sputtering, before (a) and after (b) thermal annealing at 500°C for 3 hours.

Figure 6.6 (a, b, c) shows SEM micrographs of a single Au tube. As proven by the side-view of the tube opening (Figure 6.6 b, c) pyrolysis conserves almost perfect cylindrical tube's shape. Not only single tubes, but also arrays of tubes can be fabricated on the same substrate

(Figure 6.6 d, e). Tube length was only limited by substrate dimensions (2 - 3 cm). As discussed above, the tube diameter can be tailored by varying the thickness of the metal layer. Figure 6.6 f, g shows SEM image of gold tube obtained from 20 and 50 nm thick gold films on polymer bilayer respectively.



**Figure 6.6 (a - e):** SEM micrographs of gold tubes (a) Image with rolled part and unrolled part. The rolling direction of the tube was from bottom to top in the SEM image; (b) and (c) Clearly visible open end of tube; (d) Arrays of gold tubes (top view); (e) Arrays of gold tubes; side view; show open end of tubes.



**Figure 6.6 (f - g):** (f) Gold tube formed from 20 nm layer thickness; (g) Gold tube formed from 50 nm gold layer thickness.

The Ti tube and bimetallic tubes were also synthesized using the same approach. SEM micro-graphs of Ti and Au/Ti bimetallic tubes are shown on Figure 6.7 a and b, respectively.

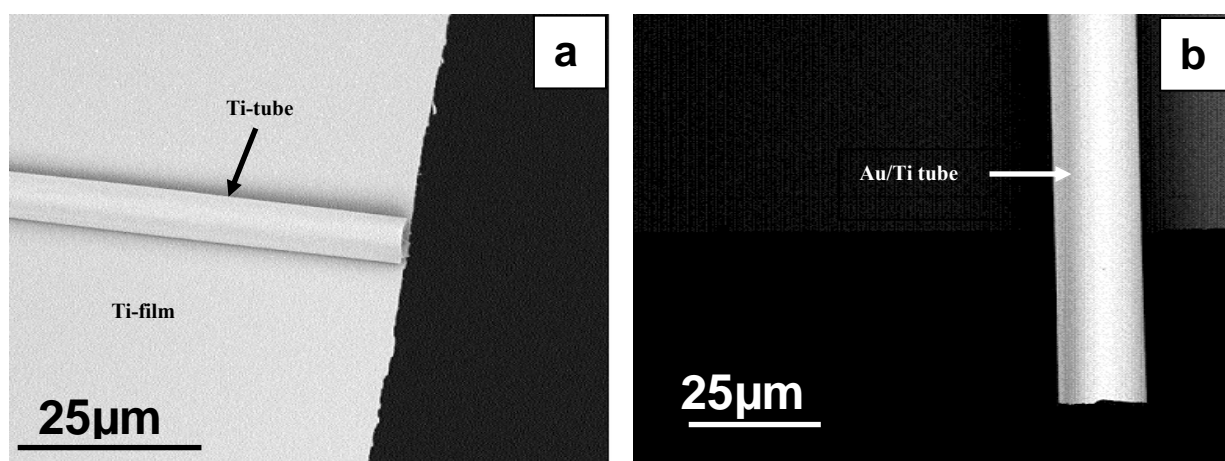


**Figure 6.7:** SEM images of metal tube (a) titanium tubes (b) Bimetallic (Au/Ti) tube.

FTIR was used to monitor the polymer removal process during pyrolysis. Figure 6.8 shows the FTIR spectrum of microtube before and after pyrolysis. For reference, FTIR spectrum of a simple PS/P4VP polymer tube is also shown. The FTIR spectra were obtained in transmission mode for samples on silicon wafer. FTIR spectra of samples before pyrolysis show the characteristic peaks of aromatic C-C out of plane bending at  $700\text{ cm}^{-1}$ , C-H bending vibration at  $833\text{ cm}^{-1}$ , aromatic C-C stretch at  $1493\text{ cm}^{-1}$ , and aromatic overtone band at  $1640$

$\text{cm}^{-1}$  and  $1719 \text{ cm}^{-1}$ . The stretching band of  $\text{CH}_2$  group at  $2856 \text{ cm}^{-1}$ ,  $2927 \text{ cm}^{-1}$ , and  $3083 \text{ cm}^{-1}$  were also clearly seen in the spectra of tube before pyrolysis. After pyrolysis at  $500 \text{ }^\circ\text{C}$ , as expected, the organic moiety was removed and only silica fingerprint region at  $1100 \text{ cm}^{-1}$  is observed which comes from the silicon wafer. Hence, it was concluded that the entire polymer was burned during pyrolysis and only metal remains at this stage.

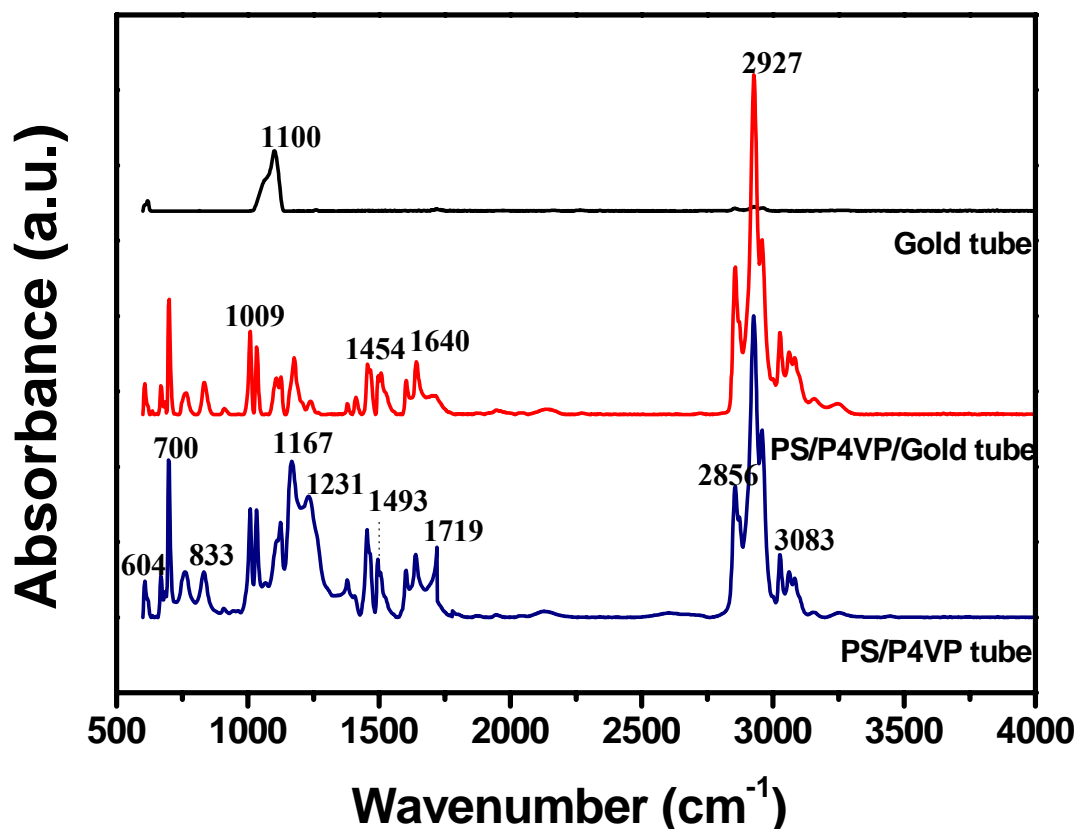


**Figure 6.8:** FTIR spectrum of PS/P4VP tube, Polymer with inner gold layer and tube after pyrolysis (only gold remains).

The metallic tubes were further characterized using X-ray photoelectron spectroscopy (XPS). Figure 6.9 shows the XPS spectra of polymer tube, polymer/gold hybrid tube and gold tube obtained after pyrolysis. It could be clearly observed that characteristic peak of polymer vanished after the pyrolysis. The characteristic signals of gold (Au  $4d_{3/2}$  and  $4d_{5/2}$ ) could be clearly observed in the XPS spectra.

The XPS analysis of Au/Ti bimetallic tube was more complex because the limited penetration depth of X-rays renders it difficult to get information about both Au and Ti in the tube. Hence, EDX was used in this case. EDX was performed on the 50 x 50  $\mu\text{m}^2$  area which comprised of both tube as well as unrolled film area.

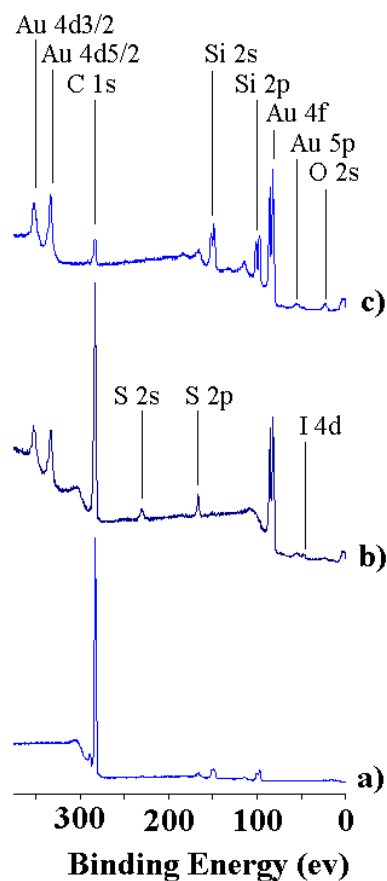


**Figure 6.9:** XPS wide-scan spectra of (a) PS/P4VP, (b) PS/P4VP/gold (c) only gold

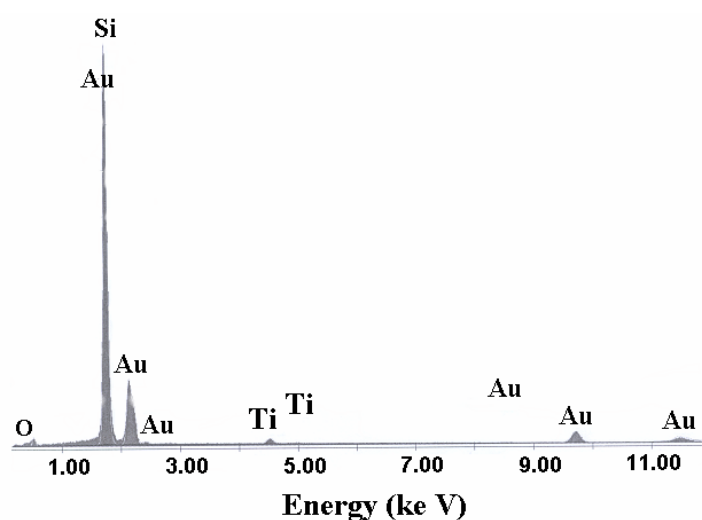


**Figure 6.10:** Energy-dispersive X-ray (EDX) spectra of Au/Ti tube.

The EDX spectra of Au/Ti tube after pyrolysis (Figure 6.10) revealed the presence of Si, Au and Ti peaks with atomic ratios 88.89: 9.39: 1.72 respectively. It was concluded from the EDX spectrum that the polymer was removed from the tube and finally Au/Ti bimetallic tube was obtained. In the EDX spectrum of tube, three peaks of gold  $M_{\alpha}$  and  $M_{\beta}$  at 2.1 keV,  $L_{\alpha}$  at 9.7 keV and  $L_{\beta}$  at 11.4 keV while two Ti peaks,  $K_{\alpha}$  at 4.5 keV and  $K_{\beta}$  at 4.9 were observed. Silicon peak was also present at 1.7 keV which was a contribution from the silicon wafer. Beside the Si peak, a small peak of oxygen was also obtained at 0.452 keV which could be due to limited oxidation of Ti and Si during the pyrolysis process.

#### **6.4 Kinetics of tube formation**

One of the interesting aspects of the self-rolling fabrication process is the possibility to control easily the tube dimensions. As discussed above, the diameter of the tubes can be preset by varying the thickness of the deposited metal film, whereas the thickness of the tube's walls (or, equivalently, the number of rolls) can be tailored by stopping the rolling at some stage simply by removing the sample from DBSA solution. Hence, it is essential to know the rate of rolling for the films with different thickness of the metal layer. Detailed investigation of polymer tube formation was reported in Chapter 4 [Kum08]. In the present work, we undertake a detailed study on rate of rolling as thickness of gold layer was varied.

Figure 6.11 shows the dependence of the rate of rolling on the gold layer thickness, for the polymer bilayer thickness kept constant. Rolling rate was found to decrease drastically as the Au layer thickness increased above 20 nm. Such a variation in rate of rolling might be related to slower relaxation of the internal stresses via plastic deformation of the gold layer.

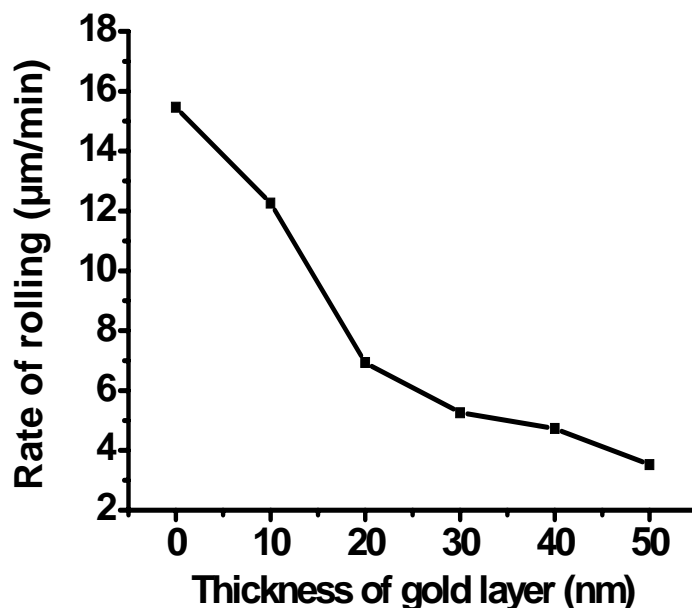


*Figure 6.11: Plot depicting rates of rolling vs thickness of gold layer*

Similarly, the diameter of tube was found to increase with the thickness in gold layer as shown in Figure 6.12. Such a variation in rate of rolling and tube diameter was obvious from the fact that the increase in the gold layer thickness made the film stiff which not only resulted in slow rolling but also allowed only small curvatures during the bending process. It must also be noted here that the variation shown in Figure 6.11 and 6.12 is specific for gold. In general, stiffer will be the metallic layer slower will be the rolling process and smaller will be the curvature of the tube.

A complete quantitative analysis of the  $D(h)$  dependence is yet not possible, since it should involve many unknown parameters, such as bending stiffness of both the polymer and the metallic layers, and take into account possible dependence of these parameters on the thicknesses of the layers. We still have not enough data to elucidate these dependencies. Nevertheless, good theoretical fit of the experimental data can be obtained in frames of the following simple model.



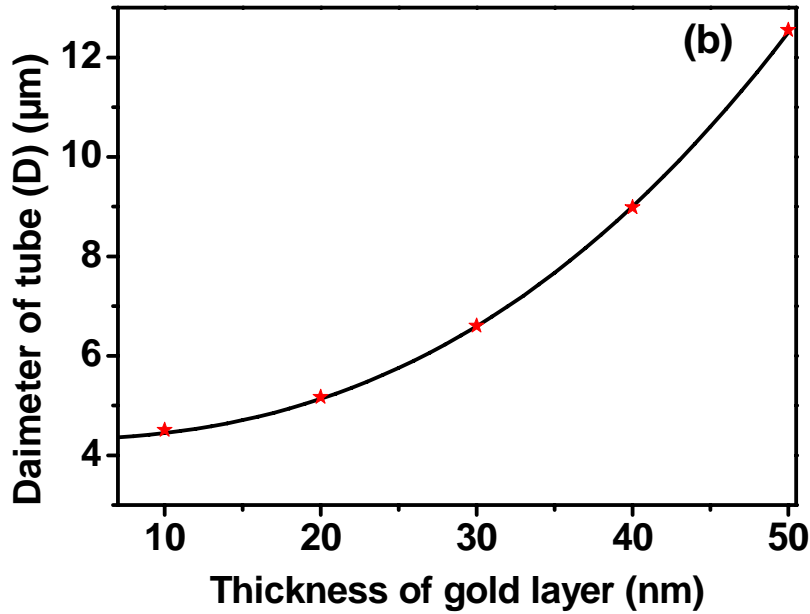


**Figure 6.12:** Plot depicting variation of tube diameter with thickness of gold layer. Solid curve represents the theoretical fit of the experimental data using eq. (4).

According to linear elasticity theory, the bending energy ( $F$ ) of a layer of elastic material, forced to curl to some curvature radius ( $R$ ) can be written as:

$$F = \frac{\kappa}{2} \int \left( \frac{1}{R} - \frac{1}{R_0} \right)^2 dA \quad (1)$$

where  $\kappa$  is the bending rigidity of the layer, and  $R_0$  is the equilibrium curvature, which has the layer in absence of external forces [Lan99]. In our simplified model, we suppose that the equilibrium curvature radius of the gold layer is very large compared to that of the polymer layer, and the corresponding curvature  $C_{0,Au} = 1/R_{0,Au}$  can be neglected. During the rolling process, the bending energy of the polymer  $F_p$  decreases, and that of the gold layer,  $F_{Au}$ , increases. The equilibrium curvature radius can be found from the equality of the absolute values of the two energies. Let  $\kappa_p$  be the bending rigidity of the polymer layer,  $R_{0,p}$  the equilibrium radius of the polymer layer, which it admits after swelling in the DBSA solution. We suppose that the dependence of the bending rigidity  $\kappa_{Au}$  of the gold layer on the thickness

has the form  $\kappa_{Au} = a \cdot h^q$ , where  $a$  and  $q$  are the constants. In the classical elasticity theory,  $a = E/12$ ,  $q = 3$ , where  $E$  is the Young modulus of gold. However, it is known that gold forms nanoscale clusters in course of magnetron sputtering deposition. This may lead to deviation of  $a$  and  $q$  from the values for the bulk material. Equating now the free energies of polymer and gold layers per unit tube length, we obtain:

$$\frac{a \cdot h^q}{R^2} = \kappa_p \left( \frac{1}{R} - \frac{1}{R_{0,p}} \right)^2 \quad (2)$$

Resolving this equation for R gives:

$$R(h) = R_{0,p} \left( 1 + B \cdot h^{q/2} \right) \quad (3)$$

or, for diameters of the tubes,

$$D(h) = D_{0,p} \left( 1 + B \cdot h^{q/2} \right) \quad (4)$$

where  $B = \sqrt{\kappa_p/a}$ . From experiment on rolling the polymer bilayer without the gold layer we know the parameter  $D_{0,p} \approx 4.3 \mu\text{m}$ . Numerical fitting of the free parameters of the model,  $B$  and  $q$ , to experimental data gives the values:  $B \approx 1.1 \cdot 10^{-4}$ ,  $q \approx 4.99$  (note that the thickness is measured in nanometres, the diameter is measured in microns, and the dimensionality of  $B$  is inverse to that of  $h^{q/2}$ ). The experimental data and the fitting curve are shown on Figure 6.12. We have no clear explanation why the parameter  $q$  exceeds almost twice that of the classical theory. Probably, the bending rigidity of a material composed of clusters may increase faster with the thickness of the film, than the rigidity of a monocrystalline material. Special study is needed to elucidate this question.

It should be noted here that there is a possibility to make gold tube without assisted polymer bilayer due to the presence of lateral strain in the gold layer. The presence of lateral strain in the gold layer was confirmed by control experiment. In control experiment a 20 nm

gold layer was sputtered on a silicon wafer with 150nm thick layer of SiO<sub>2</sub>, and the metallic layer was released by selective etch of SiO<sub>2</sub> by 1 w.t.% aqueous solution of hydrofluoric acid (HF). Indeed, we observed that in some experiments the metallic layer enrolled in 50μm thick tubes. This proves that there do exist some lateral strain in the metallic layers, created by magnetron vacuum sputtering, as well as in the layers, made by thermal evaporation and described by Mei et al [Mei08].

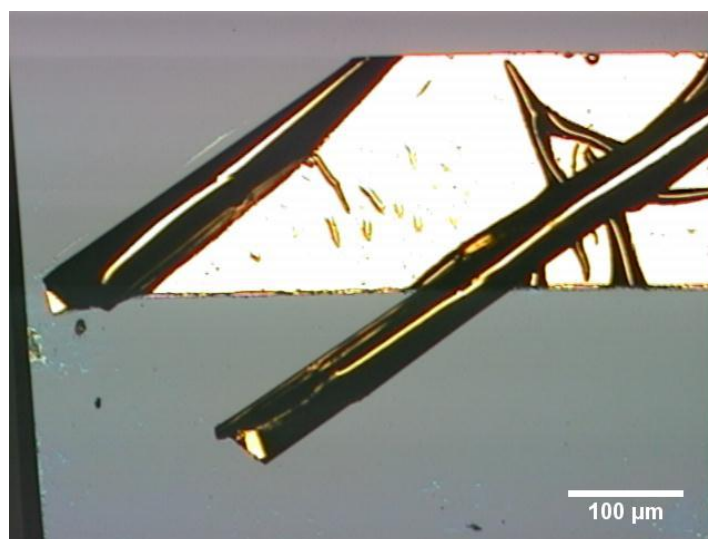


**Figure 6.13:** *Optical micrograph of gold layer rolled up without the assistance of polymer bilayer. The diameter of the tubes is approximately 50μm*

Nevertheless, the use of assisting polymer bilayer for the tube formation has several important advantages:

(a) The strain developed in the polymer due to swelling can be much more considerable than the one in bare metallic layer. This permits to obtain metallic tubes of small diameters with use of relatively thick metallic layers, which by themselves roll up in large tubes. For instance, as shown by Figure 6.6f, a 20nm thick Au layer can be rolled in approximately 5μm thick tube, whereas the same layer, used in the control experiment, rolls in the 50 μm thick tube (Figure 6.13). But, for many applications it might be necessary to have sufficiently thick shells of the

metallic tubes, to provide them better mechanical robustness, electrical and thermal conductivity, etc.

(b) The degree of swelling of the polymer, hence, the strain in it and the diameter of the tubes can be easily controlled by concentration of DBSA in the solution. The strain in the bare metallic tubes, created thermal evaporation or magnetron vacuum sputtering, cannot be controlled so easily.

(c) The use of the polymer bilayer as the assisting layer in the rolling process potentially enables creation of complex 3D metallic patterns, created by photo- or electron lithography on the top of the polymer bilayer [Detail is given in chapter 8]. Such objects as spirals, springs, rings etc. and their dimensions can be easily programmed by the direction of rolling and the dimensions of the template polymer tubes.

The hollow interior and good mechanical properties of metallic tubes may find interesting applications in microfluidic devices. In many practical cases, fluids can be introduced in the tubes simply by capillary forces. To demonstrate this, we used the titanium tube and put a drop of glycerin at the tube opening. Spreading of the liquid inside the tube was tracked by optical microscopy. Figure 6.14 shows the position of glycerine meniscus inside the tube at two different time intervals.

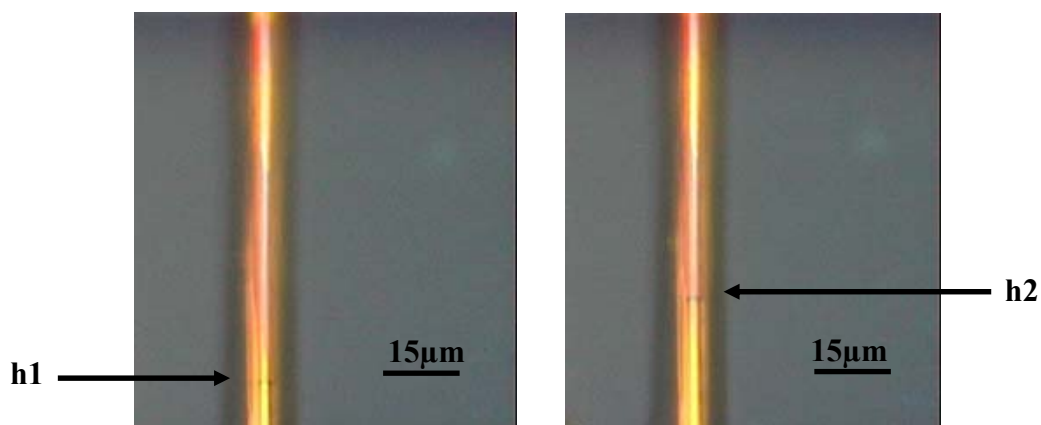


**Figure 6.14:** Flow of glycerin in titanium tube: *h1* and *h2* indicate stage of flow at a particular time

## 6.5 Conclusions

In summary, we have reported a simple and inexpensive two-step method for the synthesis of gold, titanium, and bimetallic microtubes. The metal layer is enrolled as a part of the hybrid polymer/metal tube in the first step and polymer is removed by pyrolysis in the second step. The diameter of tube can be easily tailored by thickness of the metal layer, whereas the thickness of the tube walls can be controlled by the rate and time of the tube's formation. The polymer bilayer plays the role of the support for the metallic layers, and allows to form tubular architectures of arbitrary single-metal or multi-metal thin films, even those which do not form the tubes by themselves. Moreover, the use of rolling polymer support potentially enables fabrication of complex free-standing metallic objects via enrolling of metallic patterns, which can be created by photolithography on the top of the polymer bilayer film. Metallic microtubes fabricated by self-rolling approach may find potential application as waveguides, or elements of microfluidic devices.

## *Chapter 7*

## 7. Fabrication of Silica and Silica/Metal Hybrid Tubes

### 7.1 Introduction

Recently, various architectures of silicon dioxide (silica) has been used in biological, medical and biotechnological applications [Fen07, Bar08, Cor03]. The properties of silica especially high thermal and chemical stability, biocompatibility and high strength lead to many applications. Silicon oxide has attracted more attention as a good photoluminescence material [Jia03]. Mesoscale structures of silicon oxide would be advantageous in nano and microscale electronics, optoelectronics and wave guide applications [Loc04, Sor93, Son07]. Silicon microtubes and microneedles have been successfully inserted through human skin for transdermal drug delivery [Mca99]. Silica tubes selectively transport the enantiomer that specifically binds to the antibody, relative to the enantiomer that has lower affinity for the antibody [Lee02].

In addition to single silica tubes, the hybrid mesostructures (silica-metal) have also attracted much interest in recent years as it combines advantageous properties of different chemical components. Hybrid silica-metal composites have many potential applications in medicine, physics and chemistry. For the catalytic applications, composites of silica with metals such as gold, titanium, platinum, aluminum etc. have been synthesized [Hof06]. Hybrid composite of silica with copper is demonstrated as an antibacterial material [Kim06a]. Hybrid material of  $\alpha$ -Fe<sub>2</sub>O<sub>3</sub>@SiO<sub>2</sub>@Au shows optical properties and supermagnetic characteristics at room temperature [Fan08]. These hybrid composites are also used as catalysts for the conversion of CO to CO<sub>2</sub> [Fan08]. Au@silica@CdSe-QD demonstrates switching between photoluminescence quenching and enhancement according to the silica thickness [Liu06]. Silica-Au hybrid can also be used in targeted bioimaging and therapeutics application due to biocompatibility and easiness of bioconjugation of these composites [Bik07].

A number of methods such as template based method [Li05], laser ablation [Yu98, Cha06], thermal oxidation [Hu03] and chemical vapour deposition [Wu01, Niu04] have been reported as the methods of synthesis of mesoscale silica tubes and wires. In this chapter we introduce a simple, novel and inexpensive robust method to produce silica and silica-metal hybrid tubes using self-rolling of polymer bilayer with polydimethylsiloxane (PDMS). PDMS is a precursor of silica. Pre-ceramic polymers have been widely used to synthesize ceramic film via thermal curing and pyrolysis [Sey90]. PDMS is widely used as a precursor for the silica layer. PDMS is optically clear, cheap and readily film forming polymer widely used as a structural material in microfluidics and bio-microelectromechanical systems. The surface of PDMS can be converted to silicon-oxide by various techniques such as low temperature plasma oxidation [Ala04], UV/ozone treatment [Sch03, Par03] and pyrolytic degradation [Nak05a, Nak05b].

## **7.2 Experimental**

The bilayer of P4VP and PS was deposited on the cleaned silicon wafer from chloroform and toluene solution, respectively. The bilayer was crosslinked by UV radiation emitted by a UV lamp (G8T5, TecWest Inc., USA). The estimated exposure dose was  $2.7 \text{ J/cm}^2$ . A 200 nm thickness of PDMS is deposited from the diethyl ether solution, on the crosslinked PS/P4VP. The dip-coater was used to deposit thin films. The PDMS mixture of base and its curing agent in a ratio 10:1 was degassed in vacuum and dissolved in diethyl ether. The PDMS layer was thermally crosslinked at  $120 \text{ }^\circ\text{C}$  for 2 h. Micro-structuring of the crosslinked layers was done by a sharp blade in order to provide a selective solvent the access to the bottom P4VP layer. The rolling of microstructure sample was done in aqueous solution of 4 wt% dodecylbenzene sulfonic acid (DBSA).

In order to synthesize hybrid tubes of silica and gold, a thin layer of gold (4 - 6 nm) was deposited by physical vapour deposition on crosslinked polymer multilayers. Three different



kinds of hybrid tubes were fabricated: (a) with gold layer deposited on the top of thermally crosslinked PDMS layer, (b) with gold deposited on the top of the PS layer before the PDMS layer deposition, (c) with gold deposited before and after the PDMS layer deposition. The transformation of polymer tube (PS/P4VP/PDMS) to ceramic tube was carried out in a high temperature furnace at 700 °C for 4h in oxygen atmosphere. After pyrolysis, samples were cooled to room temperature. Morphology and chemical composition of the tubes were characterized by optical microscope, EDX, IR, FIB, XPS, and SEM.

### 7.3 Results and discussion

The formation of silica or hybrid tube of silica with metal consists of a two step procedure. In the first step P4VP/PS/PDMS tube was fabricated which then is further subjected to pyrolysis in the second step to remove the polymer moiety. An optical micrograph of self-rolled polymer (P4VP/PS/PDMS) tube is shown in Figure 7.1 a. These samples are pyrolyzed at 700 °C for 4h to entirely burn the polymer moiety from the samples. Figure 7.1 b represents an optical micrograph of a tube obtained by pyrolysis of P4VP/PS/PDMS. Direction of rolling is from left to right in both samples.

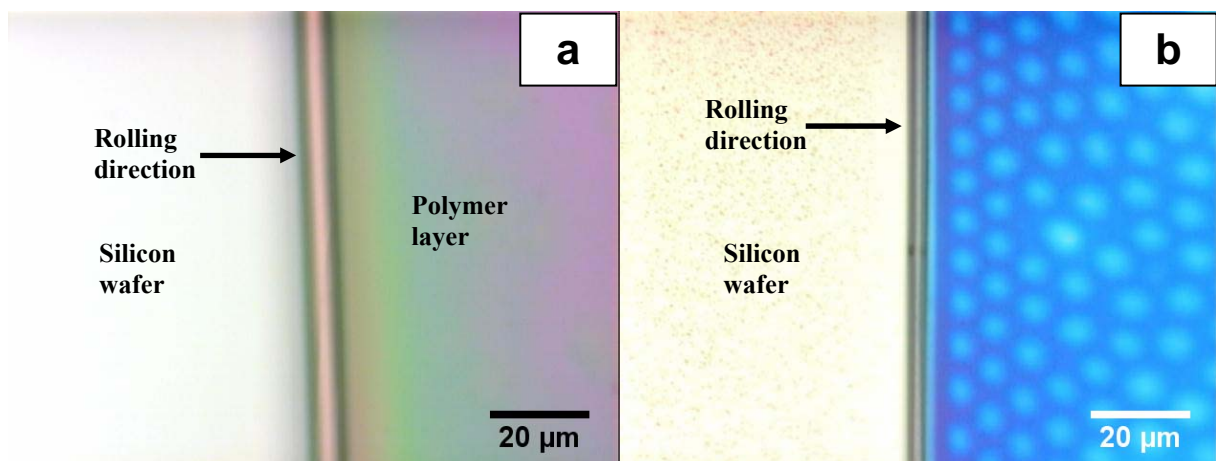


*Figure 7.1: Optical micrographs of tube (a) before pyrolysis, (b) after pyrolysis*

It is observed that large density change occurs in the pyrolysis. This densification leads to volumetric shrinkage of the tube. However, the cylindrical shape of the tube is retained in course of pyrolysis, as confirmed also by SEM.

The morphologies of pyrolyzed and un-pyrolyzed tubes were characterized in detail by SEM. Figure 7.2 shows the SEM images of polymer tube before pyrolysis. Figure 7.2 a shows the rolling direction of polymer layer from a scratch. It is obvious that polymer layers roll in opposite directions from the scratch. The cross-section of the rolled polymer layer is shown on Figure 7.2 b. The P4VP/PS and PDMS layer can be also be differentiated on this image. The polymer layer completed 3 rolls before the rolling was stopped by taking the sample out from the acidic solution.

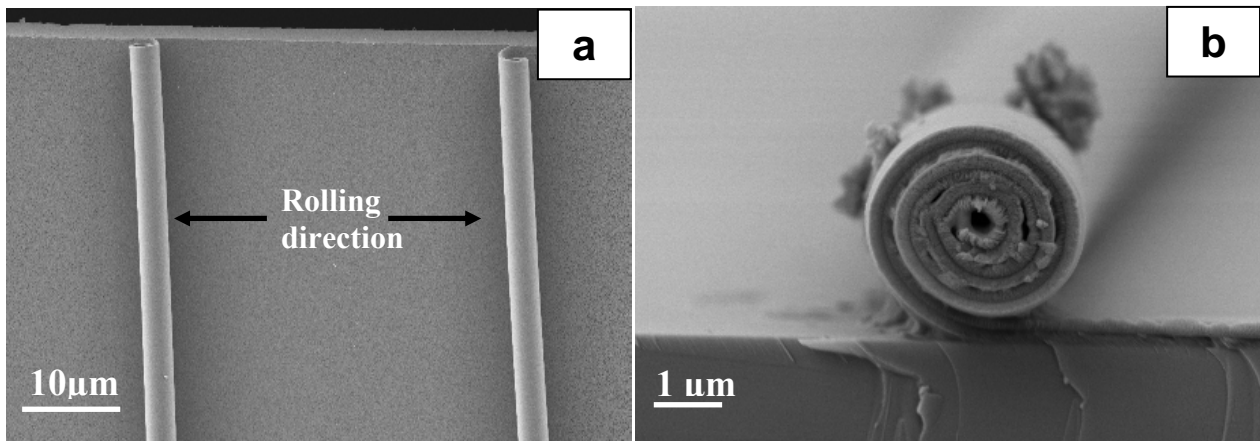


**Figure 7.2:** SEM micrographs of P4VP/PS/PDMS polymer tube before pyrolysis. (a) tubes rolled in opposite direction from the scratch, (b) clearly visible rolled polymer layers with open end of tube.

The morphology of tube's surface is changed after pyrolysis from the smooth one to wrinkled one (see Figure 7.3 a, b). Remarkably enough, the wrinkles on the pyrolyzed tube are oriented parallel to the tube's axis. The roughness of the tube surface should be due to the inhomogeneous shrinkage of the structure. PDMS shrinks in the pyrolysis process but the

tubular shape is maintained. The open end of tubes are shown by Figure 7.4 a and b. The diameter of tubes was found to be smaller than the unpyrolysed reference tube. Therefore, it is obvious that thermal decomposition of the polymer tube was accompanied with the creation of the exterior rough surface and partial mass removal from the polymer tube. This weight loss is due to removal of certain chemical functionalities during the pyrolysis. Finally, a solid silica residual tube is left after pyrolysis.

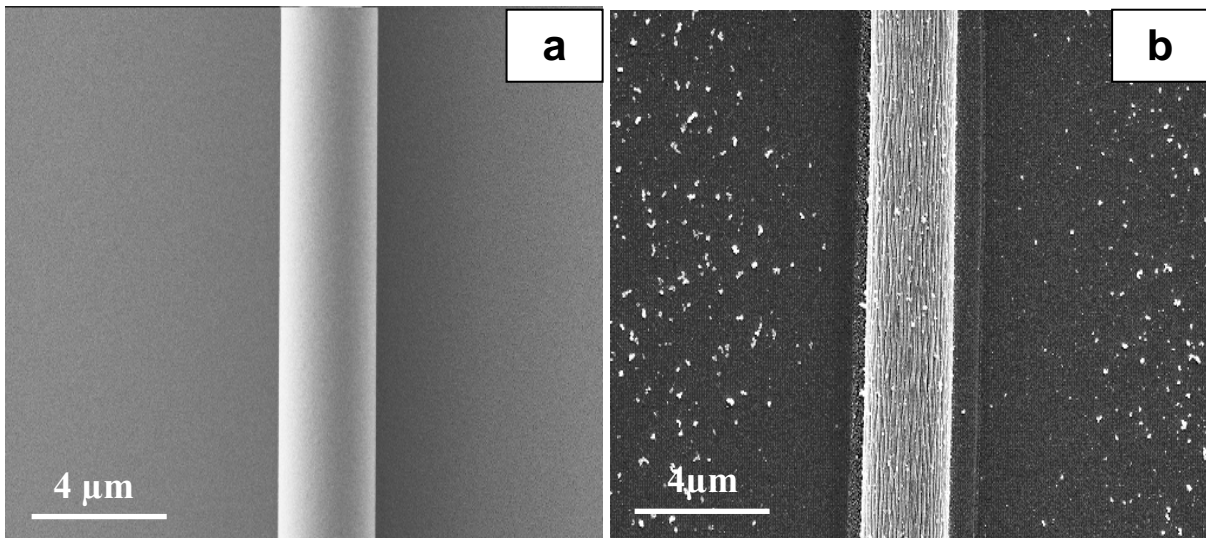


*Figure 7.3: Shows SEM micrographs of tube. (a) before pyrolysis (b) after pyrolysis.*

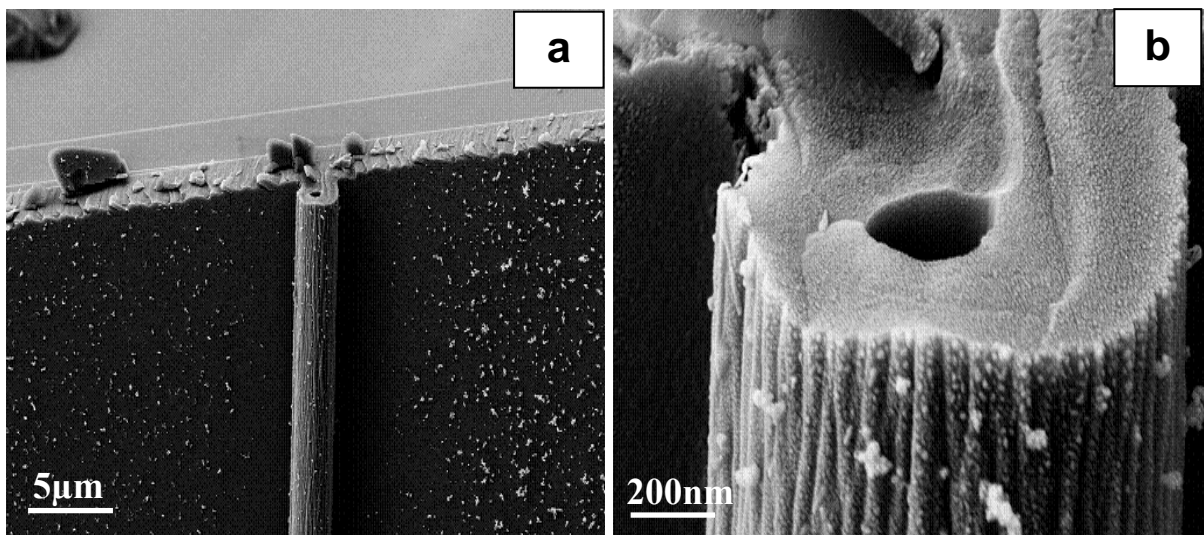
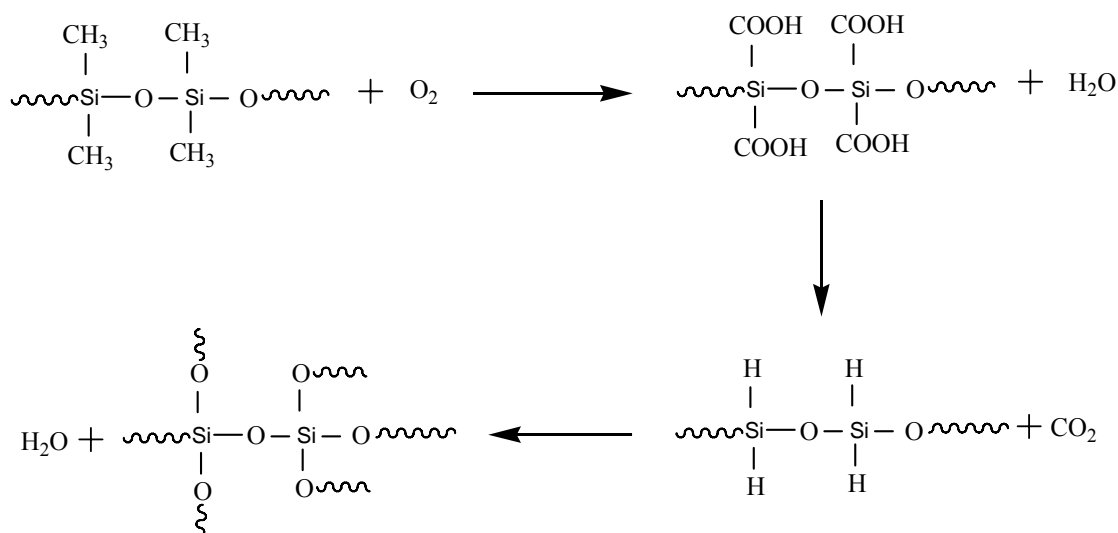


*Figure 7.4: SEM micrographs of tube with open end (a) by lower magnification (b) by higher magnification.*

It is noted here that the transformation of PDMS to silica is completed by oxidative pyrolysis. The reaction proceeds by decomposition of the PDMS producing amorphous SiO<sub>2</sub> [Cam01]. Scheme 7.1 shows the detailed reaction sequence:



**Reaction scheme 7.1:** Transformation of PDMS into silica by oxidative pyrolysis.

The transformation of silica from PDMS is confirmed by FTIR spectrum of the tube before pyrolysis and after pyrolysis. Figure 7.5 shows the spectra of pyrolyzed and unpyrolyzed sample. The characteristic peak of Si-CH<sub>3</sub> appeared at (1416, 1257, 804 cm<sup>-1</sup>) and stretching vibration of CH<sub>3</sub> and CH<sub>2</sub> bond are observed at 2959 and 2929 cm<sup>-1</sup> in unpyrolyzed samples. These characteristic peaks of Si-CH<sub>3</sub>, CH<sub>3</sub> and CH<sub>2</sub> are disappeared after pyrolysis at 700 °C.

The characteristic peaks of Si-O asymmetric stretching vibration in PDMS appeared at 1091 and 1026 cm<sup>-1</sup>. These peaks shifted to a higher wave number region after heat treatment. The shifting of Si-O to higher frequency is due to thermal transformation of PDMS to silica and formation of strong Si-O bond. These shifting in frequency are related to change in bonding characteristic, such as bond length and bond angle.

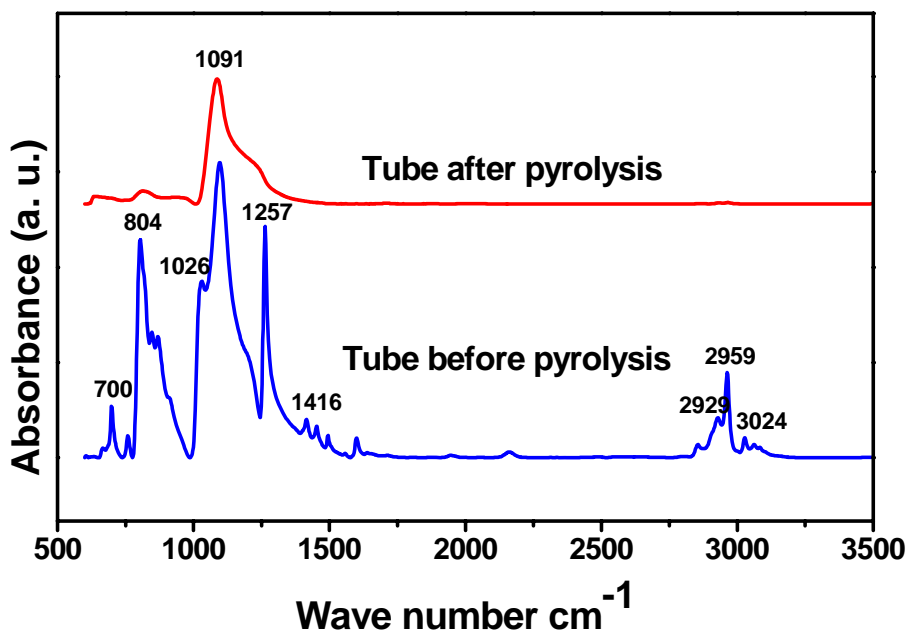


*Figure 7.5: FTIR spectrum of PDMS/PS/P4VP tube, before pyrolysis and after pyrolysis*

Energy-dispersive X-ray (EDX) was also used to determine the chemical composition of silica tube synthesized from polymer tube template. EDX spectra of silica tube after pyrolysis is presented in Figure 7.6. This spectrum revealed the presence of Si and oxygen. It is obvious from the EDX spectrum that the polymer was removed from the tube and finally silica tube was obtained. In the EDX spectrum of tube one peak of silicon at 1.7 keV and a small peak of oxygen was also obtained at 0.50 keV. The presence of oxygen peak reveals the oxidation of Si during the pyrolysis process.

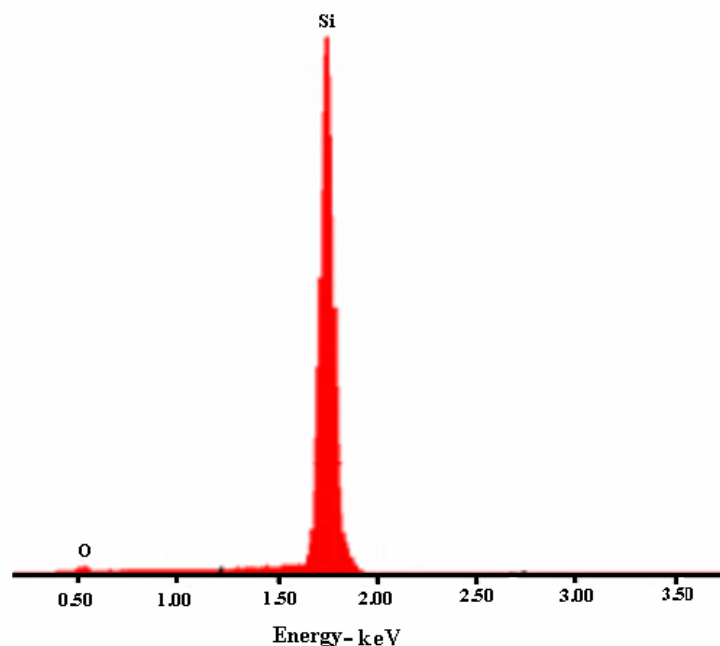


*Figure 7.6: EDX spectra of silica tube.*

The hybrid tube of silica with any metal could be synthesized using self-rolling technique. The hybrid film can be exploited for various catalytic and opto-electronic applications. In the present study we have demonstrated the formation of silica/Au hybrid tube by the same approach. A 4-6 nm thin layer of gold was deposited before or after the deposition of PDMS layer. Polymer moiety has been removed by pyrolysis and silica/Au tube obtained. Figure 7.7 shows the SEM micrographs of the hybrid tube after the heat treatment. The presence of silica and gold layer is clearly visible in the hybrid tubes. A bright thin film in the tube corresponds to the gold layer whereas thick black color represent the silica layer.

To make hybrid tube of silica with gold, the gold layer is deposited on the top of crosslinked PDMS layer [Figure 7.7 a]. The thickness of Au layer (4 - 6 nm) is very small compared to the thickness of silica film (150 - 160 nm). The hybrid layers are clearly visible on the open end of the tubes. In order to fabricate tube with gold on top of silica, the gold layer is deposited before the PDMS layer deposition [Figure 7.7 b] . The number of rolls can be calculated by the number of either gold or silica layers. SEM micrograph of the open end of the

tube presented in Figure 7.7 b is shown in Figure 7.7 c. Finally, we also fabricated tubes with the gold layer deposited both before and after the PDMS layer deposition. On the corresponding Figure 7.7 d one can see the double gold layer in the middle of two silica layers.

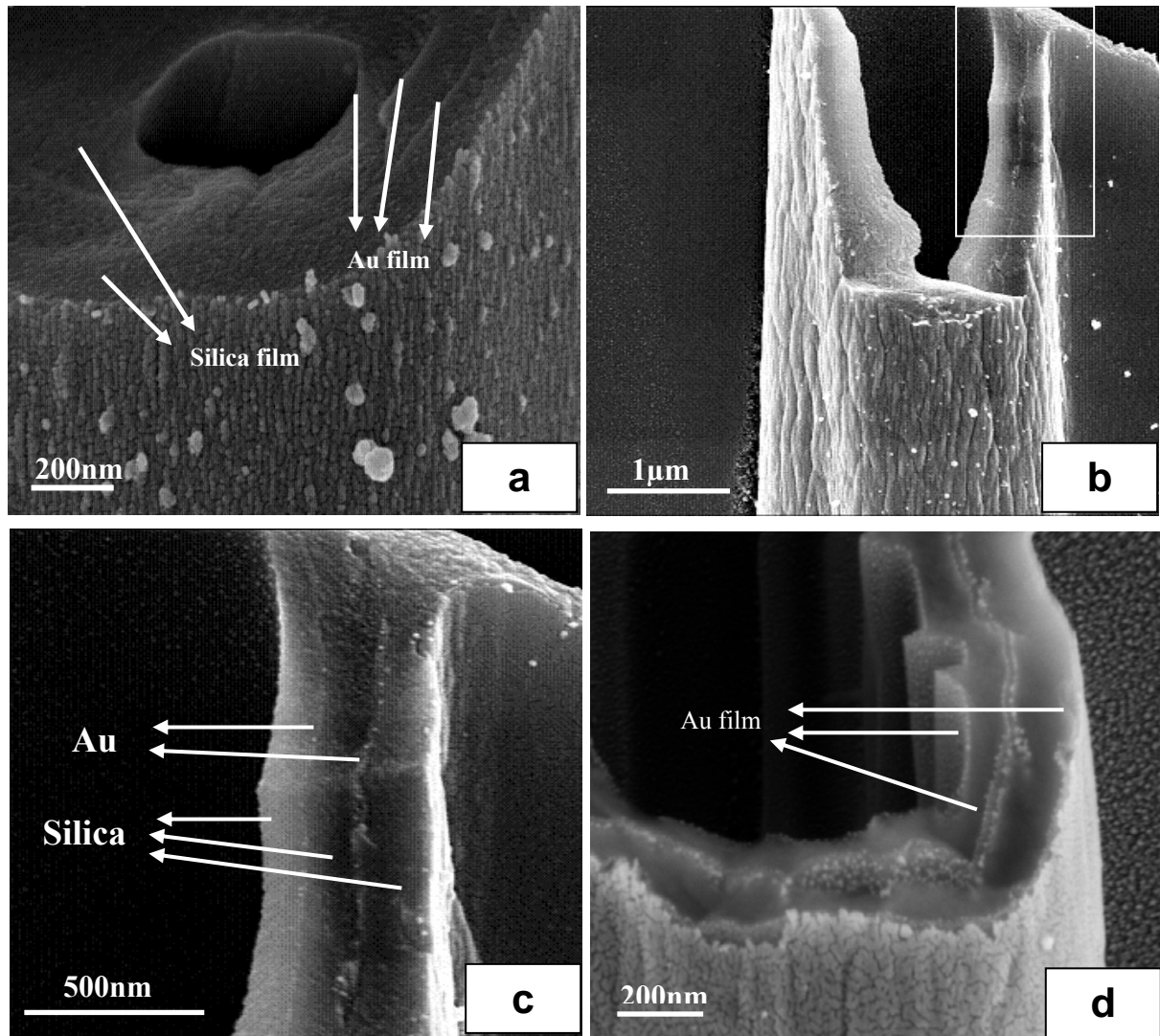


**Figure 7.7:** SEM images of silica/gold hybrid tubes, (a) gold layer is deposited on the top of thermally crosslinked PDMS layer, (b) gold film is deposited before deposition of the PDMS layer, (c) magnified image of an rectangular part of Figure b, (d) gold films are deposited before and after the PDMS layer.

The chemical composition of silica/gold hybrid tube was further characterized in detail by EDX. In Figure 7.8 EDX spectra of hybrid tube after pyrolysis is presented. The presence of Si

and Au peaks in the spectra reveal the presence of Si as well as gold in the tube. In the EDX spectrum of tube, one peak of gold  $M_{\alpha}$  at 2.1 keV, one peak of silicon at 1.7 keV is observed. Beside the Si and Au peak, a small peak of oxygen was also obtained at 0.50 keV which could be due to limited oxidation of Si during the pyrolysis process.

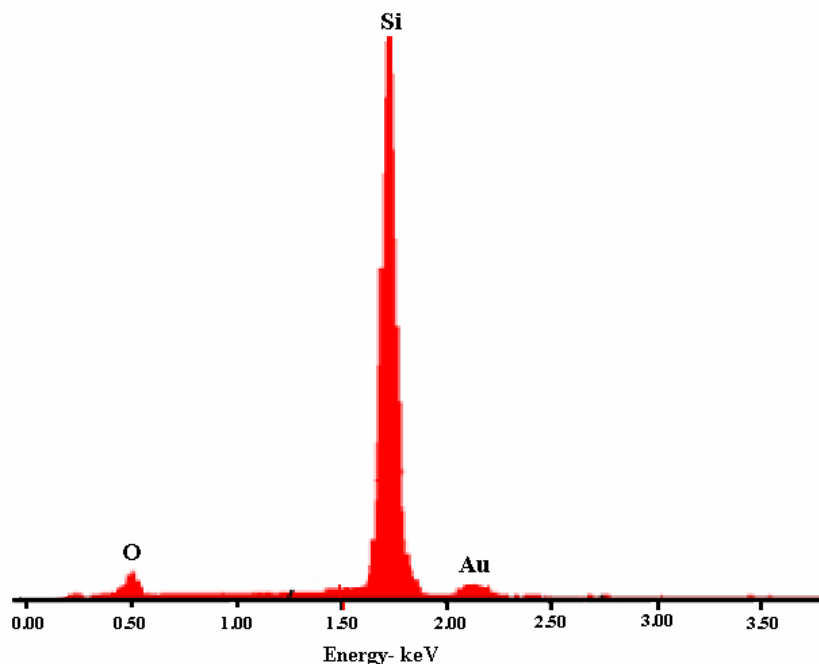


*Figure 7.8: EDX spectra of silica/Au tube.*

The surface chemistry of the silica and silica/gold hybrid tubes were further characterized by XPS. Figure 7.9 reveal the XPS spectra of polymer, silica and silica/gold hybrid tube. The XPS spectra of the polymer tube is recorded before pyrolysis whereas silica, silica/gold hybrid tubes XPS spectra were recorded after the pyrolysis of the polymer tubes. It was observed from comparing Figure 7.9 a, b and c spectra that characteristics peaks of polymer (C 1s) was drastically reduced after the pyrolysis. It can be concluded that polymer is burned out due to pyrolysis and PDMS is thermally converted into silica. The XPS spectrum of silica tube clearly shows characteristic peak of Si 2s, Si 2p, O 1s at 154 eV, 103 eV and 533.5 eV, respectively. For the silica tubes the [Si]:[O] ratio was found to  $[Si]:[O] = 0.467$ , which is very close to the stoichiometric ratio of  $SiO_2$ . The origin of the residual carbon (C 1s peak) in silica and



silica/gold tubes could be explained by non-specifically adsorbed surface contaminations, which are typical for all metal and ceramic surfaces. The characteristic signals of gold (Au 4d<sub>3/2</sub>, 4d<sub>5/2</sub> and 4f<sub>7/2</sub>) are clearly observed in the XPS spectra of hybrid tube. Furthermore, Si and O peaks also appear at their normal binding energies but the peak intensity become very poor because the gold layer covers the silica surface in hybrid tube.

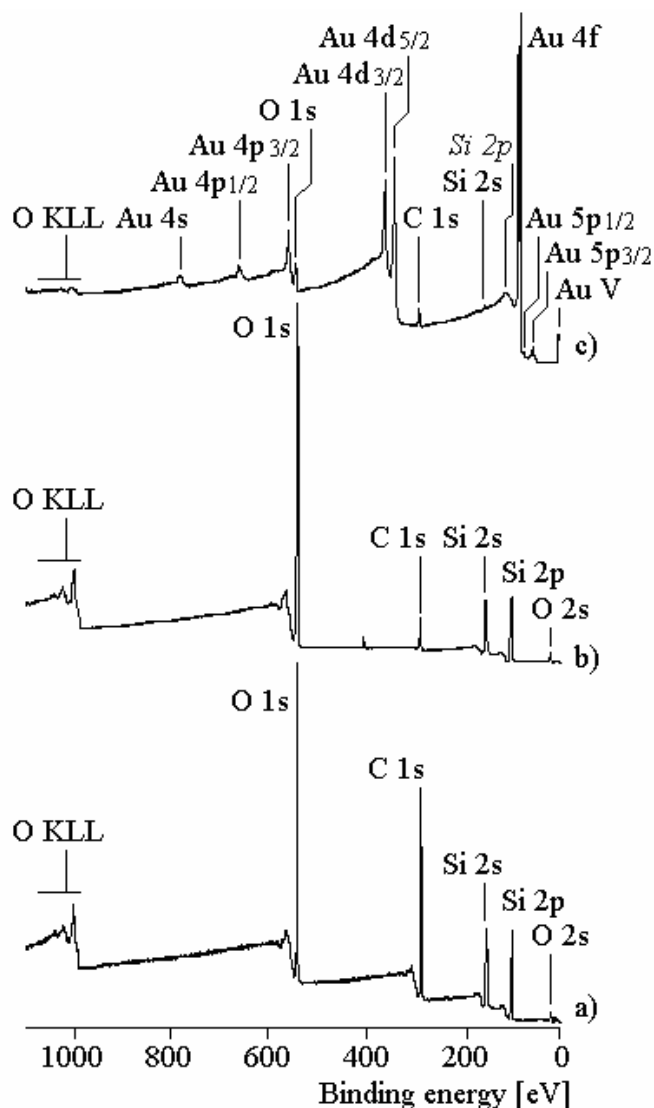


**Figure 7.9:** XPS spectra of tubes (a) PDMS/PS/P4VP (b) silica tube (c) silica/gold hybrid tube.

The fabricated tube have hollow interior throughout the length of tube. The open end of fabricated tubes was confirmed by SEM as shown by Figure 7.10 a and b. Usual approach for obtaining tube's cross-sections is simply breaking the silicon wafer substrate. However,

breaking of the substrate does not provide the tube's opening at exact position. Tube's opening can be obtained with high spatial resolution by using focussed ion beam (FIB). The NEON 40 EsB FIB used for this. Exact positioning of the tubes on the substrate and their opening at well-defined locations is important for the construction of future tube-based devices.

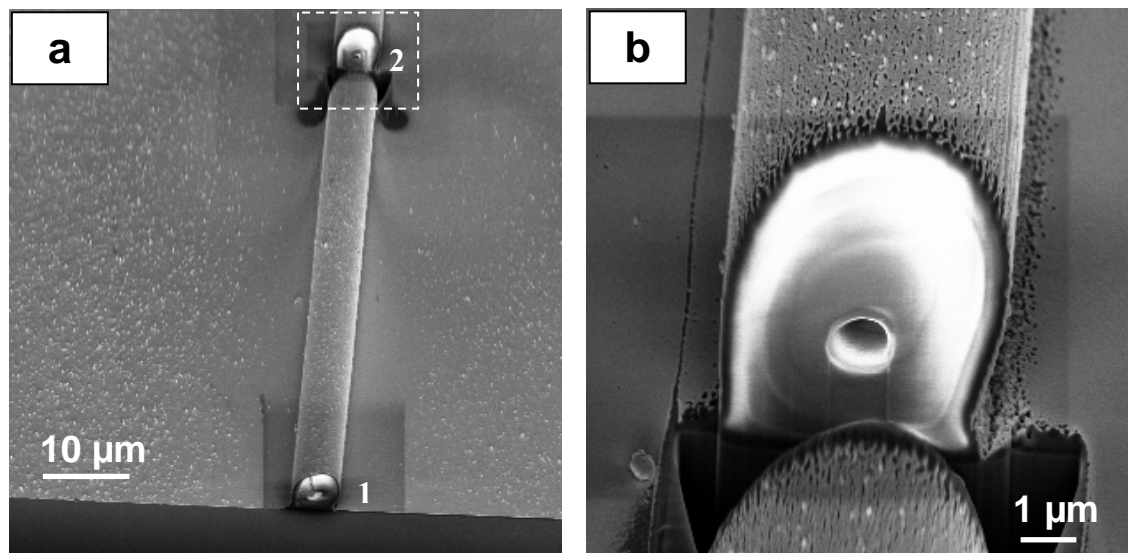


**Figure 7.10:** (a) Open end of tube is shown by FIB (mark no. 2) as well as breaking of silicon wafer (mark no. 1), (b) enlarge image of rectangular part of the Figure a.

Figure 7.10 a shows two opening of a silica tube, one opening created by breaking of substrate (mark no. 1) whereas another (mark no. 2) opening was produced by FIB technique. The FIB system work at high vacuum ( $1.69 \times 10^{-6}$  mbar). In FIB technique the samples were irradiated by 30keV  $\text{Ga}^+$  ions at 500pA ion current. A magnified image of a rectangular part of Figure 7.10 a confirms almost perfect cylindrical shape of the object [Figure 7.10 b].

#### **7. 4 Discussion**

In the past, the silica tube has been fabricated by template based method [Li05], laser ablation [Yu98, Cha06], thermal oxidation [Dai02] and chemical vapour deposition [Zhu01, Niu04]. Li et al. used human hair as a template and a precursor solution of tetraethoxysilane

was used as silica source [Li05]. The minimum diameter of the resulting silica tube was limited to 20- 30 $\mu$ m. Moreover, these approaches do not yield high aspect ratio tubes. In the present thesis we fabricated the silica tube by self-rolling approach and it was possible to obtain tubes with diameter as low as 200 nm. Furthermore, very high aspect ratio silica tube could be obtained using this approach. The diameter of the silica tube could be easily tuned by controlling the thickness of polymer layers. In the past, even though the strain driven self-rolling has been used for the fabrication of silica resonators (SiO<sub>2</sub>/Si) [Son07], however, pure silica tube could not be fabricated using this procedure. The approach discussed in this chapter makes it possible to obtain pure silica tube. Moreover, all the fabrication steps in this procedure are simple and easy to follow.

Recently, the silica/metal hybrid tubes have been investigated for their catalytic activity. The fabrication of silica/Pd, silica/Pt, and silica/gold hybrid tube were demonstrated using electroless plating [Jav09] or template method [Cha06]. Compare to these techniques the present approach is much simpler and robust for fabricating silica/metal hybrid tube of higher aspect ratio. The main advantage of the approach we see is the possibility of the combination of silica with apparently any single or multi-metals, even those that have no propensity to self-roll by themselves. Moreover, more complex micro-machined structures of silica and silica/metal hybrid can also be fabricated using this approach.

## **7.5 Conclusions**

We have demonstrated a novel effective route for the synthesis of silica and Au/silica tubes via self rolling approach. The thermal decomposition of the tubes was accompanied by the transformation of the PDMS to silica. All organic moiety has been burned by pyrolysis. The tubes were characterized by optical microscopy, FTIR, SEM, FIB and EDX. During the pyrolysis shrinkage of tubes were observed. This shrinkage process could be used for the

synthesis silica composite of smaller feature sizes and with controlled porosity. The silica and hybrid of silica have potential applications in optical device (sensors, actuators), catalytic components and tissue engineering matrices. It should be noted here, though, in this study we emphasize only on silica and silica/gold hybrid but this novel approach could also be used for the fabrication of other ceramic or ceramic/metal hybrid tubes.

## *Chapter 8*

## 8. Bubble Generation Inside the Tube

### 8.1. Introduction

Recently, single phase and multiphase flows have been studied in microfluidic devices [Gun06, Bar04, Shu07, Gun04]. Microfluidic field is an interdisciplinary area of biotechnology, chemistry, physics, biology, nanotechnology and engineering in which small volume of fluids is used [Hal08, Sto01, Squ05, Klo07, Bee02]. Microfluidic device can be used for bioanalysis [Kha02], chemical reactions [Dem06], electrical analysis of cells [Bao08], food engineering [Sku08], sensors [Cha08b, Sta05], ink-jet printing [Coo02], encapsulation and hydrodynamic self-sorting of single cells [Cha08a] and kinetic studies [Kha06b]. A very promising sub-field of micro-fluidics is the production and manipulation of microdroplets and microbubbles [Fid07, Son06b, Son03, Hue07, Tan06, Kim06b]. Droplets can be seen as self-contained microreactors that prevent sample loss, diffusion, cross-contamination. Micromanipulation of individual discrete droplets, dubbed digital microfluidics, attracts a lot of attention as a tool for very precise, economical and high rate method of chemical and biochemical research. Digital microfluidic processing is carried out on unit-sized packets of fluid which are transported, stored, mixed, reacted, or analyzed in a discrete manner using a standard set of basic instructions. The production of unit-volume droplets can be reduced a set of repeated basic operations, i.e., moving one unit of fluid over one unit of distance.

Microreaction synthesis [Kob04, Hat06], encapsulation and self-sorting of single cells [Cha08a], studies of protein crystallization [Che05, Zhe05] and the synthesis and fabrication of colloid particles [Xu05, Uta05] are the examples where controlled size droplets are used. These droplets can be used as a carrier of water soluble drugs for sustained release or targetable drug delivery. Small size droplets can be conveniently used in nanoreactors with advantages in terms of reaction efficiency, exact control on the substances and cost savings. Splitting of continuous

liquid flow in small droplets can be done by flow-dominated rupture [Tho01, Ann03, Dre03, Sto04], geometry dominated break-up [Sug01, Lin04] and generation of small gas bubbles [Gar04].

Small gas bubbles generation is one of the important technique to control the production and size of droplets formation [Xio07, Gar04, Gor04] because gas bubbles can divide the liquid stream into small droplets in narrow channels. Proper segmentation of the liquid stream and production of small droplets with very precise accuracy can be done using gas bubbles. These bubbles in microfluidic devices can be generated by flow-focusing devices [Gar04, Gor04] and using lumped gas and organic injected junction [Ara08]. In these cases the size and density of the produced bubbles can be controlled by liquid flow, gas pressure level in the liquid, and geometry of device. In order to achieve highly accuracy and repetition rate of bubble generation inside the tube, the fluid dynamics of the growth and collapse of a bubble in a small tube is studied [Ory00].

Recently, electrolysis was also used to produce small size bubbles. Splitting of water into bubbles of hydrogen and oxygen by electrical current passing through the water enables direct control of bubble size, release location and release frequency [Lee05]. The geometry of the device plays an important role in the synthesis of bubbles. Recently, self-rolling approach has been demonstrated to form nano- and microtube with accuracy control in structure, geometry and position geometry [Sch01a, Pri00]. It has been demonstrated that the self-rolled tubes can be used as a transport media for the solution and chemicals [Den04b].

In this chapter, we addressed splitting of the fluid stream by gas bubbles via an electrochemical process inside the self-rolled polymer tube. For the electrolytic bubble generation, current has to flow between two electrodes which are in contact with the liquid

substance. Hence, the polymer tube requires a continuous metal stripe inside as well as outside of the tube. Outer part of the stripe can be used to connect an external power supply and this kind of structures (tubes with external conductive contacts) could be fabricated using self-rolling technique [Pri00]. Detail description of this technique is given in Chapter 2.

## **8.2. Fabrication of bubble generation device**

The schematic view of simple polymer tube device is shown in Figure 8.1. The bilayer of P4VP (70 nm) and PS (50 nm) deposited on the cleaned silicon wafer followed by crosslinking via UV-radiations. The thin film of gold is deposited by physical vapour deposition using DC sputtering at pressure of  $2.6 \times 10^{-2}$  mbar and an operating voltage of -440V. Photolithography process was used to make patterns of gold. Small metal mask were used to make patterns of gold electrodes. PDMS and aluminium mask were also used to make bigger size patterns. A schematic view of gold patterned bilayer is shown in Figure 8.1 a. After creation of gold patterns a fine scratch was made in the middle of stripe to introduce the DBSA solution to the bottom P4VP layer [Figure 8.1 b]. Microscratched sample was immersed in the 4 wt % DBSA solution. P4VP form supramolecular complex with DBSA and resulted increase specific volume of the bottom P4VP layer. This swelling is opposed by stiff PS layers and these two opposing action, start the bending process [Detail description is given in Chapter 2.4]. Some part of gold is enrolled inside the polymer tube and remaining part is outside of the tube [Figure 8.1 c]. Furthermore, after the tube formation, it is connected to the micropump via a syringe or glass capillary to give a controlled continuous water stream. The outer stripes of electrode are connected to the power supply to start electrolysis [Figure 8.1 d]. Bartels mikrotechnik MP5 micro pump (maximum flow rate 3  $\mu$ l/min, work at 7.5 V DC) is used to control the transport of the liquid [Figure 8.2].



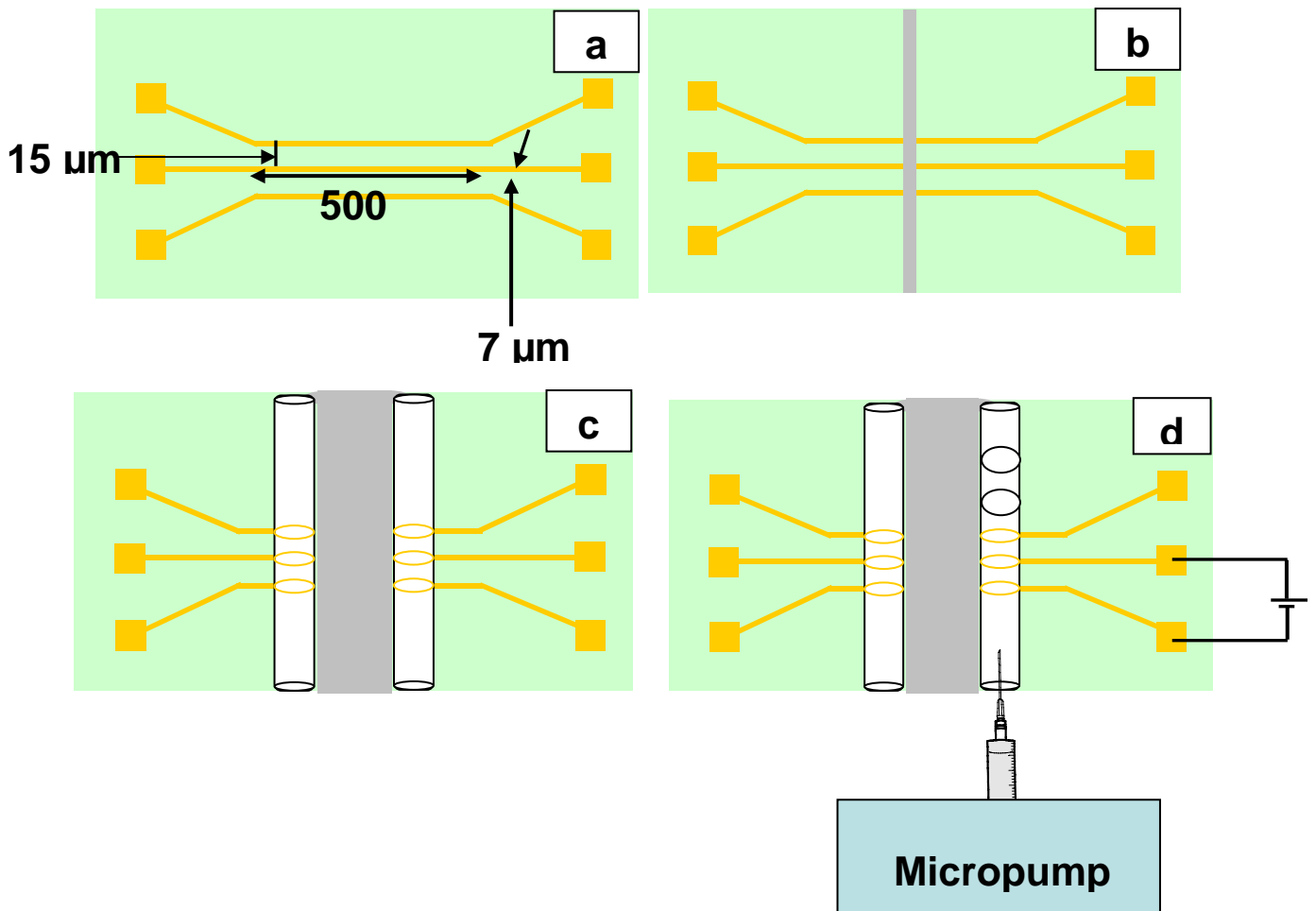


**Figure 8.1:** Schematic view of bubble generation inside the self-rolled polymer tube (a) planner pattern of gold electrodes, (b) scratched sample, (c) partially rolled gold pattern, (d) generation of bubble.

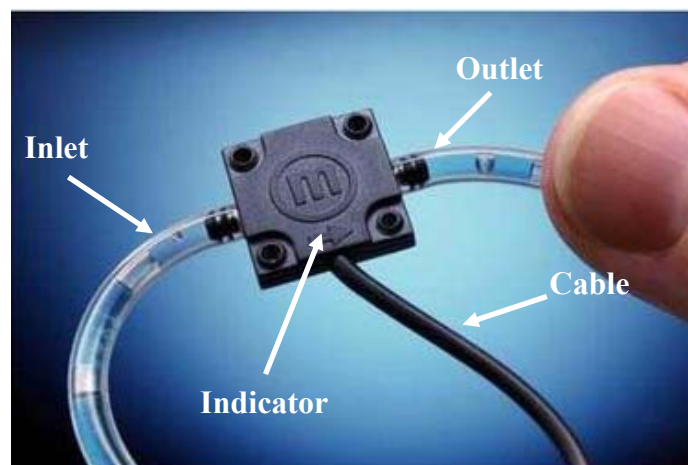


**Figure 8.2 :** Micropump mp5: showing inlet and outlet of the pump

### 8.3 Results and Discussions

In order to perform an electrolysis process inside the tube conductive stripes of gold are deposited on the crosslinked bilayer. An optical micrograph with gold patterns is shown in Figure 8.3. The light pink yellow colour represent the gold film whereas the light blue-green colour represent the crosslinked P4VP/PS bilayer. An optical micrograph with gold patterns is shown in Figure 8.3. The dimension of gold electrodes was further characterized by AFM. Figure 8.4 shows the height and phase image of gold electrode.

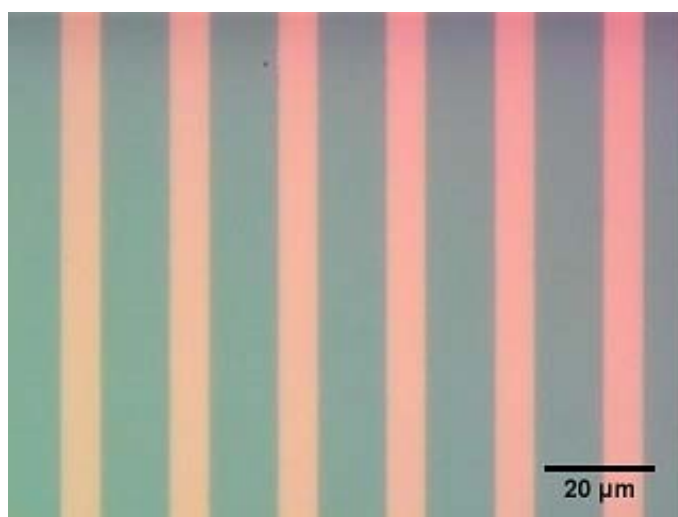


*Figure 8.3: Pattern of gold stripes on the crosslinked polymer bilayer*

The thickness of the gold electrodes was determined by the necessity to satisfy the balance between the sufficiently high conductive and mechanical integrity and the ability of the multi-layer structure to roll. We noticed that gold stripes thicker than 80 nm suppress the rolling of the bilayer, so that only the place where gold is not present are rolled up. In this work the thickness of the gold layer ranged from 30 to 50 nm.

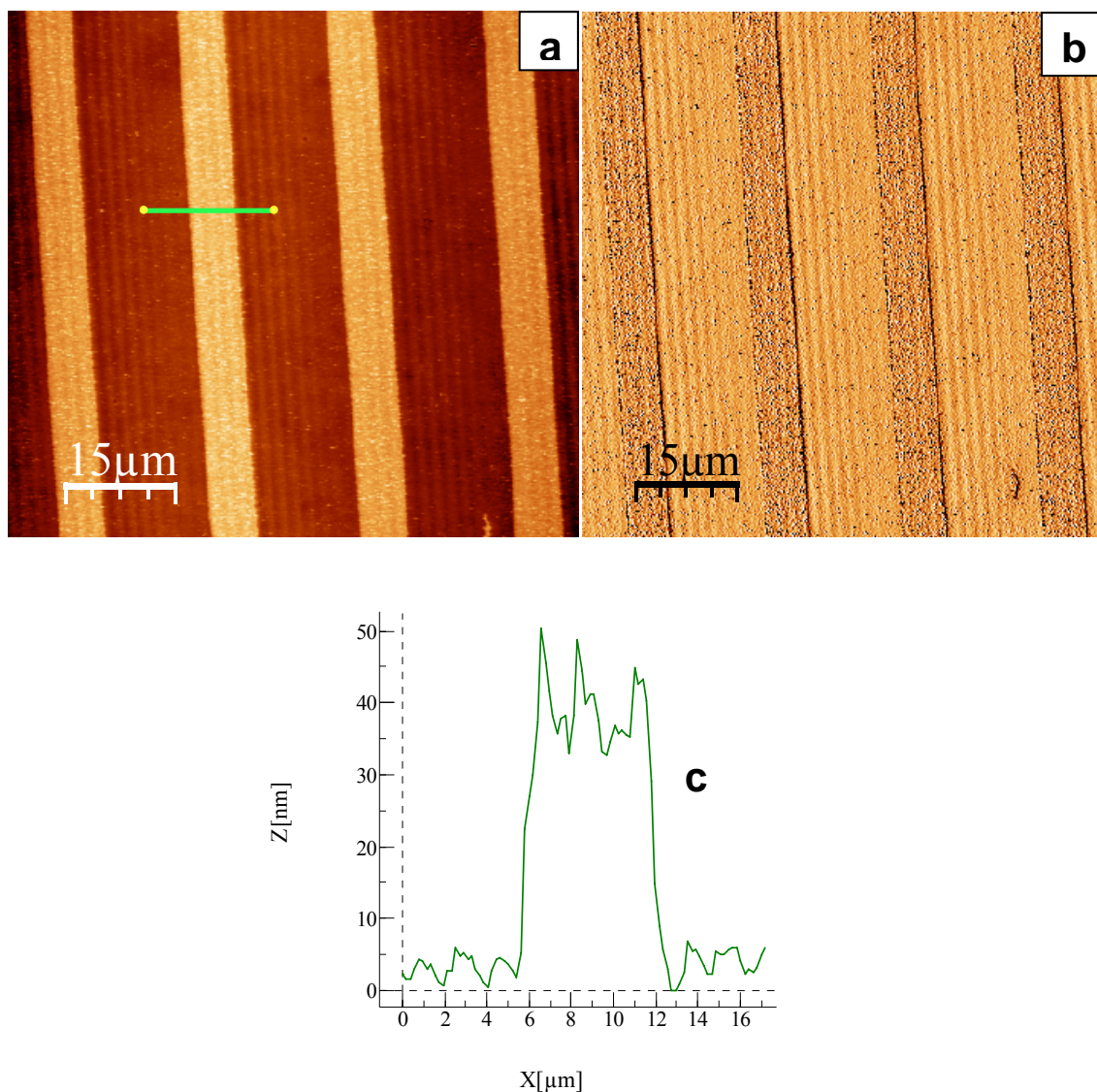


**Figure 8.4:** AFM images of gold electrodes deposited on the polymer bilayer, (a) height image, (b) phase image, (c) section profile of the height image.

After 2 - 3 rolls of gold layer in the DBSA solution the sample was taken out from the acidic solution and washed by millipore water. An optical micrograph of partially rolled stripes is shown in Figure 8.5. It is cleared from the this figure that a flat gold stripe is converted into partially rolled stripe. The flat part can be easily connected with outer power supply and these stripe worked as a electrode to perform electrolysis.

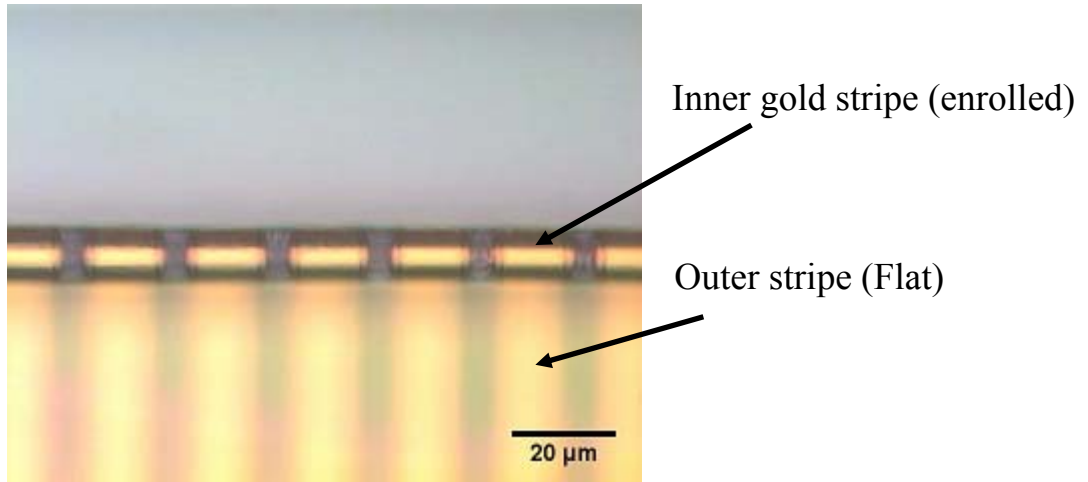


**Figure 8.5:** Gold patterns partially rolled inside the polymer tube

In order to start electrolytic bubble generation fluid should be inside the polymer tube. Fluid can be inserted in the polymer tube by two methods (a) capillary action (b) pumping inside the tubes from external fluid reservoir with use of a micropump system. We explored the both approaches.

#### **(a) Capillary action**

The capillary action, in particular the spreading of liquids in narrow tubes is the result of intermolecular attraction between the liquid and solid materials. It can be explain in terms of cohesive and adhesion forces [Lam07]. Pressure driving the fluid in (or outside) the capillary of a circular cross-section is given by the formula:  $P = 2\gamma\cos\theta/r$ , where:  $\gamma$  is liquid-air surface tension ( $\text{J/m}^2$  or  $\text{N/m}$ ),  $\theta$  = contact angle,  $r$  = radius of tube (m). The fluid is driven inside the tube if the inner surface is hydrophilic (contact angle is in the range from 0 to 90 degrees in hydrophilic). In order to change the property of inner surface from hydrophobic to hydrophilic, the polymer bilayer was treated by oxygen plasma for 2 - 3 minutes before start to roll. This reduced the contact water-surface contact angle from approximately 90 degrees (usual value for the untreated polystyrene) to a few degrees [Mur05, Ha97].

Filling of a tube with a water-based solution is shown in the Figure 8.6 by several consecutive images. This demonstration was made simply by putting a droplet on an open tube end, while the other tube end was kept in air. The rate of the fluid propagation inside the tube of given dimensions depends on the fluid viscosity. We did not quantify this phenomenon, since it is out of the scope of our present research.

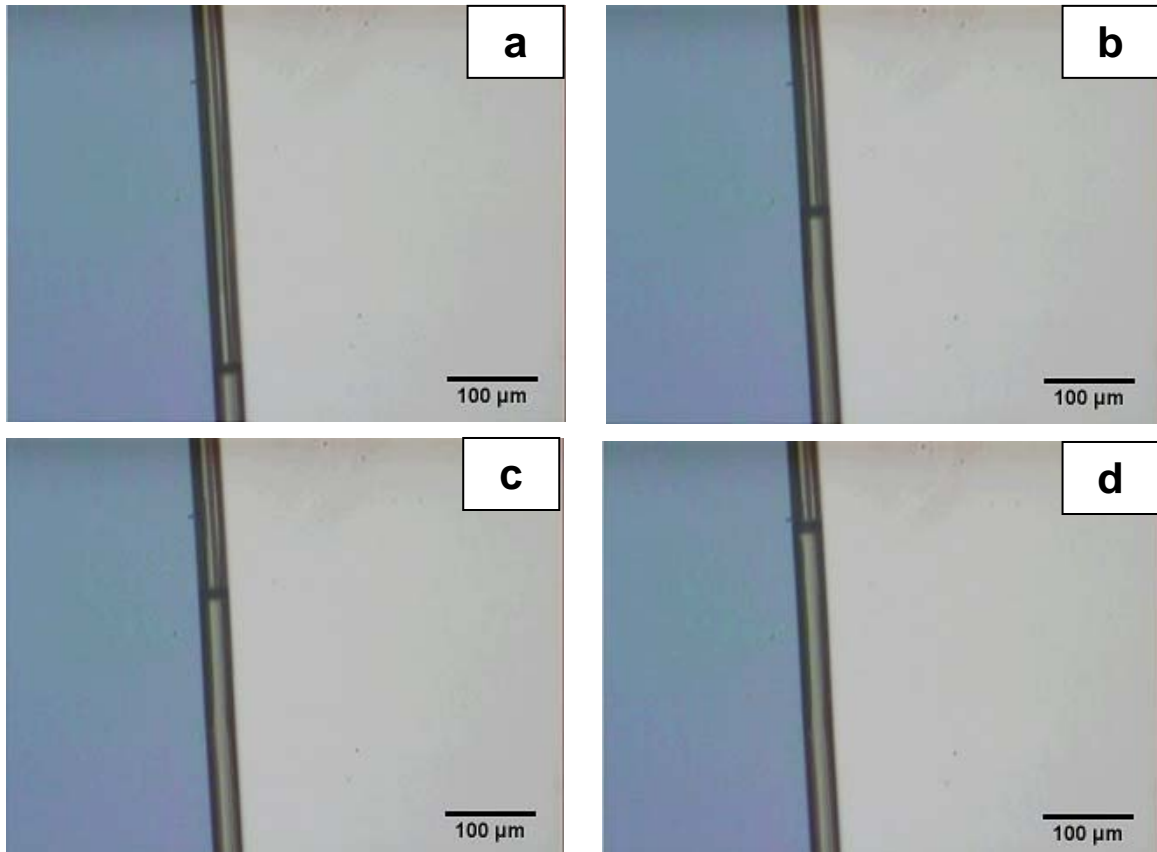
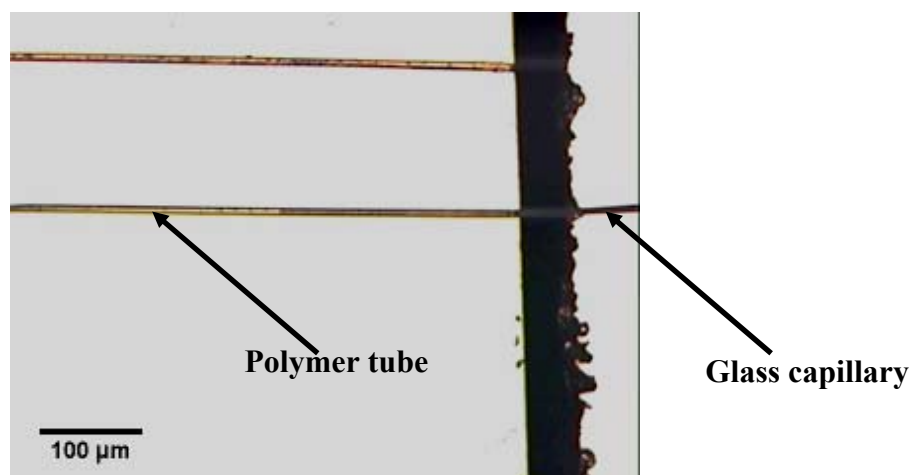


*Figure 8.6: Water rising in the polymer tube due to capillary action*

The obvious advantage of the capillary action use is the simplicity of this operation and the minimal apparatus requirements. This may be profitable for the future design of the tube-based autonomous sensor devices. The drawback of the approach is the impossibility to achieve the permanent flow with the regulated flow rate through the tube. These problems can be resolved by interfacing the tubes with an external micro-pumping system.

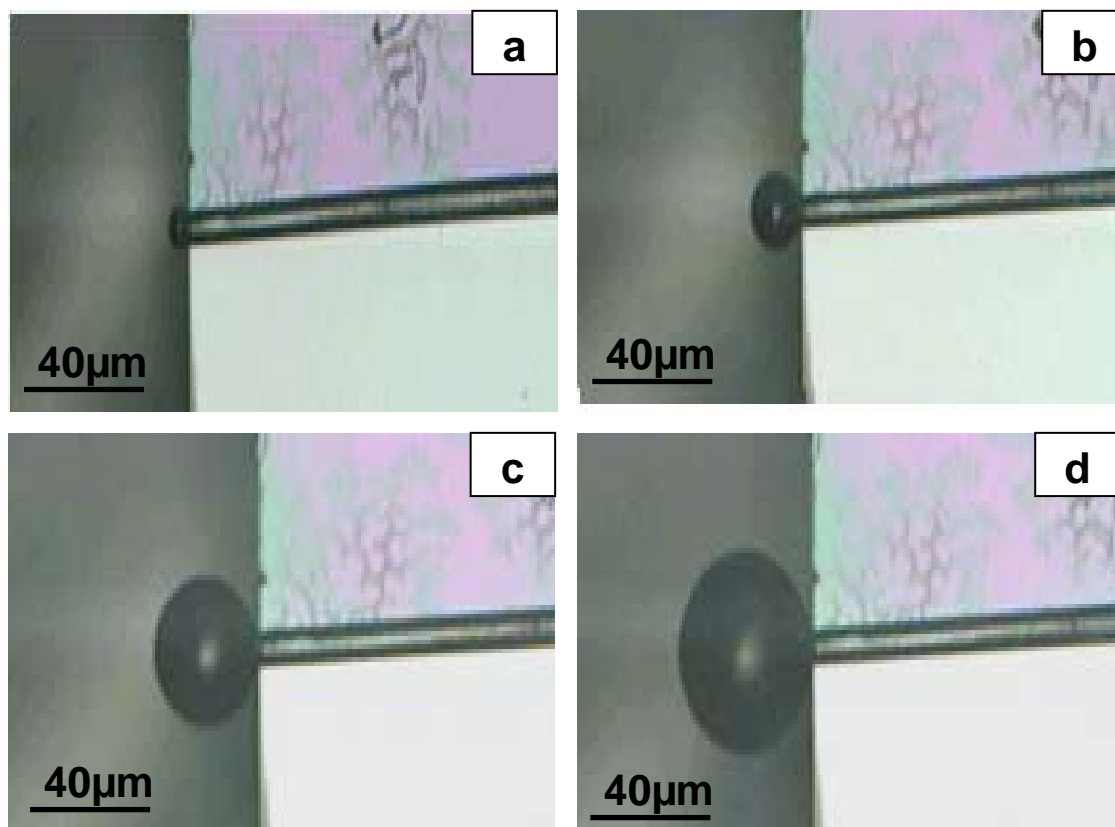
***(b) Polymer tube with external fluid reservoir***

The setup is schematically shown on the Figure 8.1 d. The self-rolled tubes are connected to the external pumping system via a few micron wide glass capillaries, made by fast stretching of 1mm-thick glass tubes heated over the flame. The insertion of glass capillary inside the polymer tube was performed under the microscope. One object either glass capillary or polymer tube was fixed on micro positioning system and other object moved towards the open end of first object. After insertion of capillary inside the polymer tube the capillary-tube connection was sealed using epoxy. A less viscous epoxy has possibility to block the open end of glass capillary or block the way inside the polymer tube by flowing through the tube-capillary connection. In order to resolve the problem of flow of epoxy inside the tube we used quite viscous epoxy. The viscosity of epoxy was controlled by waiting a certain time before applying to the capillary-tube junction sealing. The other end of the glass capillary was connected by flexible plastic tubes to the micropump and the solution reservoir. In our experiments, the glass capillary was connected only to one ending of the self-rolled tube, while the other one was left free. This configuration corresponds in principle to micro-syringes, or micro-jet printing devices [Arn00].



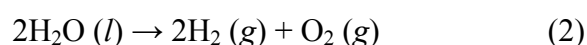
***Figure 8.7: Polymer tube with inserted glass capillary***

Figure 8.7 shows an inserted glass capillary inside the polymer tube. After sealing of tube-capillary connection by epoxy the glass capillary was connected to micro pump to control the flow of liquid.



*Figure 8.8: Generation of water droplet from capillary-tube connection*

After set up of whole device, a continuous flow of water through the polymer tube is started using micro pump. As pointed above the gold stripes were deposited on the crosslinked polymer before rolling and further some part of stripe was enrolled inside the polymer tube. The outer stripe of the gold is connected with power supply in order to start the electrolysis. Water decomposes into hydrogen ( $H_2$ ) and oxygen ( $O_2$ ) in water electrolysis due to electric current being passed through the water. Electrolysis of water is common method of  $H_2$  and  $O_2$  production in electrochemistry. The overall reaction in electrolysis can be presented by the following equation:



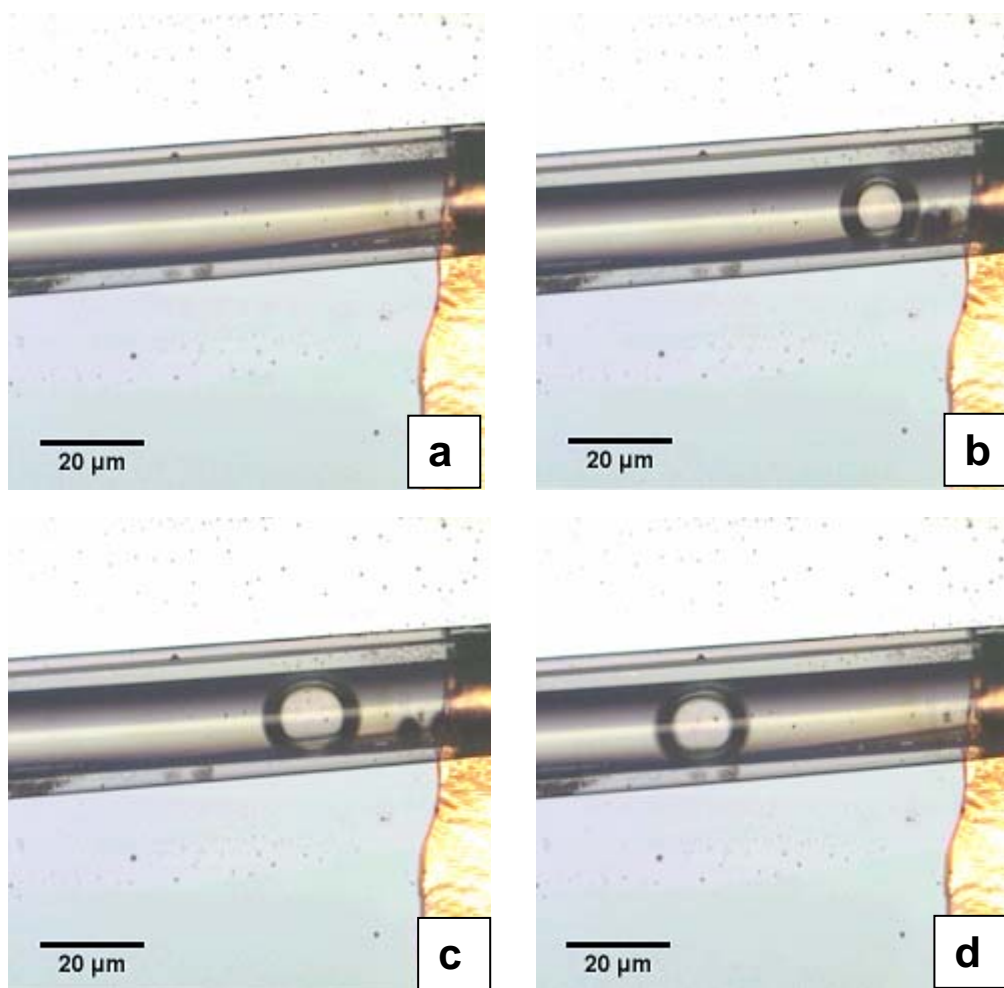


**Figure 8.9:** Generation of micron size bubble inside the polymer tube by electrolysis (a) stage before electrolysis, (b, c, and d) are the consequent figures after bubble generation.

Due to hydrolysis, oxygen and hydrogen gas are generated inside the tube and the gas bubble flow with stream of water. Some micrographs of bubble generation inside the self-rolled polymer tubes is captured by optical microscope and is shown in Figure 8.9. Figure 8.9 a reveal the stage when sufficient amount of current has not reached to start electrolysis. Once the optimum current reached upto inner electrode of tube the electrolysis process start and hydrogen and oxygen gas are produced. Figure 8.9 b, c, and d are the consequent figures showing the generation of micro bubble inside the tube.



It is obvious from the Figure 8.9 that a micron size bubble is generated inside the polymer tube by water electrolysis. This generation of bubble split the liquid stream and produce droplets in a precise manner. The generation of bubbles could be controlled by changing the applied voltage. Hence, the splitting of liquid stream can be adjusted by the flow rate of liquid or applied voltage. Electrolysis of pure water is a very slow process so little amount of iron chloride salt was added in the water.

It is also possible to estimate the volume of the bubbles generated during electrolysis using the Faraday's law of electrolysis

$$V = \frac{1}{N_A} \cdot \frac{Q}{ne^-} \cdot \frac{RT}{P} \quad (8.1)$$

where,  $V$  = volume of gas generated over a time  $t$ ,  $N_A$  = Avogadro's number,  $Q$  = total electric charge, which flows inside the tube over a time  $t$ ,  $n$  = number of electrons per ion involved in the electrolysis,  $e^-$  = electron charge,  $R$  = universal gas constant,  $T$  = temperature,  $P$  = pressure inside the bubble.

The droplets of different size can be generated by applying the electrical voltage impulses with certain time intervals. Let  $q$  be the flow rate in the tube (the volume of fluid which passes through the tube's cross-section in a time unit). Then, the volume of the droplets can be estimated as  $V_d = q\Delta t$ , where  $\Delta t$  is the time interval between the voltage pulses. In this estimation, we imply that gas is generated only at one of the electrodes. This can be realized if water contains the iron chloride salt, then, only the bubbles of chlorine are formed at the anode. Otherwise, in case of pure water electrolysis, the size of the droplets can be regulated by the distance between the electrodes. The volume of the droplet can be estimated as the volume of fluid between the two electrodes.

## 8.4 Discussion

After the development of self-rolling technology, various application of the self-rolled semiconductor tube have been demonstrated including as X-ray and visible light waveguides [Den06a] and in micro- and nanofluidic applications [Sch01c, Thu06, Gir07]. In microfluidic applications organic fluid transport within the rolled-up tube was demonstrated [Den04b, Den04c]. Similarly, the microfluidic devices made from polymer tube can be used for modular microfluidic circuits and interconnections for multipurpose applications in life science, chemistry, Bio-MEMS, and Lab-on-Chip devices [Bec02]. A detail description of the application of rolled-up polymer tubes as a transport media on the substrate is given in Chapter 4. In the present study we used integrated polymer tube for the electrolytic microbubbles generation which can be further explored for nanojet-printing.

In the previous studies on bubble generation, the bubbles were generated at the injector tip, when a submerged gas was vertically injected into a liquid under constant flow conditions [Kum70, Wra71]. The generation of bubbles was controlled by gas flow rate. At low gas rates under terrestrial conditions, single bubble emerge from the injector, detach from it, and rapidly rise to the surface of the liquid primarily due to the buoyant forces [Gad86]. An increase in gas flow rate leads to the formation of bubble-coalescence and jetting regimes [Miy82, Kyr97]. The formation of monodisperse gas bubbles using a hydrodynamic flow focusing method through capillaries and orifice has also been demonstrated in the past [Gan01, Gan04, Gor04]. It is clear from these studies that for the bubble generation one need a separate source of liquid and gas in the microfluidic devices whereas in the present system the bubbles can be generated inside the liquid stream by hydrolysis via integrated electrodes. Another disadvantage of employing gas injected bubbles is that the bubble here is excessively large and prone to coalescence. The present approach does not suffer from such disadvantages.

## 8.5 Conclusions

Self-rolling of polymer bilayers is a very convenient approach for interfacing the interior of microtubes with external electrical circuits. As shown in this chapter, it can be used in particular for creating such devices as micro-bubble generators exploiting electrolytic decomposition of fluids. To this end, the electrodes can be created on the surface of the bilayer and placed inside the tube during the self-rolling. The unrolled parts of the electrodes can be connected to external power supply, whereas the fluid can be introduced either by capillary action or micro-pumping system. The main reward of the electrolytic decomposition approach to the microbubble/microdroplet generation is the possibility to control the size of the droplets in broad limits either by varying the time intervals between the electrical impulses which generate the gas bubbles by splitting the fluid stream, or via the distance between the electrodes.

Furthermore, using the approach outlined in this chapter a device could be developed which will be able to generate droplets, containing a certain amount of nanoparticles or macromolecules. Most probably, this can be realized via the integration of the self-rolling tubes with the optical detection system, which will detect the presence of the fluorescent quantum dots or fluorescent-labelled macromolecules in the space of fluids between the electrodes. The optical detection system should be able then to trigger the electrical pulse splitting the fluid stream by the droplets.

## *Chapter 9*

## 9. Summary and outlook

In this thesis, exploration of self-rolling approach for the formation of polymeric, metallic and ceramic micro and submicron size objects has been demonstrated. The tubes were fabricated using strain driven self-rolling phenomena of P4VP/PS thin bilayer film. Swelling of P4VP layer occurred in the acidic solution which was opposed by stiff PS and it induced the film to roll into tubes because of the strain developed in the film. Strain was generated in acidic solution due to unequal swelling of polymer layers. Photolithography route was used for the formation of polymer rolled-up tubes in high quantity and of good quality. The position and arrangement of the tubes on the substrate are precisely defined by UV-photolithography. Directional rolling of crosslinked layer was performed by asymmetric photopatterning for the production of single tubes. The UV-radiation which crosslink the bilayer, was used stepwise in order to create asymmetric patterns of polymer layers. The copper TEM grids were used as a photomask. The fabricated tubes were characterized by optical microscopy and SEM.

The dependence of the tube's dimensions on the thickness of polymer layers and on the fabrication parameters (UV radiation dose, solvent selectivity) was studied. Thickness of the bilayer film was found to be the dominating factor to determine the tube's dimension. Diameter of the tubes increased with increasing the thickness of bilayer and it decreased with increasing the UV exposure time. Rate of rolling was faster in higher acidic solution compared to that in lower acidic solution. Furthermore, the method of gradient film preparation was used to study a broad range of parameters in a single experiment. The study of various experimental parameters would be helpful in the fabrication of polymer tube of desired dimensions. Moreover, the transportation of the fluid through the polymer microtube was observed. The presence of PSA molecules inside the polymer tube was detected with fluorescence microscope. Rhodamine dye was used for fluorescent labelling of the PSA molecules. Such

study in further detail may help to explore the behaviour of single molecule in confined media of polymer tube.

Some complex geometries like toroids and triangles were also fabricated using strain driven self-rolling approach of polymer film. The toroids formation proceeds from a circular opening in the film made by photolithography or by mechanical scratching followed by immersion of patterned sample in aqueous solution of DBSA. DBSA forms supramolecular complexes with pyridine rings of P4VP and increases the specific volume of the polymer. Since the PS layer is neutral in this solution, bilayer film develops strain due to unequal swelling of polymers in solution of DBSA and hence the film bends and scrolls in order to minimize its free energy. The increasing radius of the toroid causes lateral strain in the film, such that the strain isolines are closed concentric circles centered at the middle of the lithographic window. Furthermore, the kinetics of toroid formation was also studied. The equilibrium dimensions of toroid were determined by the balance of the bending and the stretching energies of the film. The width of the rolled-up bilayer was larger for the films with higher values of the bending modulus and smaller values of the effective stretching modulus. Possibility to functionalize the hidden walls of the tubes is one of the major advantages of the self-rolling approach. One can modify the surface of the film prior to rolling by magnetron sputtering of metal and upon rolling, micro-toroids with metallized inner surface could be obtained. The toroids with metallic inner surface are promising for the future research as IR-frequency range resonators.

Furthermore, we explored the self-rolling approach of polymer bilayer for the fabrication of metallic and multimetallic tubes. In a typical fabrication scheme, the multilayer consists of the bottom P4VP film, the intermediate PS film, and the top metallic or bimetallic film. The internal stress and the bending moment are induced in the film due to swelling of the bottom

P4VP layer after dipping the sample into aqueous solution of DBSA. The length of the tubes and the direction of rolling are determined by mechanical patterning of the film, whereas the tube diameter is tailored by varying the thickness of the polymer and metallic layers. After rolling, polymer template is removed by pyrolysis resulting in pure metal microtubes. The metallic tubes were characterized by optical microscopy, SEM, EDX, XPS and FTIR. Various combinations of metals could be used to fabricate multimetallic tubes from the self-rolling approach. From this approach, even those metals that have no propensity to self-roll could be rolled with help of polymer layers and then could be converted in pure tubes. Metallic microtubes fabricated by self-rolling approach may find applications in such fields as IR-waveguiding, microfluidics, enzyme bi-reaction, chemical and biochemical sensing.

Moreover, the procedure of strain driven self-rolling of polymeric material was also applied for the synthesis of ceramic tube. PDMS was used as a precursor of the silica and it is thermally transformed into silica. We synthesized silica tube using the self-rolling of P4VP/PS/PDMS trilayer film. Polymer template was removed by pyrolysis which also converts PDMS into silica. The fabricated tubes were characterized by optical microscopy, FTIR, SEM, FIB and EDX. The shrinkage of tubes were observed during pyrolysis due to chemical transformation of PDMS into silica and polymer removal. The hybrid tubes of silica with gold were also synthesized using this technique. To make hybrid tube the gold is deposited by physical vapour deposition on the crosslinked polymer. Pre-ceramic polymer processing have advantages over traditional ceramic processing techniques like, ease of processing from liquid precursors, tailorable chemistry and structure, and relatively low pyrolysis temperatures. Hybrid of silica and metal could be used for the catalytic applications.

Furthermore, an electrolysis reaction was demonstrated inside the self-rolled polymer tube to split the liquid stream in microsize droplets. A thin stripe of metal is partially enrolled

inside the polymer tube. In partially enrolled stripe, some part of stripe is inside the polymer tube whereas remaining part is outside from the tube. This partially rolled-up stripe is further used to make external ohmic contact. This external contact provides an electric current to the interior of tube and electrolysis process is performed. Furthermore, the closed planar electric circuits could be transfer to the interior of the tube by rolling. The micron-size bubbles were generated due to electrolysis. The potential application of this study is to fabricate nanoject-printing device as will be discussed later. Moreover, the synthesis of integrated-circuit device could be used for a great variety of practical applications in future.

Futher studies on the self-rolling approach could be extended on the basis of experimental details described in the present thesis. Since this approach combines highly developed planar methods of surface modification and self-organized formation of 3D micro- and nanostructures, the surfaces of tubes could be easily functionalized using photolithography, micro-contact printing, vacuum sputtering of metals, ion beams, plasma chemical activation etc. and this open novel and broad opportunities for mesoscale engineering of the tube-based devices. The self-rolled polymer tube or toroids with metallized inner surface could be used as waveguides for IR-radiation [Har00]. Toroids can also be used for the study of the behaviour of quantum dots or cells in confined space. In order to introduce this kind of study dots or cells could be encapsulated from the solution during the rolling.

The research on the self-rolled polymer tube can be extended by exploring these tubes as highly sensitive chemical or biological sensors. It was found during this work that polyelectrolyte molecule (conductive polymers) could be captured during the flow of polyelectrolyte solution in the self-rolled tube. Moreover, these polyelectrolyte molecules could further be stretched in the confined space of polymer tube. The hydrodynamic forces can be used for stretching of the molecule and then it could be deposited between two gold



electrodes [Figure 9.1 a]. The deposited molecule will work as a bridge between two electrodes. Alternatively, one can also stretch the molecule or make thin film of conductive molecules between two gold electrodes before rolling of polymer layer and later it could be transferred to the interior of the tube during rolling of the surface. Outer stripes could be used as electrodes to measure the conductivity. This kind of device will have potential application in chemical or biological sensor since when some conductive moiety comes in contact with bridge molecule, the ionic current change [Figure 9.1 b]. Hence, such sensors could be used to detect the conductive moiety.

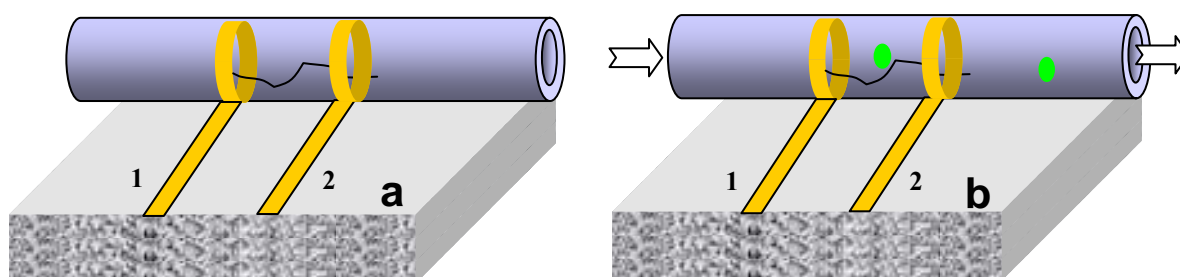


**Figure 9.1:** Schematic view of fabrication of bio chemical sensor using self-rolling procedure (a) Polymer tube with partially rolled gold electrodes with stretched conductive polymer. (b) Introduction of bioactive agent

Polymer based sensor are more sensitive for a wider range of gases even at low concentration at room temperature and the electric conductivity of these sensors can be switched between conducting and insulating state through doping and undoping cycles [Mia86]. The stretching of conductive molecule also provides the possibility to control and manipulate molecules to achieve particular functions at molecular scale. Hence, stretched molecule could be used for the fabrication of future miniaturized micro- and nanoelectronic devices.

Moreover, self-rolled polymer tube can be used to make nano-jet printing device. The generation of bubble inside the self-rolled tube has been demonstrated in this thesis and this can be explored for the formation of printing device [Figure 9.2]. In this device generated gas bubble push a droplet (with particle) outside the tube and with help of nanoplotter one can put these droplets in a fixed place and fabricate a patterned assembly of particles.

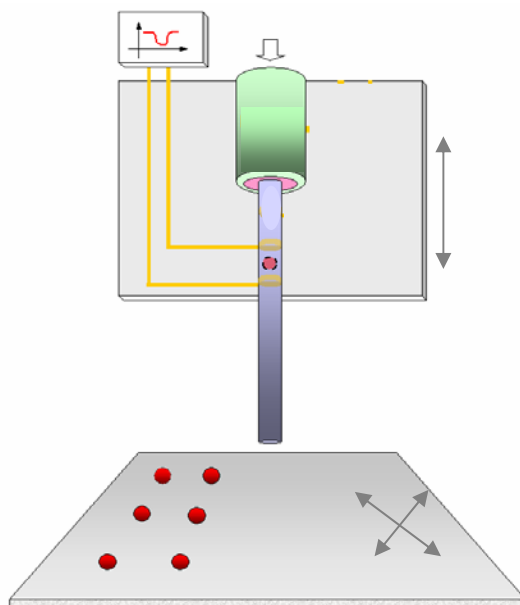


**Figure 9.2:** *Fabrication of nano-jet printing using self-rolled polymer tube*

Furthermore, large quantities of calibrated rolled-up tubes can be used in the formation of smart membranes. These smart membranes can be formed by polymer/metal hybrid tube. In order to fabricate smart membrane, a thin film of nickel and gold can be deposited on the crosslinked P4VP/PS bilayer. After tube formation these rolled-up tubes could be separated from the substrate using a sharp object and dispersed in a curable polymer and align by magnetic field or electric field. The curable matrix is cured after the alignment and then sliced-up by microtone to facilitate the open end of tubes. The synthesized tubes will have a sequence of Au/Ni/PS/P4VP layer from inner wall to outer wall. The gold is a standard substrate for the bio-molecules, hence, these tubes can be used to study the behaviour of DNA, biocatalysts, antibodies.

In the present work polymer, metal, ceramic and metal-ceramic hybrid films were transformed into various objects including microtubes, microtoroids etc. using strain driven self-rolling phenomena of P4VP/PS thin bilayer film. In future, study of the self-rolling approach of polymer layers can be explored for the synthesis of complex three-dimensional objects like solenoids, electrochemical capacitors, or supercapacitors of metal and ceramic [In06]. The easy control of dimension and accuracy in positioning of the tube could be used with the mature silicon based integrated circuit and micro-electro-mechanical systems.

## References

- [Ade90] Adema G. M., Turlik I., Hwang L.T., Rinne G. A., Berry M., *IEEE, Trans. Componets, Hybrids. Manuf. Tech.* **1990**; 13(4), 766.
- [Ade91] Adem E., *VG scientific XPS handbook, VG Scientific Limited, East Grinstead, 1991.*
- [Ala04] Alavi K. F., Gedde U. W., *Polym. Degrad. Stabil.* **2004**; 84 (3): 469.
- [Alc05] Alcoutlabi M., McKenna G. B. *J. Phys.: Condens. Mater* **2005**; **17**: R461.
- [And76] Andrade J. D., *ACS Symp. Series, 31, Am. Chem. Soc. Washington DC* **1976**; 1.
- [Ann03] Anna S. L., Bontoux N., Stone H. A., *Appl. Phys. Lett.* **2003**; 82: 364.
- [Ara08] Arakawa T., Yamamoto T., Shoji S., *Sens. Actu. A* **2008**; 243: 58.
- [Arm03] Armani D. K., Kippenberg T. J., Spillane S. M., Vahala K., *Nature* **2003**; 421: 905.
- [Arm07] Armani A. M., Srinivasan A., Vahala K. J., *Nano Lett.* **2007**; 7(6): 1823.
- [Arn00] Arndt K. F., Kuckling D., Richter A., *Polym. Adv. Technol.* **2000**; 11: 496.
- [Azz87] Azzam, R. M., Bashara N. M., *Ellipsometry and Polarized Light; North-Holland Publishing Company: Amsterdam* **1987**.
- [Bao08] Bao N., Wang J., Chang L., *Anal. Bioanal. Chem.* **2008**; 391: 933.
- [Bar96] Bradbury, S. and Evennett, P., *Fluorescence microscopy., Contrast Techniques in Light Microscopy., BIOS Scientific Publishers, Ltd., Oxford, United Kingdom* **1996**.
- [Bar04] Baroud C. N., Willaime H., *Compt. Rend. Phys.* **2004**; 5: 547.
- [Bar08] Barik T. K., Sahu B., Swain V., *Parasit. Res.* **2008**; 103 (2): 253.
- [Bec02] Becker H., Locascio L. E., *Talanta* **2002**; 56: 267.
- [Bee02] Beebe D. J., Mensing G. A., Walker G. M., *Annu. Rev. Biomed. Eng.* **2002**; 4: 261.

- [Ben99] Benoit D., Chaplinski V., Braslau R., Hawker J. C., *J. Am. Chem. Soc.* **1999**; 121: 3904.
- [Bie00] Biesalski M., Rule J., *Langmuir* **2000**; 16: 1943.
- [Bik07] M. Bikram, A. M. Gobin, R.E. Whitmire, J. L. West, *J. Cont. Rel.* **2007**;123: 219.
- [Bli94] Blitz J. P., Augustine S. M., *Spectroscopy* **1994**; 9 (8): 28.
- [Bog00] Bognitzki M., Hou H., Ishaque M., Frese T., Hellwig M., Schwarte C., Schaper A., Wendorff J. H., Greiner A., *Adv. Mater.* **2000**; 12 (9): 637.
- [Bra90] Brannon P. L., Harland R. S., *Absorb. Polym. Tech., Elsevier, Amsterdam* **1990**; Ch 1-4.
- [Bra03] Bradley K., Gabriel J. P., Star A., Grüner G., *Appl. Phys. Lett.* **2003**; 83: 3821.
- [Bri98] Briggs D., *Surface analysis of polymers by XPS and static SIMS*, Cambridge University Press, **1998**.
- [Bro07] Brown M. A., Rosakis A. J., Feng X, Huang Y., Üstündag E., *Int. J. Solids Struct.* **2007**; 44 (6): 1755.
- [Buf76] Buffet P. H., Borel J. P., *Phys. Rev. A.* **1976**; 13: 2287.
- [Cac87] Caceres P., Pierola I. F., *Makromol. Chem. Rapis Commun.* **1987**; 8: 573.
- [Cai00a] Cai M., Painter O., Vahala K. J., *Phys. Rev. Lett.* **2000**; 85: 74.
- [Cai00b] Cai M., Painter O., Vahala K. J., Sercel P. C., *Opt. Lett.*, **2000**; 25: 1430.
- [Cam01] Camino G., Lomakin S. M., Lazzari M., *Polymer* **2001**; 42 : 2395.
- [Cav07] Cavallo F., Songmuang R., Ulrich C., Schmidt O. G., *Appl. Phys. Lett.* **2007**; 90: 193120.
- [Cha95] Chastain J., King R. C., *Handbook of X-ray photoelectron spectroscopy. Eden Prairie: Physical Electronics Inc, 1995*.
- [Cha06] Chaudhary Y. S., Ghatak J., Bhatta U. M., Khushalani D., *J. Mater. Chem.* **2006**; 16: 3619.

- [Cha08a] Chabert M., Viovy J. L., *PANS* **2008**; 105 (9): 3191.
- [Cha08b] Charlot S., Gue A. M., Tasselli J., Marty A., Abgrall P., Esteve D., *J. Micromech. Microeng.* **2008**; 18: 17003.
- [Che90] Chescoe D., Goodhew P. J., *The operation of transmission and scanning electron microscopes; Oxford University press* **1990**
- [Che05] Chen D. L., Gerdts C. J., Ismagilov R. F., *J. Am. Chem. Soc.* **2005**; 127: 9672.
- [Cho06] Chou A., *Science* **2006**; 313: 164.
- [Chu08] Chun I. S., Verma V. B., Elarde V. C., Kim S. W., Zuo J. M., Coleman J. J., Lia X., *J. Crystal Growth* **2008**; 310: 2353.
- [Coo02] Cooley P., Wallace D., Antohe B., *J. Assoc. Lab. Auto.* **2002**; 7 (5): 33.
- [Cor03] Coradin T., Nassif N., Livage J., *Appl. Microbio. Biotech.* **2003**; 61 (5): 429.
- [Cro93] Crooks R. M., Sun L., Xu C., Hill S. L., Ricco A. J., *Spectroscopy* **1993**; 8 (7), 28.
- [Day99] Dayal U., Mehta S. K., Choudhari M. S., Jain R., *J. Macromol. Sci-Rev Macromol. Chem. Phys.* **1999**; C39: 507.
- [Deg80] Delly J. G., *Photography Through the Microscope, Eastman Kodak Company* 1980.
- [Dem06] Demello A. J., *Nature* **2006**; 442: 394.
- [Den02] Deneke Ch., Müller C., Jin-Phillipp N. Y., Schmidt O. G., *Semicond. Sci. Technol.* **2002**; 17: 1278.
- [Den04a] Deneke Ch., Jin-Phillipp N. Y., Loa I., Schmidt O. G., *Appl. Phys. Lett.* **2004**; 84: 4475.
- [Den04b] Denke Ch., Schmidt O. G., *Physica E* **2004**; 23: 269.
- [Den04c] Deneke Ch., Schmidt O. G. *Appl. Phys. Lett.* **2004**; 85(14): 2914.
- [Den06a] Deneke Ch., Schmidt O. G., *Appl. Phys. Lett.* **2006**; 89: 123121.

- [Den06b] Deneke Ch., Zschieschang U., Klauk H., Schmidt O. G., *Appl. Phys. Lett.* **2006**; 89: 123121.
- [Din98] Dini D., Decker F., *Electrochimica Acta* **1998**; 43 (19-20): 2919.
- [Dre03] Dreyfus R., Tabeling P., Willaime H., *Phys. Rev. Lett.* **2003**; 90: 144505/1
- [Eba06] Ebara M., Hoffman J. M., Hoffman A. S., Stayton P. S., *Lab Chip* **2006**; 6: 843.
- [Fan08] Fang C. L., Qian K., Zhu J., Wang S., Lv X., Yu S. H., *Nanotechnology* **2008**; 19: 125601.
- [Fed06] Fedorchenko A. I., Wang A. B., mashanov V. I., Huang W. P., Cheng H. H., *Appl. Phys. Lett.* **2006**; 89: 43119.
- [Fen07] Feng J., Yan W., Gou Z., Weng W., Yang D., *J. Mat. Sci.: Mater. in Medicine* **2007**; 18: 2167.
- [Fid07] Fidalgo L. M., Abell C., Huck W. T. S., *Lab Chip* **2007**; 7: 984
- [Flo53] Flory P. J., *Principles Polym. Chem.*, Cornell U. Press, **1953**.
- [Fre00] Freund L.B., *J. Mech. Phys. Solids* **2000**; 48: 1159.
- [Fuj98] Fujinami Y., Hayashi H., Ebe A., Imai O., Ogata K., *Mater. Chem. Phys.* **1998**; 54 (1-3): 102.
- [Fuj06] Fujikawa S., Takaki R., Kunitake T., *Langmuir* **2006**; 22 (21): 9057.
- [Gan01] Ganan-Calvo A. M., Gordillo J. M., *Phys. Rev. Lett.* **2001**; 87: 274501.
- [Gan04] Ganan-Calvo A. M., *Phys. Rev. E* **2004**; 69: 27301.
- [Gar04] Garstecki P., Gitlin I., Diluzio W., Whitesides G. M., Kumacheva E., Stone H. A., *Appl. Phys. Lett.* **2004**; 85 (13): 2649.
- [Gie03] Giessibl F., *Rev. Mod. Phys.* **2003**; 75 (3): 949.
- [Gir07] Giordano C., Todaro M. T., Salhi A., Martiradonna L., Viola I., Passabi A., Carbone L., Gigli G., Passaseo A., De Vittorio M. *Microelectron. Eng.* **2007**; 84: 1408

- [Gol81] Goldstein, G. I., Newbury D. E., Echlin P., Joy D. C., Fiori C., Lifshin E., *Scanning Electron Microscopy and X-ray Mmicroanalysis*. New York: Plenum Press, **1981**.
- [Gol01] Golod S. V., Prinz V. Ya., Mashanov V. I., Gutakovsky A. K., *Semicond. Sci. Technol.* **2001**; 16 (3): 181.
- [Gol03] Goldstein J. I., Newbury D. E., Echlin P., Joy D. C., Lyman C. E., Lifshin E., Sawyer L. C., Michael, J. R., *Scanning Electron Microscopy and X-Ray Microanalysis*, Springer **2003**.
- [Gol04] Golod S. V., Prinz V. Ya., Wägli P., Zhang L., Kirfel O., Deckhardt E., Glaus F., David C., Grützmacher D., *Appl. Phys. Lett.* **2004**; 84 (17): 3391.
- [Gol05] Golod S. V., Prinz V. Ya., Mashanov V. I., *Thin Solid Films* **2005**; 489: 169.
- [Gor04] Gordillo J. M., Cheng Z., Ganan-Calvo A. M., Marquez M., Weitz D. A., *Phys. Fluids* **2004**; 16 (8): 2828.
- [Gri86] Griffiths P. R., J. A. Dehaseth, *Fourier Transform Infrared Spectrometry*. New York: Wiley, **1986**.
- [Gun04] Gunther A., Khan S. A., Thalmann M., Trachsel F., Jensen K. F., *Lab Chip* **2004**; 4: 278.
- [Gun06] Gunther A., Jensen K. F., *Lab Chip* **2006**; 6: 1487.
- [Guo06] Guoa Z., Zhao T. S., Shi Y., *Phys Fluids* **2006**; 18: 67107.
- [Ha97] Ha S.-W., Hauert R., Ernst K.-H., Wintermantel E., *Surf. Coat. Tech.* **1997**; 96: 293.
- [Hal08] Hallow D. M., Seeger R. A., Kamaev P. P., Prado G. R., LaPlaca M. C., Prausnitz M. R., *Biotech. Bioeng.* **2008**; 99 (4): 846.
- [Har00] Harrington J., *Fiber Integ. Opt.* **2000**; 19: 211.
- [Har05] Harnish B., Robinson J. T., Pei Z., Ramström O., Yan M., *Chem. Mater.* **2005**; 17: 4092.



- [Hat06] Hatakeyama T., Chen D. L. L., Ismagilov R. F., *J. Am. Chem. Soc.* **2006**; 128: 2518.
- [Hel73] Helfrich W. Z., *Naturforsch.* **1973**; 28: 693.
- [Het05] Hetsroni G., Mosyak A., Pogrebnyak E., Yarin L. P., *Int. J. Heat Mass Transfer* **2005**; 48: 1982.
- [Hin06] Hinterdorfer P., Dufrene Y. F., *Nature Methods* **2006**; 3: 5.
- [Ho98] Ho C. M., Tai Y. C., *Annu. Rev. Fluid Mech.* **1998**; 30: 579.
- [Hof06] Hoffmann F., Cornelius M., Morell J., Fröba M., *Ange. Chem. Int. Ed.* **2006**; 45 (20): 3216.
- [Hop04] Hopkins A. R., Lipeles R. A., Kao W. H., *Thin Solid Films* **2004**; 447: 474.
- [Hu03] Hu J.Q., Jiang Y., Meng X. M., Lee C. S., Lee S. T., *Chem. Phys. Lett.* **2003**; 367: 339.
- [Hua05] Huang M., Boone C., Roberts M., Savage D. E., Lagally M. G., Shaji N., Qin H., Blick R., Nairn J. A., Liu F., *Adv. Mater.* **2005**; 17 (23): 2860.
- [Hue07] Huebner A., Srisa-Art M., Holt D., Abell C., Hollfelder F., deMello A. J., Edel J. B., *Chem. Commun.* **2007**; 1218.
- [Ich96] Ichikawa T., Nakajima T., *In: Polym. Mater. Encyclo. Salamone (Ed), CRC, Boca Raton (Florida)* **1996**; 8051.
- [In06] In H. J., Kumar S., Horn Y. S., Barbastathis G., *Appl. Phys. Lett.* **2006**; 88: 83104.
- [Hub03] Huber D.L., Manginell R. P., Samara M. A., Kim B. I., Bunker B. C., *Science* **2003**; 301: 352.
- [Ika96] Ikkala O., Ruokolainen J., Torkkeli M., Serimaa R., Brine G. T., *Macromol. Symp.* **1996**; 112: 191.
- [Ikk95] Ikkala O., Ruokolainen J., Brinke G., Torkkeli M., Serimaa R., *Macromolecules.* **1995**; 28: 7088.

- [Ion06] Ionov L., Houbenov N., Sidorenko A., Stamm M., Minko S., *Adv. Func. Mater.* **2006**; 16: 1153.
- [Ita06] Itaka K., Yamashiro M., Yamaguchi J., Yaginuma S., Haemori M., Koinuma H., *Appl. Surf. Sci.* **2006**; 252(7): 2562.
- [Iye03] Iyer K. S., Zdyrko, B., Malz H., Pionteck J., Luzinov I., *Macromolecules* **2003**; 36(17): 6519
- [Jan07] Janssen G. C. A. M., *Thin Solid Films* **2007**; 515 (17): 6654.
- [Jav09] Javaid R, Tanaka D. A. P, Kawanami H, Suzuki T. M. *Chem. Lett.* **2009**; 38 (2): 146.
- [Jia03] Jian J., Chen X., Ma Y., Li X., *J. Phys. Condens. Matter* **2003**; 15: 8177.
- [Jou91] Jou J. H., Hsu L., Yeh S., Shyy T., *Thin Solid Films* **1991**; 201(1): 69.
- [Kac02] Kaczmarek H., Kowalonek J., Szalla A., Sionkowska A., *Surf. Sci.* **2002**; 507-510: 883.
- [Kan06] Kanakubo M., Hiejima Y., Minami K., Aizawa T., Nanjo H., *Chem. Commun* **2006**; 1828.
- [Kel00] Kelly P.J., Arnell R.D., *Vacuum* **2000**; 56: 159.
- [Ker70] Kern W. A., D. A. Poutinen, *RCA Rev. vol.* **1970**; 31: 187.
- [Kha02] Khandurina J., Guttman A., *J. Chromatography A* **2002**; 943: 159.
- [Kha06a] Khang D. Y., Jiang H., Huang Y., Rogers J. A., *Science* **2006**; 311 (5758): 208.
- [Kha06b] Khalis I. M., Qiaosheng P., Alvarez J. C., *Angew. Chem. Int. Ed.* **2006**; 45 (35) : 5829
- [Kim99] Kim J. S., Paik K. W., Oh S.H., *J. Appl. Phys.* **1999**; 86 (10): 5474.
- [Kim06a] Kim Y. H., Lee D. K., Cha H. G., Kim C. W., Kang Y. C., Kang Y. S., *J. Phys. Chem. B* **2006**; 110: 24923.
- [Kim06b] Kim S. J., Song Y. A., Skipper P. L., Han J., *Anal. Chem.* **2006**; 78 (23): 8011.

- [Kip06] Kipp T., Welsch H., Strelow C., Heyn C., Heitmann D., *Phys. Rev. Lett.* **2006**; 96: 77403.
- [Klo07] Klostranec J. M., Xiang Q., Farcas G. A., Lee J. A., Rhee A., Lafferty E. I., Perrault S. D., Kain K. C., Chan C. W., *Nano Lett.* **2007**; 7 (9): 2812.
- [Kob04] Kobayashi J., Mori Y., Okamoto K., Akiyama R., Ueno M., Kitamori T., Kobayashi S., *Science* **2004**; 304: 1305.
- [Kul89] Kulicke W. M., Nottelmann H., *Adv. Chem. Ser.* **1989**; 223: 15.
- [Kum08] Kumar K., Luchnikov V., Nandan B., Senkovskyy V., Stamm M., *Euro. Polym. Jour.* **2008**; 44 (12): 4115.
- [Kum70] Kumar, R., Kuloor N. R., *Adv. Chem. Eng.* **1970**; 8: 255.
- [Kyr97] Kyriakides N.K., Kastrinakis E.G., Nychas S. G., Goulas A. *Canad. J. Chem. Eng.* **1997**; 75: 684.
- [Lak99] Lakowicz J. R., ed. *Principle of Fluorescence Spectroscopy. 2<sup>nd</sup> ed. Plenum Press, New York 1999.*
- [Lam07] Lambert P., Capillary Forces in Microassembly, *Series Microtech. MEMS 2007*; XXII, 263.
- [Lan86] Landau L. D., Lifshitz E. M., *Theory of Elasticity, 15 (Pergamon, New York, 1986).*
- [Lan99] Landau, L. D.; Lifshitz, E. M.; *Theory of Elasticity, Reed Elsevier Publishing, 1999*; Chap. 18.
- [Lee02] Lee S. B., Mitchell D. T., Trofin L., Nevanen T. K., Söderlund H., Martin C. R., *Science* **2002**; 296. (5576): 2198.
- [Lee05] Lee S., Sutomo W., Liu C., Loth E., *Int. J. of multiphase flow* **2005**; 31: 706
- [Lel04] Lelea D., Nishio S., Takano K., *Int. J. Heat Mass Transfer* **2004**; 47: 2817.
- [Lic05] Lichtman J. W., Conchello J. A., *Nature methods* **2005**; 2 (12): 919.
- [Li05] Li N., Li X., Wang W., Qiu S., *Mater. Chem. Phys.* **2005**; 91: 223.

- [Li06] Li, Z. Y., Zhang, Z. Y., Scherer, A., Psaltis, D. *Opt. Express* **2006**; 14(22): 10494.
- [Li08] Li X., *J. Phys. D: Appl. Phys.* **2008**; 41:193001
- [Lin04] Link D. R., Anna S. L., Weitz D. A., Stone H. A., *Phys. Rev. Lett.* **2004**; 92: 54503/1.
- [Liu06] Liu N. G., Prall B. S., Klimov V. I., *J. Am. Chem. Soc.* **2006**; 128: 15362.
- [Loc04] Lockwood D. J., Pavesi L., *Silicon Photonics, Book Series: Topics in Applied Physics* **2004**; 94: 1.
- [Luc05] Luchnikov V., Sydorenko O., Stamm M., *Adv. Mater.* **2005**; 17 (9): 1777.
- [Luc06] Luchnikov V., Stamm M., Akhmadaliev C., Bischoff L., Schmidt B. J., *Micromech. Microeng.* **2006**; 16 (8): 1602.
- [Luc07] Luchnikov V., Stamm M., *Physica E* **2007**; 37 (1-2): 236.
- [Luc08] Luchnikov V., Kumar K., Stamm M., *J. Micromech. Microelect.* **2008**; 18 (3): 35041.
- [Mal99] Mala G. M., Li D., *Int. J. Heat Fluid Flow* **1999**; 20:142.
- [Mar94] Martin C. R., *Science* **1994**; 266: 1961.
- [Mar98] Marzolin C., Terfort A., Tien J., Whitesides G. M., *Thin Solid Films* **1998**; 315 (1-2): 9.
- [Mar03] Martin C. R., Kohli P., *Nat. Rev. Drug Disc.* **2003**; 2: 29.
- [Mca03] Mcallister D. V., Wang P. M., Davis S. P., Park J. H., Canatella P. J., Allen M. G., Prausnitz M. R., *Proc Natl Acad Sci U S A* **2003**; 100:13755.
- [Mca99] McAllister D.V., Cros F., Davis S. P., Matta L. M., Prausnitz M. R., Allen A. G., *Proc. 10th Int. Conf. Solid State Sens. Actu. (Transducers'99), Technical Digest, Chicago, USA; 1999*: 1098.
- [Mei08] Mei Y., Huang G., Solovev A. A., Urena E. B., Mönch I., Ding F., Reindl T.; Fu R. K. Y., Chu P. K., Schmidt O. G. *Adv. Mater.* **2008**; 20: 4085.

- [Men04] Mendach S., Schumacher O., Heyn Ch., Schnüll S., Welsch H., Hansen W., *Physica E* **2004**; 23: 274.
- [Mia86] Miasik J. J., Hooper A., Tofield B. C. J. *Chem. Soc. Faraday Trans.1* **1986**; 82: 1117.
- [Miy82] Miyahara T., Terakado H., Takahashi T. *J. Chem. Eng. Jpn* **1982**; 45: 454.
- [Mou95] Moulder J. F., Stickle W. F., Sobol P. E., Bomben K. D., *Handbook of X-ray Photoelectron Spectroscopy*, ed. Jill Chastain and Roger C. King Jr.: *Physical Electronics, Inc.*, USA. **1995**, 11.
- [Mur00] Murphy D. B., *Fundamentals of Light Microscopy and Electronic Imaging*. *Cambridge University Press; illustrated edition* **2000**.
- [Mur05] Murakami T. N., Fukushima Y., Hirano Y., Tokuoka Y., Takahashi M., Kawashima N., *Appl. Surf. Sci.* **2005**; 249 (1-4): 425
- [Mön01] Mönch W., *Semiconduct. Surf. Interfaces*, Springer, Berlin; **2001**.
- [Nak05a] Nakade M., Ichihashi K., Ogawa M., *J. Ceram. Soc. Japan* **2005**; 113 (4): 280
- [Nak05b] Nakade M., Ichihashi K., Ogawa M., *J. Porous Mater.* **2005**; 12: 79.
- [Nar95] Narayanan P. V., *J. Biomat. Sci. Polym. Edi.* **1995**; 6 (2): 181.
- [Nik03] Nikishkov G. P., *J. Appl. Phys.* **2003**; 94 (8): 5333.
- [Nas05] Nastaushev V. Yu., Prinz V. Ya., Svitashva S. N., *Nanotechnology* **2005**; 16: 908.
- [Niu04] Niu J., Sha J., Zhang N., Ji Y., Ma X., Yang D., *Physica E* **2004**; 23: 1.
- [Nur06] Nurmukhametov R. N., Volkova L. V., Kabanov S. P. *J. Appl. Spectro.* **2006**; 73 (1):55.
- [Oca03] Ocampo J. M. Z., Vaccaro P. O., Fleischmann T., Wang T. S., Kubota K., Aida T., Ohnishi T., Sugimura A., Izumoto R., Hosoda M., Nashima S., *Appl. Phys. Lett.* **2003**; 83: 3647

- [Oco92] O'connor D. J., Sexton B. A., Smart R. St. C., *Surface analysis method in materials science, Springer-Verlag, Heidelberg, 1992.*
- [Ohl00] Ohlidal I., Franta D., *Ellipsometry of thin film systems, in Progress in Optics, 41, ed. E. Wolf, Elsevier, Amsterdam 2000*, 181.
- [Omi08] Omidian H., Park K., *J. Drug Deliv. Sci. Technol.* **2008**; 18 (2): 83.
- [Ory00] Ory E., Yuan H., Prosperetti A., Popinet S., Zaleski S., *Phys. Fluid.* **2000**; 12 (6): 1268.
- [Par03] Park H. B., Han D. W., Lee Y. M., *Chem. Mater* **2003**; 15 (12): 2346
- [Poo90] Pool R., *Science* **1990**; 247: 1410.
- [Po94] Po R., *A patent survey, J Macromol. Sci. Rev. Macromol. Chem. Phys.* **1994**; C34: 607.
- [Pri00] Prinz V. Ya., Seleznev V. A., Gutakovsky A. K., Chehovskiy A. V., Preobrazenskii V. V., Putyato M. A., Gavrilova T. A., *Physica E* **2000**; 6: 828.
- [Pri01] Prinz V. Ya., Grützmacher D., Beyer A., David C., Ketterer B., Deckardt E., *Nanotechnology* **2001**; 12: 399.
- [Pri02] Prinz V. Ya., Chehovskiy A. V., Preobrazhenskii V.V., Semyagin B. R., Gutakovsky A. K., *Nanotechnology* **2002**; 13:231.
- [Pri03a] Prinz V. Ya., *Microele. Eng.* **2003**; 69: 466.
- [Pri03b] Prinz A.V., Prinz V.Y., Seleznev V.A., *Microele. Eng.* **2003**; 67: 782.
- [Pri03c] Prinz A V., Prinz V. A., *Surf. Sci.* **2003**; 532-535: 911.
- [Pri04a] Prinz V. Ya., *Physica E* **2004**; 23: 260.
- [Pri04b] Prinz V. Ya., *Physica E* **2004**; 24: 54.
- [Pri06] Prinz V. Ya, Golod S. V, *J. Appl. Mech. Tech. Phys.* **2006**; 47 (6): 867.
- [Pru98] Prucker O., Schimmel M., Tovar G., Knoll W., R uhe J., *Adv. Mater.* **1998**; 10 (14): 1073.
- [Pur46] Purcell E. M., *Physical Review* **1946**; 69: 681.

- [Qin05] Qin H., Shaji N., Merrill N. E., Kim H. S., Toonen R. C., Blick R. H., Roberts M. M., Savage D. E., Lagally M. G., Celler G. *New J. Phys.* **2005**; 7: 1.
- [Rab02] Rabiei P., Steier W. H., Zhang C., Dalton L. R., *J. Lightwave Tech.* **2002**; 20(11): 1968.
- [Ran75] Ranby R., Rabek J. F., *Photodeg. Photooxi. Photostab. Polym.*, Wiley, New York **1975**. pp.167.
- [Rob06] Roberts M. M., Klein L. J., Savage D. E., Slinker K. A., Friesen M., Celler G., Eriksson M. A., Lagally M. G., *Nat. Mater.* **2006**; 5: 388.
- [Ros91] Rost F., *Quantitative fluorescence microscopy. Cambridge University Press, Cambridge, United Kingdom 1991*.
- [Ros95] Rost, F., *Fluorescence microscopy. Vol. II. Cambridge University Press, Cambridge, United Kingdom 1995*.
- [Ros03] Rosseinsky D. R., Glidle A., *Electrochem. Soc.* **2003**; 150 (9): C641.
- [Rus85] Russell, S. D., Daghljan, C. P., *J. Elect. Microsc. tech.* **1985**; 2 (5): 489.
- [Rus96] Ruisanchez I., Potokar P., Zupan J., V. Smolej, *J. Chem. Inf. Comput. Sci.*, **1996**; 36(2): 214.
- [Sch01a] Schmidt O. G., *Nature* **2001**; 410: 158.
- [Sch01b] Schmidt O. G., Jin-Phillipp N. Y., *Appl. Phys. Lett.* **2001**; 78: 3310
- [Sch01c] Schmidt O. G., Schmarje N., Deneke C., Müller C., Jin-Phillipp N. Y., *Adv. Mater.* **2001**; 13 (10): 756.
- [Sch02a] Schmidt O. G., Deneke C., Manz Y. M., Müller C., *Physica E* **2002**; 13: 969.
- [Sch02b] Schmidt O. G., Deneke C., Schmarje N., Müller C., Jin-Phillipp N. Y., *Mater. Sci. Eng. C* **2002**; 19 : 393.
- [Sch02c] Schmidt O. G., Deneke Ch., Kiravittaya S., Songmuang R., Heidemeyer H., Nakamura Y., Zapf-Gottwick R., Müller C., Jin-Phillipp N. Y., *J. Sel. Topics in Quant. Electr.* **2002** ; 8(5): 1025.

- [Sch02d] Schmidt O. G., Deneke Ch., Nakamura Y., Zapf-Gottwick R., Müller C., Jin-Phillipp N. Y., *Adv. Sol. State Phys.* **2002**; 42: 231.
- [Sch03] Schnyder B., Lippert T., Kötz R., Wokaun A., graubner V. M., Nuyken O., *Surf. Sci.* **2003**; 532: 1067.
- [Sch05] Schumacher O., Mendach S., Welsch H., Schramm A., Heyn C., Hansen W. *Appl. Phys. Lett.* **2005**; 86: 143109.
- [Sel03] Seleznev V., Yamaguchi H., Hirayama Y., Prinz V. Ya., *Jpn. J. Appl. Phys. Part 2* **2003**; 42: L791.
- [Sey90] Seyferth D., *Adv. Chem. Ser.* **1990**; 224: 565
- [Sha06] Sharma S., Buchholz K., Lubner S. M., Rant U., Tornow M., Abstreiter G., *J. Microelectromech. Syst.* **2006**; 15(2):308.
- [Shi72] Shirley D.A., *Phys. Rev. B* **1972**; 5: 4709.
- [Shu07] Shui L., Eikel J. C. T., Berg A. V. D, *Sens Actu. B* **2007**; 121 : 263.
- [Sil81] Silverstein R. M., Bassler G. C., Morrill T. C., *Spectrometric Identification of Organic Compounds*, 4<sup>th</sup> Ed., New York: Wiley **1981**: 166.
- [Sil88] Silverstein R. M., Bassler G. C., Morrill T. C., *Spectrometric Identification of Organic Compounds*, 5<sup>th</sup> Ed. New York: Wiley, **1988**.
- [Sku08] Skurtys O., Aguilera J. M., *Food Biophysics* **2008**, 3: 1.
- [Smi79] Smith A. L., *Applied Infrared Spectroscopy*. New York: Wiley, **1979**.
- [Son03] Song H., Tice J. D., Ismagilov R. F., *Angew. Chem. Int. Ed.* **2003**; 42: 767.
- [Son06a] Songmuang R., Denke C. H., Schmidt O. G., *Appl. Phys. Lett.* **2006**; 89: 223109.
- [Son06b] Song H., Chen D. L., Ismagilov R. F., *Angew. Chem. Int. Ed.* **2006**, 45, 7336.
- [Son07] Songmuang R., Rastelli A., Mendach S., Denke Ch., Schmidt O. G., *Microele. Eng.* **2007**; 84: 1427.
- [Sor93] Soref R. A., *Proceedings of the IEEE* **1993**; 81 (12 ): 1687.
- [Spa07] Sparks D., Cruz V., Najafi N., *Sens. Actu. A-Phys.* **2007**; 135: 827.



- [Squ05] Squires T. M., Quake S. R., *Rev. Mod. Phys.* **2005**; 77 (3): 977.
- [Sta05] Stavitskiy S. M., Edel J. B., Li Y., Samiee K. T., Luo D., Craighead H. G., *Nanotechnology* **2005**; 16: S314
- [Ste08] Stemmann A., Heyn Ch., Köppen T., Kipp T., Hansen W., *Appl. Phys. Lett.* **2008**; 93: 123108.
- [Sto01] Stone H. A., Kim S., *AIChE* **2001**; 47 (6): 1250.
- [Sto04] Stone H. A., Stroock A. D., Ajdari A., *Annu. Rev. Fluid Mech.* **2004**; 36: 381.
- [Sto09] Stoney G. G., *Proc Royal Society. London. Series A* **1909**; 82 (553): 172.
- [Str08] Strelow Ch., Rehberg H., Schultz C. M., Welsch H., Heyn Ch., Heitmann D., T. Kipp, *Phys. Rev. Lett.* **2008**; 101, 127403
- [Sug01] Sugiura S., Nakajima M., Iwamoto S., Seki M., *Langmuir* **2001**; 17, 5562.
- [Sun06] Sun Y. G., Choi W. M., Jiang H. Q., Huang Y. Y., Rogers J. A., *Nat. Nanotech.* **2006**; 1 (3): 201.
- [Tak08] Takei K., Kawashima T., Kawano T., Takao H., Sawada K., Ishida M., *J. Micromech. Microeng.* **2008**; 18: 35033.
- [Tan06] Tan Y.C., Cristini V., Lee A. P., *Sens. Actuat. B* **2006**; 114 (1): 350
- [Teg04] Tegenfeldt J. O., Prinz C., Cao H., Huang R. L., Austin R. H., Chou S. Y., Cox E. C., Sturm J. C., *Anal. Bioanal. Chem.* **2004**; 378: 1678.
- [The99] Thess A., Boos W., *Phys. Fluids* **1999**; 11(12): 3852.
- [Tho01] Thorsen T., Roberts R. W., Arnold F. H., Quake S. R., *Phys. Rev. Lett.* **2001**; 86: 4163.
- [Thu06] Thurmer D. J., Deneke C., Mei Y. F., Schmidt O. G., *Appl. Phys. Lett.* **2006**; 89: 223507.
- [Tim25] Timoshenko S., *J. Opt. Soc. Am.* **1925**; 11: 233.
- [Tom05] Handbook of Ellipsometry Harland G. Tompkins, Eugene A. Irene, *William Andrew Publishing, Norwich, NY, USA*, **2005**.

- [Tsu97] Tsui Y.C., Clyne T.W., *Thin Solid Films* **1997**; 306: 23.
- [Uta05] Utada A. S., Lorenceau E., Link D. R., Kaplan P. D., Stone H. A., Weitz D. A., *Science* **2005**; 308; 537.
- [Vah03] Vahala K. J., *Nature* **2003**; 424: 839.
- [Voi01] Voigt J., Shi F., Edinger K., Güthner P., Rangelow I. W., *Microelect. Eng.* **2001**; 57-58: 1035.
- [Vor02] Vorob'ev A. B., Prinz V. Ya., *Semicond. Sci. . Technol.* **2002**; 17(6): 614.
- [Win92] Windischmann H., *Critical Rev. Solid State Mater. Sci.* **1992**; 17 (6): 547.
- [Wol00] Wolf E., *Progress in Optics. New York: Elsevier Science* **2000**; 41.
- [Wol01] Wolf S. A., Awschalom D. D., Buhrman R. A., Daughton J. M., Molnár S. V., Roukes M. L., Chtchelkanova A. Y., Treger D. M., *Science* **2001**; 294 (5546): 1488.
- [Wra71] Wraith, A. E., *Chem. Eng. Sci.* **1971**; 26: 1659.
- [Wu01] Wu X. C., Song W. H., Wang K. Y., Hu T., Zhao B., Sun Y. P., Du J. J., *Chem. Phys. Lett* **2001**; 336: 53.
- [Xia98] Xia Y., Whitesides G. M., *Annu. Rev. Mater. Sci.* **1998**; 28: 153.
- [Xio07] Xiong R., Bai M., Chung J. N., *J. Micromech. Microeng.* **2007**; 17: 1002.
- [Xu05] S. Q. Xu, Z. H. Nie, M. Seo, P. Lewis, E. Kumacheva, H. A. Stone, P. Garstecki, D. B. Weibel, I. Gitlin and G. M. Whitesides, *Angew. Chem. Int. Ed.* **2005**; 44: 724.
- [Yal06] Yalcin A., Popat K C., Aldridge J C., Desai T A., Hryniewicz J., Chbouki N., Little B E., King O., Van V., Chu S., Gill D., Washburn A. M., Ünlü M. S., Goldberg B. B., *IEEE Journal of Selected Topics in Quantum Electronics* **2006**; 12: 148.
- [Yan03] Yan M., Harnish B., *Adv. Mater.* **2003**; 15 (3): 244.

- [Yeo06] Yeoh T., Mason M., Feinberg Z., Leung M., Tasci M., Elarde V. C., Coleman J. *J. Mater. Res. Soc. Symp. Proc.* **2006**; 924 : Z06.
- [Yin01] Yin Y., Xia Y., *Adv. Mater.* **2001**; 13 : 267.
- [Yu98] Yu D. P., Hung Q. L., Ding Y., Zhang H. Z., Bai Z. G., Wang J. J., Zhou Y. H., Qian W., Xiong G. C., Feng S. Q., *Appl. Phys. Lett.* **1998**; 73: 3076.
- [Zha04] Zhang L., Golod S. V., Deckardt E., Prinz V., Grützmacher D., *Physica E* **2004**; 23: 280.
- [Zhe05] Zheng B., Gerdtts C. J., Ismagilov R. F., *Curr. Opin. Struct. Biol.* **2005**; 15: 548.
- [Zho93] Zhong Q., Inniss D., Kjoller K., Elings V. B., *Surf. Sci. Lett.* **1993**; 290: L688.
- [Zoh08] Zohuriaan M. J., Kabiri K., *Iran. Polym. J.* **2008**; 17 (6): 451.

## Appendix

### Appendix 1 (A1):

General expression for the free energy functional of the film (eq 5.1) can be simplified in frames of the following assumptions: a)  $\rho \ll L$ , b)  $L \ll R_0$ , c)  $r_2^{-1} \ll r_1^{-1} \approx \rho^{-1}$  (see the definitions of the symbols in the main text). Below we use the cylindrical system of coordinates.

Energy relaxation via rolling. Before rolling, the curvature radii of the film aspire to infinity, and the first term in the free energy functional (eq 5.1) can be written as:

$$F_i^{bend} \approx \int \left[ \frac{1}{2} \kappa \left( \frac{1}{\infty} + \frac{1}{\infty} - \frac{2}{\rho} \right)^2 + \bar{\kappa} \left( \frac{1}{\infty} \right) \right] dA = \frac{4}{2} \kappa \rho^{-2} \int dA \quad (A1)$$

After scrolling, the free energy term associated with bending became, according to the assumption (c):

$$F_f^{bend} \approx \int \left[ \frac{1}{2} \kappa \left( \frac{1}{\infty} + \frac{1}{\rho} - \frac{2}{\rho} \right)^2 + \bar{\kappa} \left( \frac{1}{\infty \rho} \right) \right] dA = \frac{1}{2} \kappa \rho^{-2} \int dA \quad (A2)$$

Thus, the free energy difference due to bending moment relaxation is:

$$\Delta F_{bend} = F_f^{bend} - F_i^{bend} = -\frac{3}{2} \kappa \rho^{-2} \int_{R_0}^R 2\pi r dr = -\frac{3\pi\kappa}{2\rho^2} (R^2 - R_0^2) \quad (A3)$$

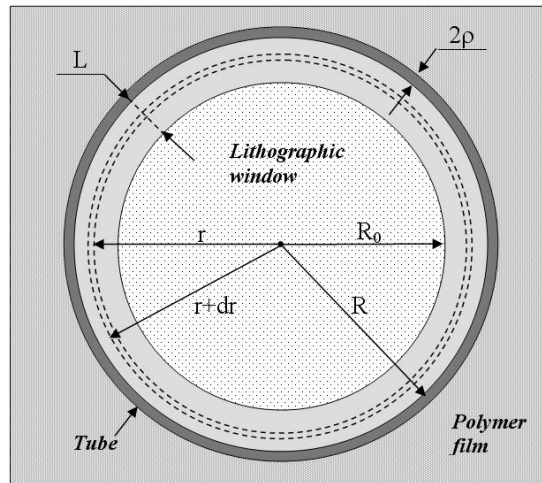


**Figure A1.** The scheme illustrating the notations used in the text.

Work on the film stretching due to rolling. Let be  $r$  the radius of a circular element of surface of the width  $dr$ , prior to rolling (see Figure A1). By the assumption (b), any element of surface has, *after rolling*, approximately the same distance to the centre:  $r \rightarrow R$ . There, the elongation of the surface element upon rolling can be written for all elements of surface as

$$\Delta l = 2\pi(R-r). \text{ The work of the in-plane stretching of is } dF_s = (1/2)Y \frac{\Delta l^2}{l} dr = \pi Y \frac{(R-r)^2}{r} dr.$$

Here,  $Y$  is the effective stretching stiffness of the bilayer film. The elastic energy stored in the film upon rolling is:

$$\Delta F_{stretch} \approx \pi Y \int_{R_0}^R \frac{(R-r)^2}{r} dr = \pi Y \left[ R^2 \ln \frac{R}{R_0} - 2R(R-R_0) + \frac{1}{2}(R^2 - R_0^2) \right] \quad (A4)$$

Combining (A3) and (A4) gives:

$$\begin{aligned} \Delta F &= \Delta F_{bend} + \Delta F_{stretch} = -\frac{3\pi\kappa}{2\rho^2}(R^2 - R_0^2) + \pi Y \left[ R^2 \ln \frac{R}{R_0} - 2R(R-R_0) + \frac{1}{2}(R^2 - R_0^2) \right] = \\ &= \pi Y R_0^2 \left\{ -\frac{3\kappa}{2\rho^2 Y} \left[ \left( \frac{R}{R_0} \right)^2 - 1 \right] + \left( \frac{R}{R_0} \right)^2 \ln \frac{R}{R_0} - 2 \frac{R}{R_0} \left( \frac{R}{R_0} - 1 \right) + \frac{1}{2} \left[ \left( \frac{R}{R_0} \right)^2 - 1 \right] \right\} \end{aligned} \quad (A5)$$

Let us introduce the dimensionless units,

$$\text{Note that } \frac{R}{R_0} = 1+x \quad \text{and} \quad \Delta \tilde{F} = \frac{\Delta F}{\pi Y R_0^2} \quad x = \frac{R-R_0}{R_0} = L/R_0$$

Then, (A5) can be rewritten as:

$$\Delta \tilde{F} = -A(2x+x^2) + (1+x)^2 \ln(1+x) - 2x(1+x) + \frac{1}{2}(2x+x^2) \quad (A6)$$

$$\text{where } A = \frac{3\kappa}{2Y\rho^2}$$

Since  $x \ll 1$  by the assumption (b),  $\ln(1+x) \approx x - \frac{x^2}{2} + \frac{x^3}{3} + \dots$

To the 3 eldest terms by  $x$ , the free energy difference of the rolled and unrolled states of the strained bilayer reads:

$$\Delta\tilde{F} = -A(2x + x^2) + \frac{x^3}{3} \quad (\text{A7})$$

The function has the minimum at  $x_e = A + \sqrt{A^2 + 2A} \approx \sqrt{2A}$  (marked by dashed line on the Figure 5.6). Thus, the equilibrium width of the rolled-up layer is:

$$L_e \approx \frac{R_0}{\rho} \sqrt{\frac{3\kappa}{Y}} \quad (\text{A8})$$

Since  $x \ll 1$ , there should be  $A \ll 1$ , i.e.  $\kappa \ll Y\rho^2$ . This means that the model is self-consistent if bending stiffness of the film is sufficiently small.

## **Appendix 2 (A2): Fabrication of other polymeric architectures by self-rolling of P4VP/PS bilayer**

### ***(I) Formation of dozen cm long tube:***

It is obvious in the self-rolling approach that the length of the tube depends on the length of substrate, hence, we fabricated long tubes from dozens of centimetres to meters by this approach. In order to make long tube concentric scratch was made using a sharp blade [Figure A2 (I) a]. An optical as well as SEM micrographs of concentric tubes are given in the Figure A2 (I) b and c, respectively. These long polymer tubes can be explored for potential use as chromatographic columns.

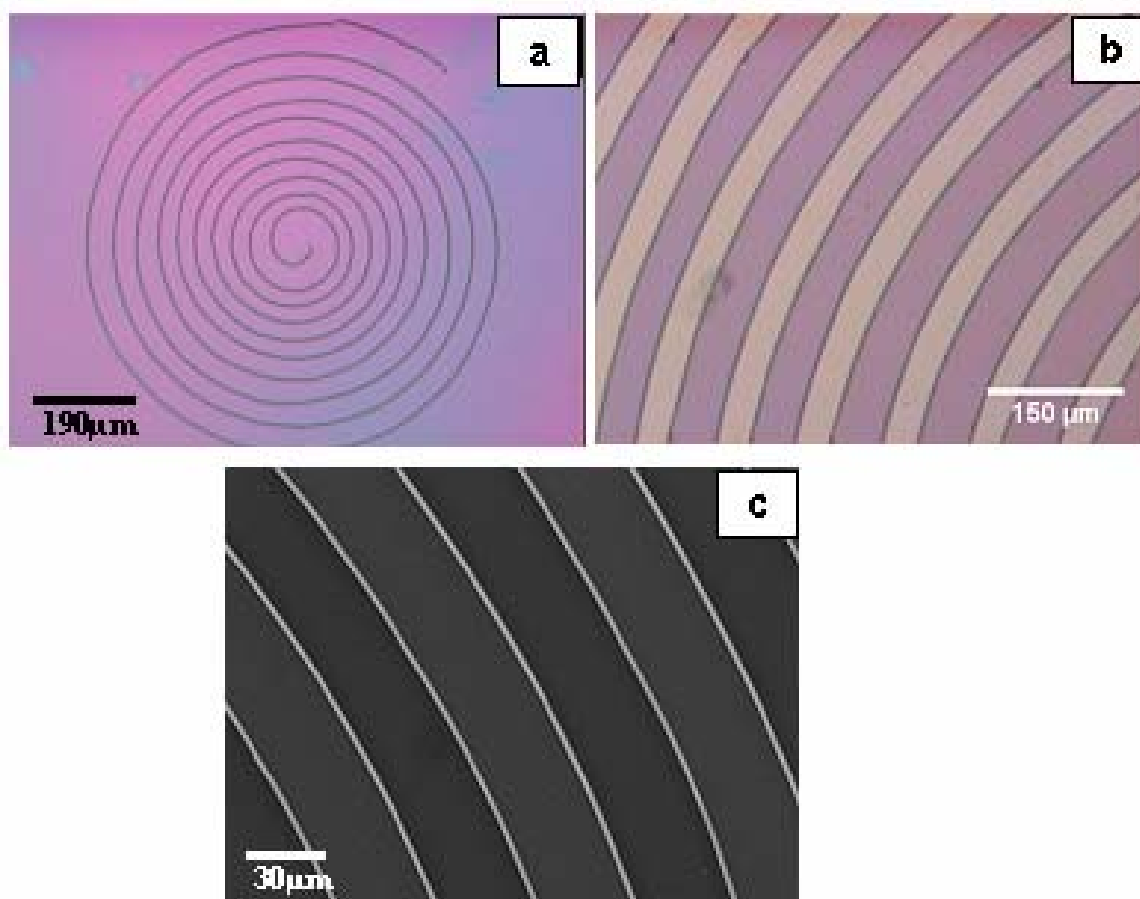


**Figure A2 (I):** (a) Optical micrograph of concentric pattern of the P4VP/PS bilayer (b) Optical figure of the concentric tube formed from self-rolling of P4VP/PS (c) SEM micrograph the tube

### **(II) Fabrication of triangle**

A pedal-like flower architecture of InGaAs/GaAs was synthesized using strain-driven rolling of InGaAs/GaAs bilayer [Chu08]. Here, we also fabricated a triangularly arranged tubes from the strain driven rolling of P4VP/P4VP bilayer. A SEM micrograph of a polymeric triangle is shown in Figure A2 (II).

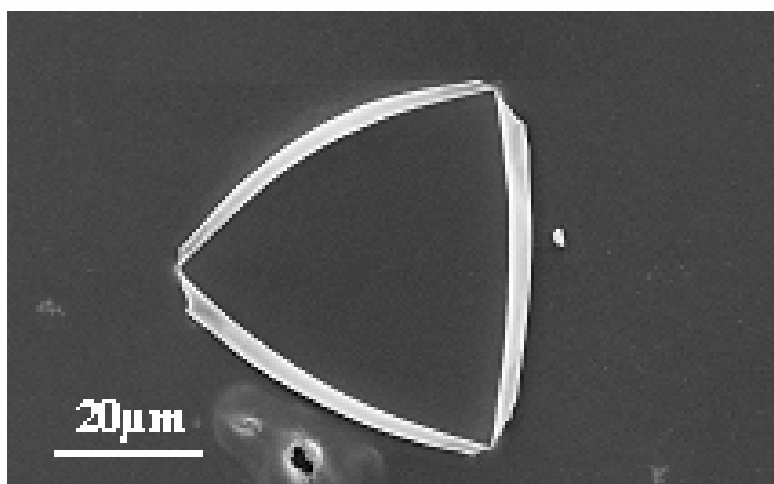


**Figure A2 (II):** A SEM micrograph of a triangularly arranged P4VP/PS tube

### **(III) Fabrication of toroids using epoxy droplet as mask**

It was observed that we can use very small droplet of epoxy as a mask for the production of micro-toroids. Using this kind of mask we can produce toroids of different dimension easily on one sample. A bilayer with developed pattern using small epoxy as droplet presented in Figure A2 (III). The surface of edges is not very sharp in this case [Figure A2 (III) a] compare to patterns using TEM grid as a mask or mechanical scratching but these rough surface are enrolled during the rolling process inside the tube and finally the smooth surface of toroids appeared [Figure A2 (III) b].

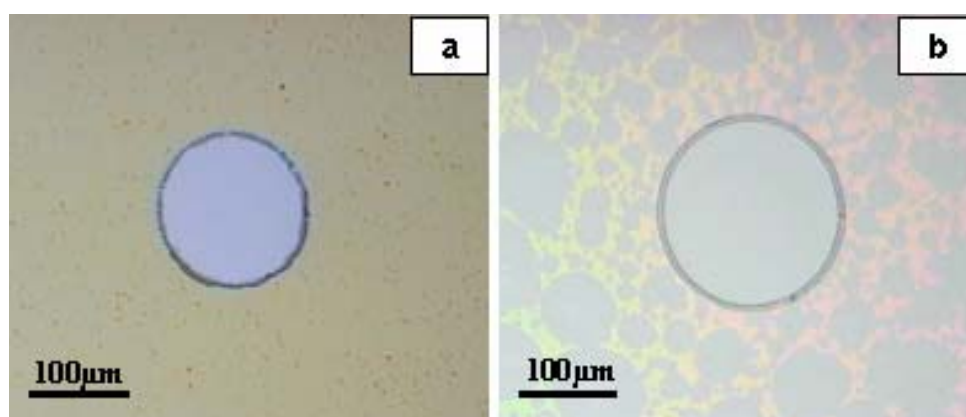


**Figure A2 (III):** Formation of toroids (a) Optical micrographs of circular pattern which formed using small droplet of epoxy during UV-crosslinking (b) Micrograph of toroid in dry state.



## Publications

- **Kamlesh Kumar**, Bhanu Nandan, Valeriy Luchnikov, E. Bhoje Gowd, Manfred Stamm, “Formation of single metal and bimetallic tubes from self-rolled polymer technique” **Langmuir (in press)**.
- **Kamlesh Kumar**, Valeriy Luchnikov, Bhanu Nandan, Volodymyr Senkovskyy, Manfred Stamm, “Formation of Self-rolled Polymer Microtubes Studied by Combinatorial Approach” **European Polymer Journal 44, (2008), 4115**.
- Valeriy Luchnikov, **Kamlesh Kumar**, Manfred Stamm “Toroidal hollow-core microcavities produced by self-rolling of strained polymer bilayer films”. **Journal of Micromechanics and Microengineering 18, (2008), 35041**.
- **Kamlesh Kumar**, Bhanu Nandan, Valeriy Luchnikov, Petr Formanek, Frank Simon, Manfred Stamm, “Synthesis of ceramic tubes from self-rolled polymer method” **Manuscript in progress**.

## Conferences

- **Kamlesh Kumar**, Valeriy Luchnikov, Manfred Stamm, “Toroidal Microcavities Produced by Self-Rolling of Strained Polymer Bilayer”, **Spring Meeting of the German Physical Society (DPG)**, Dresden, Germany, (2009).
- **Kamlesh Kumar**, Bhanu Nandan, Valeriy Luchnikov, E. Bhoje Gowd, Manfred Stamm “Fabrication of Metallic/Bimetallic Microtubes using Self-rolled Polymer Tubes as Templates”, **Spring Meeting of the German Physical Society (DPG)**, Dresden, Germany, (2009).
- **Kamlesh Kumar**, Valeriy Luchnikov, Bhanu Nandan, Manfred Stamm, “*Self-rolled polymer microtubes*”, **2<sup>nd</sup> young polymer scientists conference**, Terni, Italy (2008).
- **Kamlesh Kumar**, Valeriy Luchnikov, Manfred Stamm, “*Self-rolled polymer microtubes and toroidal microcavities*”, **Spring Meeting of the German Physical Society (DPG)**, Berlin, Germany, (2008).
- **Kamlesh Kumar**, Valeriy Luchnikov, Manfred Stamm, “*Self-rolled polymer micro- and nanotubes*” in **11<sup>th</sup> Dresden Polymer Discussion**. - Meißen, (2007)

## Curriculum Vitae

**Kamlesh Kumar**

**Personal details:**

Date of Birth : 19.07.80

Nationality : Indian

**Qualification:**

- 02.2006-07.2009      PhD student in the department of Chemistry of Technical University of Dresden (Supervisor: Prof. M. Stamm) and visiting scientist in Institute of Polymer Research, Dresden.
- 06.2005- 11.2005      Research fellow (Supervisor: Prof. Ann-Christine Albertsson) at Fiber and Polymer Technology, Royal Institute of Technology, KTH, Stockholm, Sweden.
- 07.2003-05.2005      M.Tech. (Master of Technology) in Polymer Science & Engineering (Supervisor: Prof. Indira K. Varma) from Indian Institute of Technology, Delhi, India.
- 07.2000-10.2002      M.Sc. (Master of Science) in Chemistry with specialization in Physical Chemistry from University of Rajasthan, Jaipur, India.
- 07.1997-06.2000      B.Sc. (Bachelor of Science) with Chemistry, Botany and Zoology from University of Rajasthan, Jaipur, India.
- 07.1995-06.1996      Senior Secondary Examination
- 07.1993-06.1994      Secondary Examination

## **Versicherung**

Hiermit versichere ich, dass ich die vorliegende Arbeit ohne unzulässige Hilfe Dritter und ohne Benutzung anderer als der angegebenen Hilfsmittel angefertigt habe; die aus fremden Quellen direkt oder indirekt übernommenen Gedanken sind als solche kenntlich gemacht. Die Arbeit wurde bisher weder im Inland noch im Ausland in gleicher oder ähnlicher Form einer anderen Prüfungsbehörde vorgelegt.

Die vorliegende Arbeit wurde unter der wissenschaftlichen Betreuung von Prof. Dr. Manfred Stamm an dem Leibniz-Institut für Polymerforschung Dresden angefertigt. Keine frühere erfolglose Promotionsverfahren statt gefunden haben. Die Promotionsordnung der Technischen Universität Dresden der Fakultät Mathematik und Naturwissenschaft erkenne ich an.

Kamlesh Kumar

Dresden, Germany